DRA

(NASA-CR-169945) DEVELOPMENT OF A HIGH CAPACITY TOROIDAL Ni/Cd CELL Final Report (EIC, Inc., Newton, Mass.) 114 p HC A06/MF A01 CSCL 10C

N83-19273

Unclas G3/44 15206

FINAL REPORT

DEVELOPMENT OF A HIGH CAPACITY TOROIDAL Ni/Cd CELL

Contract No. NAS3-21274

Covering period from January 2, 1979 to February 28, 1981

G. L. Holleck
J. S. Foos
J. W. Avery
V. Feiman

EIC Laboratories, Inc.
55 Chapel Street
Newton, Massachusetts 02158

Prepared for

NASA-Lewis Research Center
21000 Brookpark Road
Cleveland, Ohio 44135

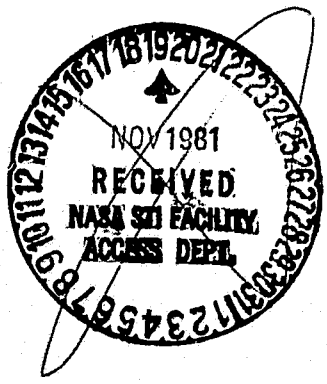

July 1981

ABSTRACT

In this report we describe two different specific designs for the implementation of a toroidal Ni/Cd cell concept originally developed at NASA. They consisted of a double swaged and a swaged-welded configuration. Toroidal prototype cells of both designs were manufactured and evaluated. We have demonstrated that large capacity toroidal Ni/Cd cells are feasible. In practice they do probably not offer significant advantages over conventional Ni/Cd cells. Mechanical contacts for high rate cells are judged as not feasible since their quality slowly degrades in the oxidizing cell environment.

TABLE OF CONTENTS

TABLE OF CONTENTS
(continued)

LIST OF ILLUSTRATIONS

LIST OF ILLUSTRATIONS
(cotninued)

LIST OF ILLUSTRATIONS
(continued)

LIST OF ILLUSTRATIONS
(continued)

LIST OF TABLES

I. INTRODUCTION

This contract effort is part of an overall program to provide electrical storage technology for photovoltaic power systems in the multikilowatt range on the low earth orbiting satellites that are foreseen in the late 1980s.

The emphasis here is on a new concept in nickel-cadmium battery design which can offer better thermal management, higher energy density and much lower cost than the state-of-the-art.

The described effort was based on a NASA toroidal Ni/Cd cell concept. It was critically reviewed and used to develop two new cell designs for practical implementation. One is a double swaged and the other a swaged-welded configuration. The concepts and their practical implementation are described in Sections II and III. Section III.5 contains a summary discussion and conclusions.

II. DEVELOPMENT OF A SWAGED TOROIDAL Ni/Cd CELL

1. Objective and Design Approach

1.1 Introduction

NASA developed a new concept in Ni/Cd battery design which can potentially offer better thermal management, higher energy density and much lower cost than the state-of-the-art. A graphical illustration of the concept is shown in Fig. 1. The concept is based on a toroidal shape of the cell containing a wound core of electrodes. Conceptual assembly involves inserting two can halves around the wound core and into each other. The two cell halves would be separated by a nylon spacer and act also as the electrical contacts. Cell sealing would be achieved by a swaging process.

1.2 Program Objective

The objective of the present program was to assess the feasibility of the toroidal Ni/Cd concept by building and evaluating prototype cells. Since there existed no past experience with this construction method detailed procedures, parts and fixtures had to be developed. In the following we discuss in detail our initial design approach.

1.3 Review of Design Requirements

1.3.1 General Remarks

The packaging of the cell is a key to success and no prior experience exists with the toroidal cell configuration. The single most important question is: whether or not a hermetic seal can be made with this construction. Other expected problems such as, e.g., electrical continuity and the resistance at the interface and in the long electrode strips will then be subsequently solved. The overcharge mode of hermetically sealed Ni/Cd cells deserves however, special consideration here since it impacts diretly on cell can design.

Hermetically sealed Ni/Cd cells are limited by the nickel oxide electrode. On overcharge, they evolve oxygen at the nickel oxide electrode which migrates to the cadmium electrode where it is reduced. The internal pressure generated depends primarily on (a) overcharge rate, (b) electrolyte fill level of the separator, (c) presence of inert gas.

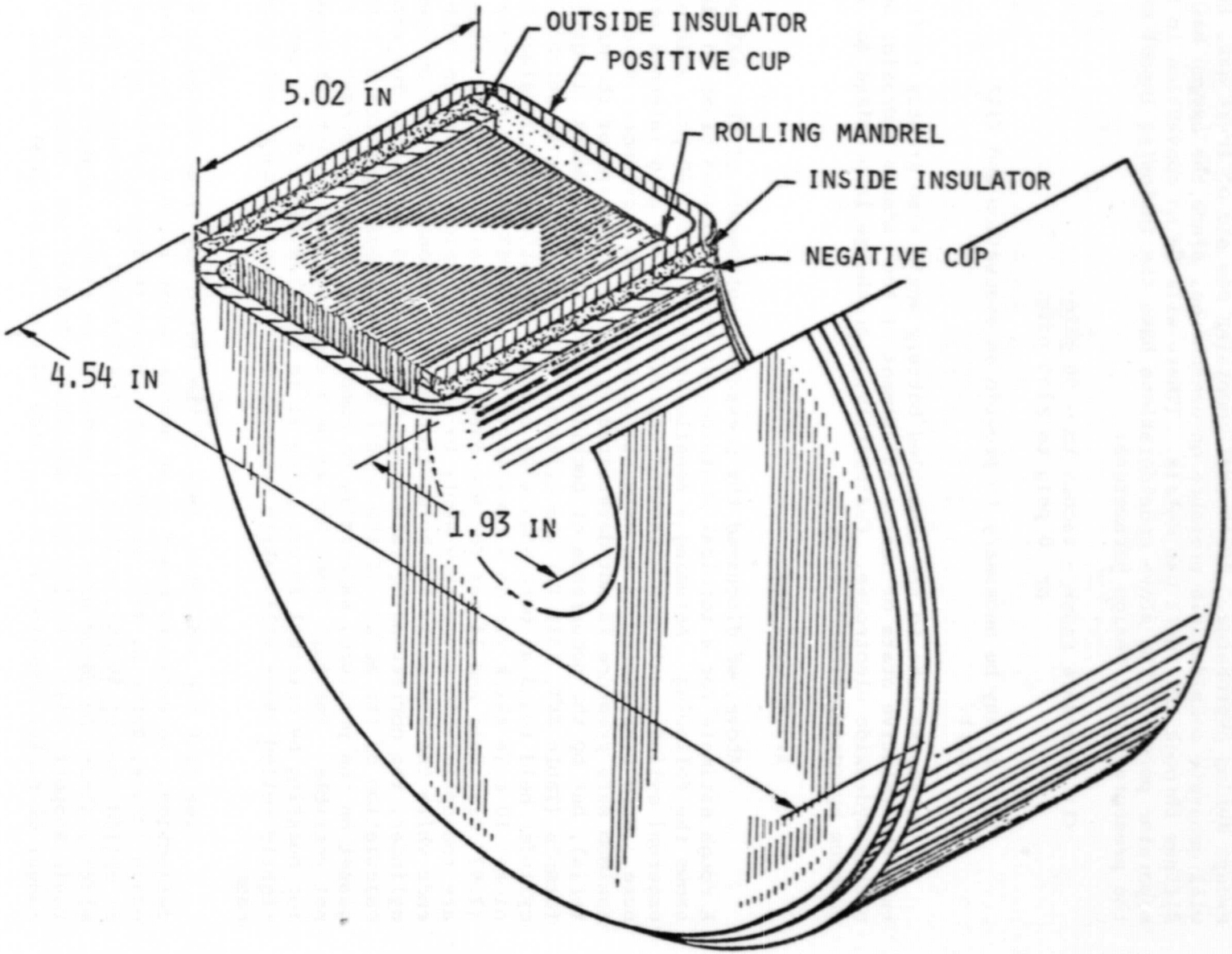

Fig. 1. 100 ampere-hour toroidal Ni/Cd cell.

To optimize O_2 gas transport in fairly electrolyte saturated stacks, the cells are evacuated prior to sealing and will be at negative pressure except during overcharge. If the cell contains one atm of inert gas, it will generate considerable pressure on overcharge, since the oxygen has to diffuse through the inert gas matrix. (There will be no convection in the separator pores). The above considerations have the following impact on the pressure vessel design parameters:

(1) pressure range - vacuum to ~ 50 psig
or 0 psig to ≥100 psig

(2) it may be necessary to provide an evacuation and fill port.

An access tube to the assembled battery would also greatly facilitate the relative state of charge adjustment of the cadmium hydroxide and nickel hydroxide electrodes. Customarily, a precharge is provided for the cadmium hydroxide electrode.

1.3.2 Cell Can

Above, we discussed the pressure requirements of the cell case. A rough estimate for a toroidal container of the dimensions given in Fig. 1 shows the following. Assuming a tensile strength of 50,000 psi, a 10 mil external cylinder wall can withstand approximately 200 psig internal pressure. More problematic is an external pressure onto a cylinder. Here, the maximum safe pressure is not determined by the yield stress of the material, but by the occurrence of buckling. For example, Roark (1) gives a formula (Table XVI, #31) for the critical external pressure at which a thin cylinder held round at both ends will buckle. Substitution of values for nickel 10 mils thick yields a buckling pressure of 53 psi for the inner (1.92" dia) wall and 14 psi for the outer (4.54" dia) wall. These values are too optimistic since they apply to a cylinder held circular on both ends while the cup walls are held circular only on one end. For an open cylinder, the corresponding values are only about 13 and 7 psi. The exact calculation of the effect of the double wall thickness separated by a nylon gasket on the pressure, especially on compression (external pressure) is not possible. The cell stack has to be discounted as a structural support for buckling by external forces since it is too flexible. Even a very tightly rolled stack will easily compress many times the case wall thickness.

The flat top and bottom face of the toroid may show considerable deflection. An estimate based on an annular plate rigidly fixed at both edges (Roark, Table X, #77) yields, for a plate thickness of 10 mils with an aplied load of 50 psi, a deflection of 140 mils. This estimate is optimistic, since the edges have been assumed to be rigidly clamped although their supports will actually give somewhat. In addition, there may be the danger of pucker buckling at the outside edge of the toroidal vessel.

In summary, the smooth walled pressure vessel will most probably require more than 0.01 inch material to safely withstand all conditions anticipated in the high capacity Ni/Cd cell.

1.3.3 Cell Seal

The most serious problems are associated with the cell seal. They relate to the forces needed to swage the nickel can and the pressure which has to be maintained on the nylon gasket in relation to the forces which can be exerted onto the can structure during the sealing process.

To produce and maintain hermeticity, the contact pressure of the nylon gasket has to exceed the maximum operating pressure of the cell. This pressure on the gasket has to be maintained permanently or cell leakage will occur.

For purposes of estimating the loads to be placed on the case structure, let us assume that the pressure in the insulators is in the range of 75-100 psi and that the tensile strength of the nickel is 50,000 psi. Pressure in the outside insulator will be balanced by tensile hoop stresses in the outside cylindrical part of the positive cup and by compressive hoop stresses in the outside cylindrical part of the negative cup. If the positive cup is 0.010" thick, 100 psi internal pressure will produce a hoop stress of 22,600 psi. This may be acceptable if the assumed material strength is correct and the seal pressure can be well controlled. The negative cup, however, is prone to buckling failure under relatively small loads, as was discussed earlier.

In summary, to maintain the compression necessary for hermeticity on the gasket the resistance to buckling of the compressively stressed portion of the vessel wall has to be increased.

1.3.4 Assembly Procedure

There are several fundamental problems in forming a seal by expanding the inner cylinder and reducing the outer cylinder of the toroid independent of the specific procedure used to achieve this. The most severe problems result from cell wall buckling under compression and from the negligible energy storage of the plastic gasket material.

We have discussed above that the maximum permissible external load on a thin wall cylinder is not limited by plastic flow of the material but by buckling. In normal swaging or deep drawing procedures, the buckling is prevented by a closely fitting internal support mandrel. In our case, the cell interior is not accessible and the electrode roll is much too resilient to act as such a support. The stress that can be applied before buckling becomes a problem will be somewhat larger than the 15 psi mentioned above, since in the redrawing deformation occurs successively in a limited area which gets a certain amount of support from the neighboring material. Theoretically, the maximum compressive force on the inner vessel wall has

to be only equal to the sealing pressure. This implies careful swaging or redrawing of the outside to yield exactly this level of compression at the inside, and then absolutely maintaining the position of the outer wall without allowing any elastic relaxation. In practice, this appears an impossible control problem as will be more evident later. An alternative procedure involves the redrawing of the outside enough to also slightly redraw the inside at the same time. To compress the inner cell wall to the yielding point (say to 50,000 psi) would require application of an external pressure of around 200 psi. Of course, the wall would need strong external supports to avoid buckling under that pressure.

The problem associated with maintaining permanent compression on the gasket material can best be illustrated by the sketch in Figure 2. For this discussion, we assume that buckling is no problem.

Let us examine in more detail the process of redrawing the outside diameter of the cell (similar arguments apply to the inside diameter). In the redrawing process, a cylindrical ring whose inside diameter is somewhat smaller than the outside diameter of the positive cup is pressed over the cup applying radial forces and reducing the cup diameter. If the size difference (interference) between the redrawing die and the cup outside diameter is large enough, the contracting positive cup may compress the insulator against the negative cup sufficiently to generate the desired sealing pressure. If the interference is higher still, the yield stress of both the positive and negative cup may be exceeded, and further increase in die-cup interference will result in little increase in insulator pressure.

After the redrawing die has passed over the cell, the elastic compression in the cups will relax. This relaxation will be about equal for both walls. Due to the relaxation of the gasket compression, the outside cup will pass through the point of 0 stress and be under a slight expansion while the inside cup remains under slight compression. The associated elastic force is the compressive force on the nylon gasket. To illustrate the magnitude of the forces involved, let us consider the following:

To compress the cup wall which forms the inside support for the outside insulator to its yield point, the nylon must exert a radial pressure of around 200 psi. Assuming nylon to have an elastic modulus of 5×10^5 psi, a radial pressure of 200 psi will elastically deform the 30 mil thick insulator about 1.2×10^{-5} in. (0.012 mils). Since the inner and outer cup walls constraining the insulator are both in compression inside the drawing die and both equally stressed (yielding), they will both expand together when the die forces are removed and the elastic energy stored in the cup walls will be dissipated. The compressed nylon will relax too, inducing compressive stresses in the inner cup and tensile stresses in the outer cup. The magnitude of these induced stresses, however, will be very small. If, for example, the total strain in the nylon insulator were

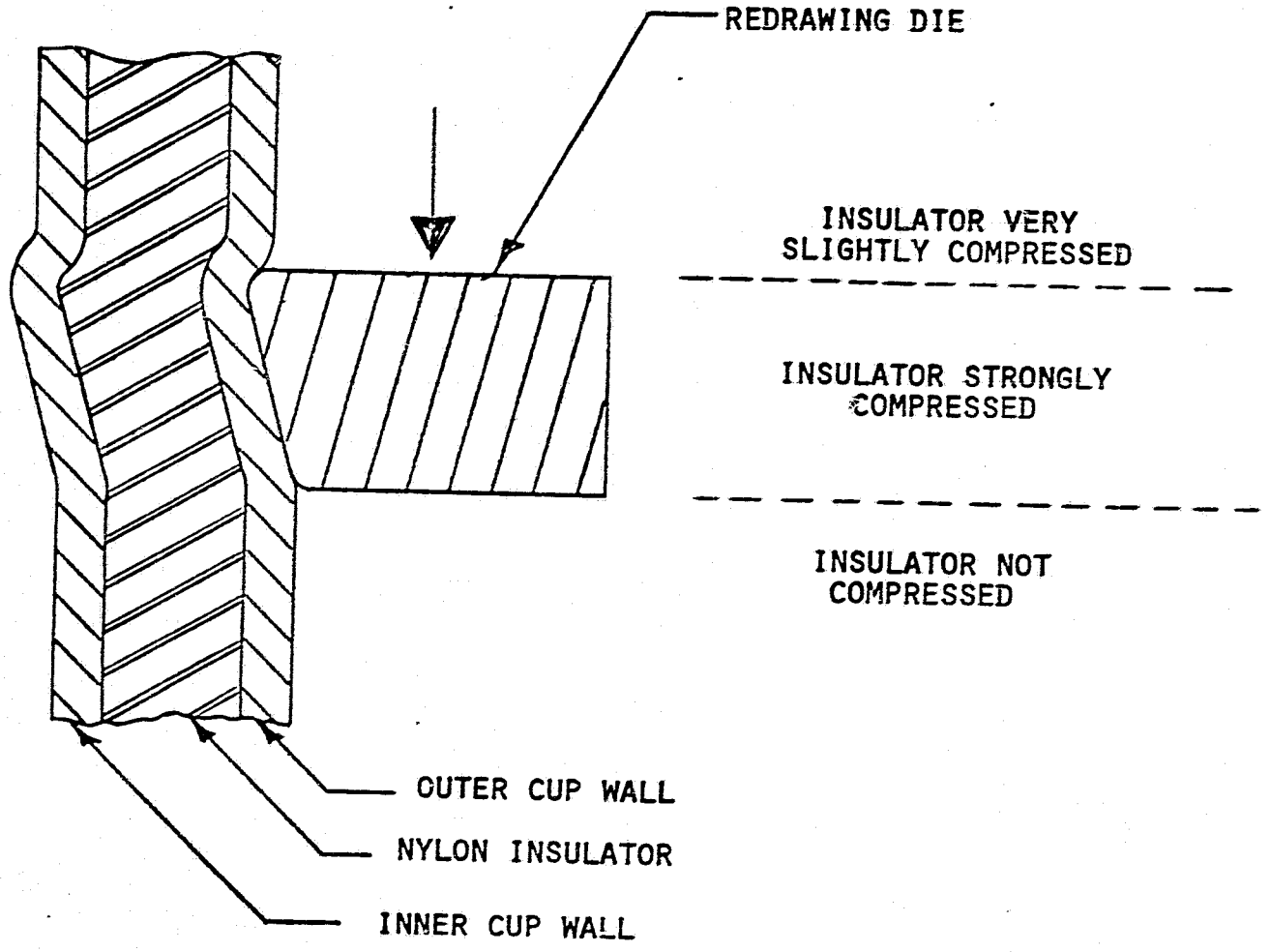

Fig. 2. Insulator compression in a redrawing operation.

transferred to the outer cup wall, i.e., the radius of the outer wall were expanded by 1.2×10^{-5} in. while the radius of the inner wall was held constant, the resulting contact pressure between the nylon and the outer wall would be about 1 psi. To support a sealing pressure of 100 psi, we calculate the necessary wall thickness from the buckling pressure equation used earlier (Roark, Table XVI, #31) to be about 25 mils. A similar stiffness could also be achieved with a thinner wall thickness and suitable reinforcing ribs.

Such solutions would allow suitable compression of the gasket, but would not support the higher loads which could result from overcompression due to an undersized restrainer, for example. Insurance of sealing pressures within acceptable limits (say 75 to 100 psi) would require very close control of tolerances in all components (less than 0.0005 in. on the radius of the can and swaging ring). Such stringent requirements are not feasible with state-of-the-art technology. If higher capacity cells with larger outer diameters are considered, the problem of avoiding buckling will become increasingly more severe.

The above considerations show that it is imperative to prevent the elastic relaxation after the plastic deformation. This means, in practice, that the sleeve would basically have to also be the drawing tool. The friction forces involved in the drawing process, even if well lubricated, are considerable and require in all probability significantly increased wall thickness for the retaining sleeves.

Other practical problems are associated with supporting the cell structure during the redrawing procedure, since only the exterior of the toroidal pressure vessel is accessible. Substantial forces are transmitted not only perpendicular to the vessel wall, but also in the axial direction. Here, too, the danger of collapse exists especially at the outside where the wall curvature is relatively small. These difficulties are, however, of less fundamental nature and can probably be handled, e.g., by constructing support jigs and using several drawing passes with only small diameter reductions in each pass.

In summary, the fundamental problem is in permanently pressurizing the sealing gasket without buckling the outside diameter of the inner cup. The specific method of pressurization is of secondary importance. Swaging or redrawing will create an excellent fit (small clearances) between the cups and the insulator, but unless the elastic relaxation after the redrawing process is prevented, no appreciable permanent pressure remains on the seal.

1.4 Specific Design Approach

To overcome the main problems identified in the original NASA design we have developed a cell design with corrugations.

This cell design obtains its stiffness and the necessary retention of compressive sealing force from a suitable use of corrugations. Figure 3 shows an illustration. In this modified redrawing concept, we would reduce the outside of the positive cup (or expand the inside of the negative cup) only in several narrow bands around the cell. Here, corrugations have been rolled into the outside and inside diameters of the cell opposite mating corrugations in the other cup which were formed when the cup was made. This mechanical interlocking has the dual advantage of securing the case together under internal pressure loading and of increasing the sealing pressure in the nylon as the internal pressure increases. Two mechanisms here allow the sealing pressure to remain after removal of the external forming forces in contrast to the unrestrained redrawing method discussed earlier. First, the small deformed bands are held in compression by the relatively larger adjacent cylindrical areas. Second, the nylon, no longer in bulk compression, can act in a much more elastic manner.

Based on a preliminary stress analysis, a circumferential corrugation of semicircular cross section with a 0.040 in. radius would be suitable. Such corrugations would be applied about every quarter inch.

To provide added strength and reduce head deflection, we have also shown ribs at the top and bottom of the cell. As an example, 36 radial ribs, of half-circular cross section with 0.075 in. radius appear in a preliminary calculation to yield acceptable deflections and stress levels with 0.010" material. In addition, these ribs will facilitate cell sealing, since they provide a positive interlock for holding the cell without requiring significant pressure during the swaging operation.

In summary, this cell design appears most attractive. It retains all desirable features of the toroidal NASA design and has the following special features:

(1) Strong, lightweight cell case.

(2) An excellent interlocking seal which improves with cell pressure.

(3) A controllable cell assembly procedure.

2. Development of Cell Closure Process

Development of suitable parameters for the swaging process was a crucial step. As discussed earlier, the general procedure of forming, for example, the outer can seal consists of pregrooving the inner can followed by grooving of the outer can. In the following subsections we discuss the effect of the insulator, groove shape and depth of the can material properties and of various forming procedures on the nature of the resulting closure seal.

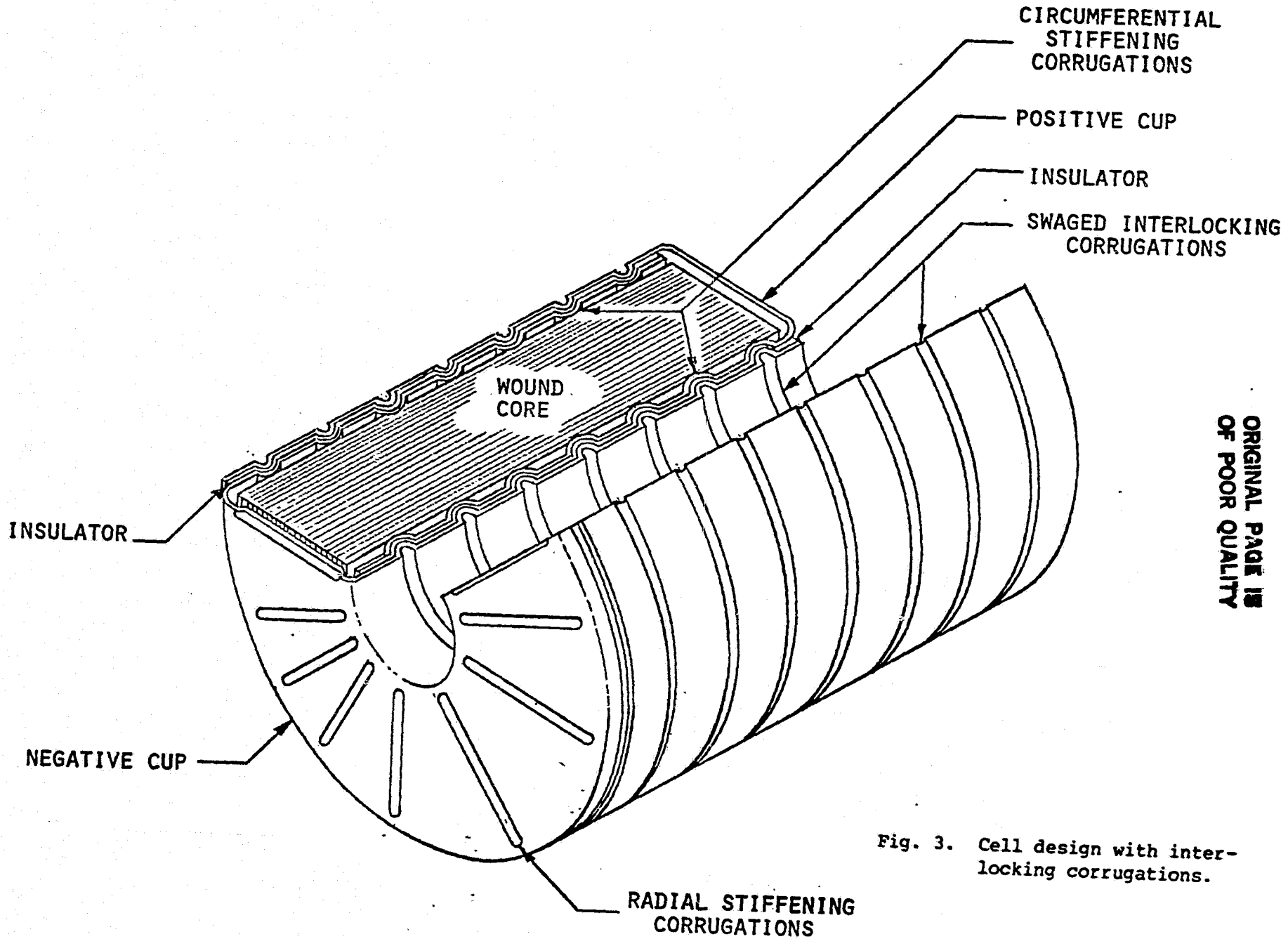

Fig. 3. Cell design with interlocking corrugations.

2.1 Insulator

To achieve a good reliable seal, a seamless nylon tube gasket is required. Such tubes can easily be extruded, however, for small quantities the cost is prohibitive. We explored therefore the formation of suitable tubular gaskets from sheet stock. Both heat and solvent sealing techniques were explored. Under carefully controlled conditions, satisfactory seals were made by heat sealing, however, the procedure was not reproducible and the seals were susceptible to cracking. As an alternative, an adhesive procedure has been investigated which gives a lapped seal as shown below.

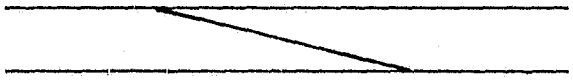

Nylon Seal

The difficulty in making such a seal lies in beveling the connecting ends of the nylon film at a constant angle over the width of the film (5"). In addition flat mating surfaces are required to make a good adhesive bond. Using a hardened steel jig, schematically shown in Figure 4, good beveled mating surfaces were produced by grinding of the nylon edge. The other edge of the nylon is given the appropriate matching bevel and the edges are joined using aqueous phenol. The bonded area is clamped, cured and the phenol removed in boiling water. The 10:1 angle of the chamfering jig allows a 0.32" overlap in the 0.032" nylon film. By this technique we produced bonds which were as strong and flexible as the original nylon.

In later experiments we also employed elastomeric insulator seals. They offer a larger elastic deformation and can easier seal small channels such as inhomogeneities in the metal surface. Elastomers which show good chemical resistances to concentrated base are listed in Table 1 along with temperature, hardness, and compression set characteristics. A Shore A hardness of 70-80 is considered the most suitable compromise for seal applications. Compression set refers to the ability of an elastomer to return to its original shape after compressive stress. A typical seal was fabricated from 0.031 inch Neoprene sheet (70 Duro).

Neoprene was used because, in addition to its resistance to potassium hydroxide, it is commonly available in a variety of sheet thicknesses and hardnesses; and can be bonded to itself using a variety of adhesives. The insulating cylinder is constructed from sheet using a 0.25" lap joint. After the joint has cured the excess rubber in the joint area is removed using a small sanding drum to give an even lapped seal (see Fig. 5 below).

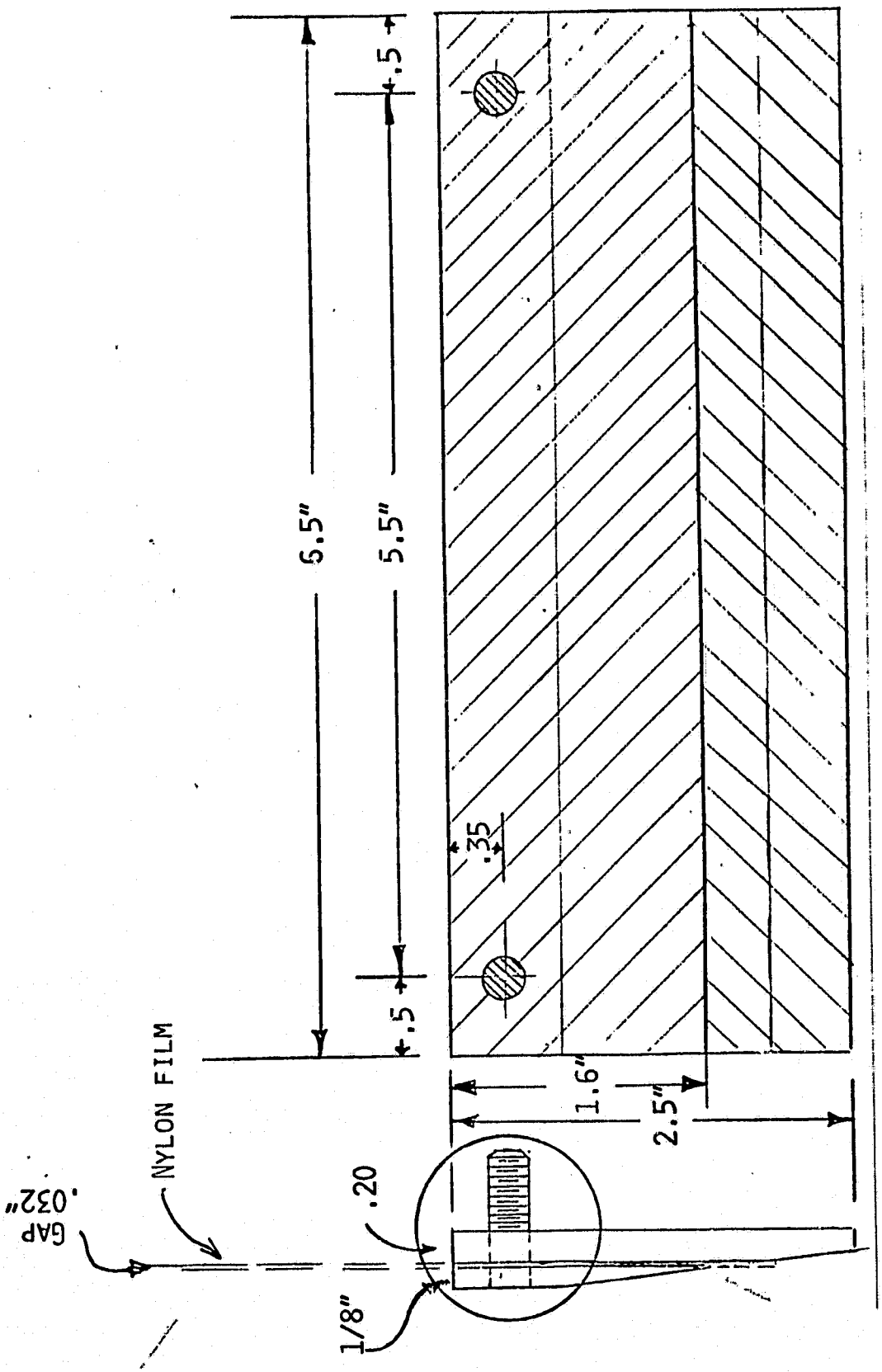

Fig. 4. Nylon beveling jig.

Table 1

Elastomer Properties

Elastomer	Aikali Resistance	Temperature Range, F	Hardness Shore, A	Compression Set
Isobutylene-Isoprene (Butyl)	Good	-50 to 300	40-80	Fair to good
Chloroprene (Neoprene*)	Good	-60 to 225	30-90	Good to excellent
Chlorinated Polyethylene	Excellent	-60 to 300	40-90	Excellent
Chlorosulfonated Polyethylene (Hypalon*)	Excellent	-50 to 325	50-90	Poor to fair
Ethylene-Propylene	Excellent	-70 to 350	30-90	Good to excellent
Epichlorohydrin	Good	-80 to 325	40-90	Poor to fair

*DuPont

Reference: Seal Compound Manual, Parker Seal Co.; "Guide to Selecting Elastomers," Product Engineering, July, 1978; "Elastomers" Machine Design, March, 1978.

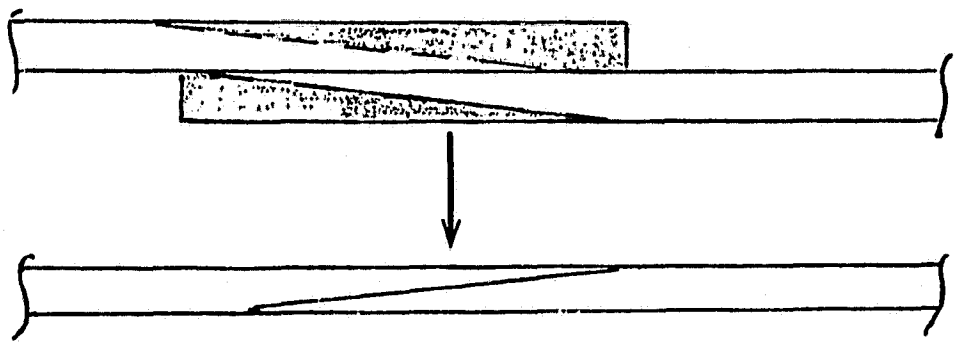

Fig. 5. Neoprene lapped seal.

The adhesive used in making the seal is Bostik 1142 applied as described on the container. It was evaluated along with Atlantic Brand Neoprene Bonding Cement and Devcon Rubber as to the strength of the bond produced and resistance of the bond to KOH. Cyanoacrylics are known to be brittle and have low resistance to base. Initial tests using short cure times (less than 24 hrs) and immersion of the joint in 30% KOH for three days showed some loss in bond strength. However, when the Bostik adhesive was cured over 24 hrs and subjected to KOH for three days the joint appeared as strong as the rubber itself. Ultimately seamless elastomeric tubes can be manufactured by a variety of processes.

2.2 The Swaging Process

2.2.1 Analysis of Groove Profiles

The hermetic seal between the two half cans is achieved by compression of the nylon gasket between grooves in the inner and outer cell walls. Number and dimension of the seal forming compression bands depends on the relative shape and dimension of the inner and outer grooves and thus on the forming wheels.

Three types of seals are illustrated in Figures 6 and 7 involving (1) three point compression, (2) side compression and (3) bottom compression. Major factors used in evaluating the relative merits of the seal types include the total area of compression in the seal and the magnitude of the compressive force making that seal. However, it is also of importance to evaluate the possibility of executing the seal formation in practice.

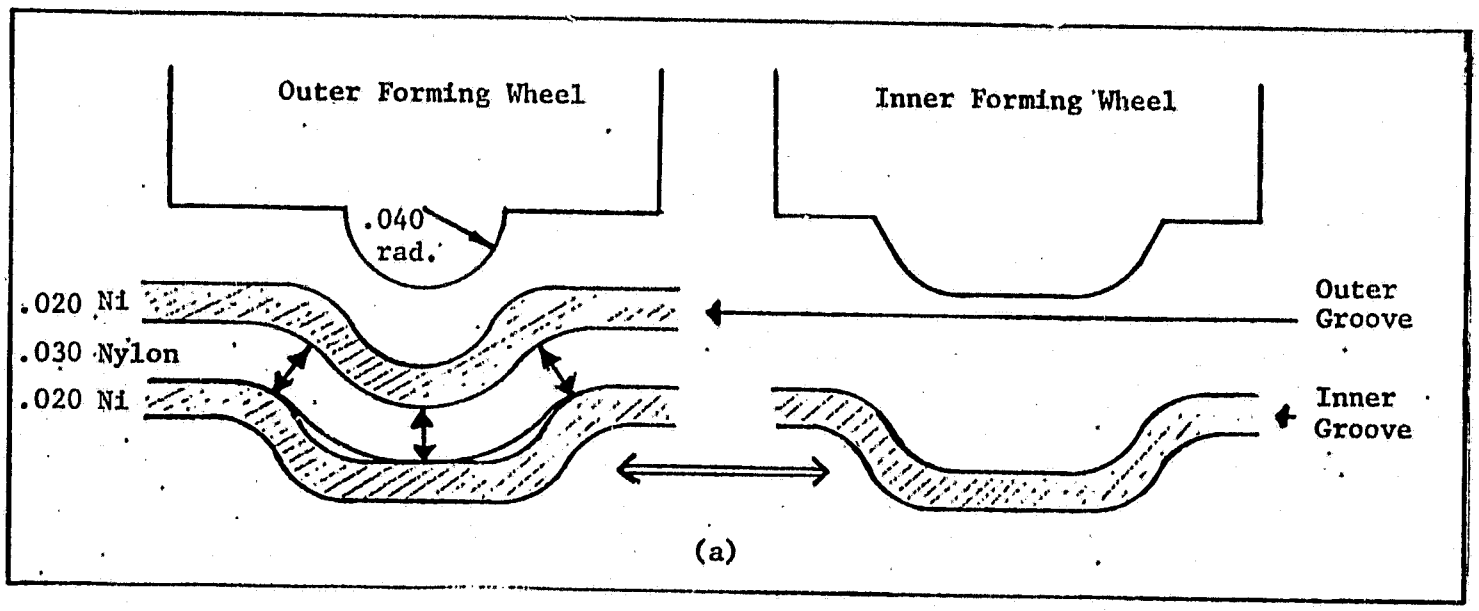

Fig. 6. Cross-section of can seal showing three areas of compression (~ X10).

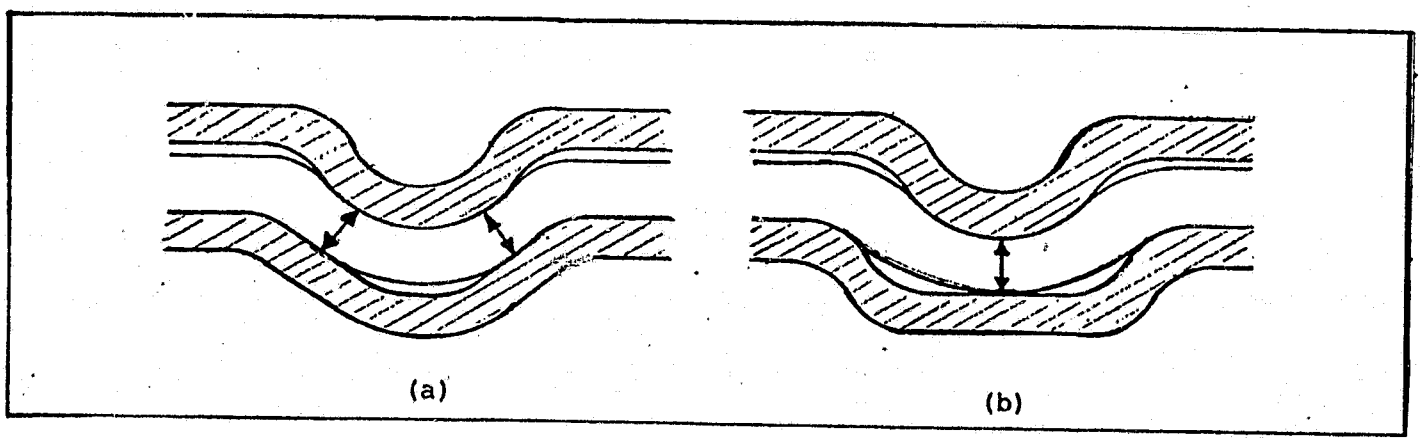

Fig. 7. Cross-section of can seal showing side contact (left) and bottom contact (right) seals (~ X10).

To maximize the quality of the seal one might wish to maximize the area of compression by using 3-point contact or side contact seals. However, these seals distribute the wall stress over a greater area than the bottom contact seal. This may cause a reduction in compressive force per unit area which could decrease the quality of the seal. This is a trade-off that will require further investigation.

The multi-contact seals also require greater accuracy in their assembly. Small errors in groove placement would cause loss of compressive seal at one or more points and any subsequent shift in relative groove position could lead to total seal loss. The bottom contact seal would be less sensitive to variations in cell assembly due to less stringent demands for exact groove placement. The major factors in forming wheel design are width and depth of the grooving bead. The detailed shape of the grooving bead, especially of the outer forming wheel, appears to be of lesser importance due to the smoothing effect of the deforming metal.

2.2.2 Experimental Exploration of Grooves and Seals

2.2.2.1 Metal Grooving

The development of experimental techniques for the formation of sealing grooves was carried out on cylinder sections and cans. Electroformed nickel cans were obtained from a commercial electroformer (Plating for Electronics, Inc., Waltham, MA). The cans (4.54 and 4.66 in. OD) were quite uniform (±2 mil) from top to bottom except in the immediate vicinity of the bottom edge. Around the circumference, however, the thickness varied widely from 17 mil over 2/3 of the circumference to a minimum of ~6 mil in the remaining third. Although such cans are ultimately not acceptable we considered them useful in exploring the effect of thickness and pretreatment on the swaging step. Fixtures were designed to be used with a standard lathe. Figures 8 and 9 show typical forming wheels and the inner can support mandrel.

Swaging of corrugations into the as-received cans resulted in breaking of the metal in the thin areas. The cans proved to be highly stressed as generally experienced with deposits from normal Watts plating baths. In order to relieve the stresses the cans were heat treated at 750°C in a H_2-N_2 atmosphere. After heat treating the metal working was greatly facilitated, however, workhardening led eventually to reoccurrence of tears across the bottom of the grooves in the thin metal cans.

Sections were cut from grooved material and mounted in epoxy. After grinding the specimen to a representative cross-section, the cross-section was polished and photographed. Figures 10 and 11 show such cross-sections from 18 mil Watts deposit, unannealed and annealed respectively. The unannealed cans resisted grooving and metal thinning was observed particu-

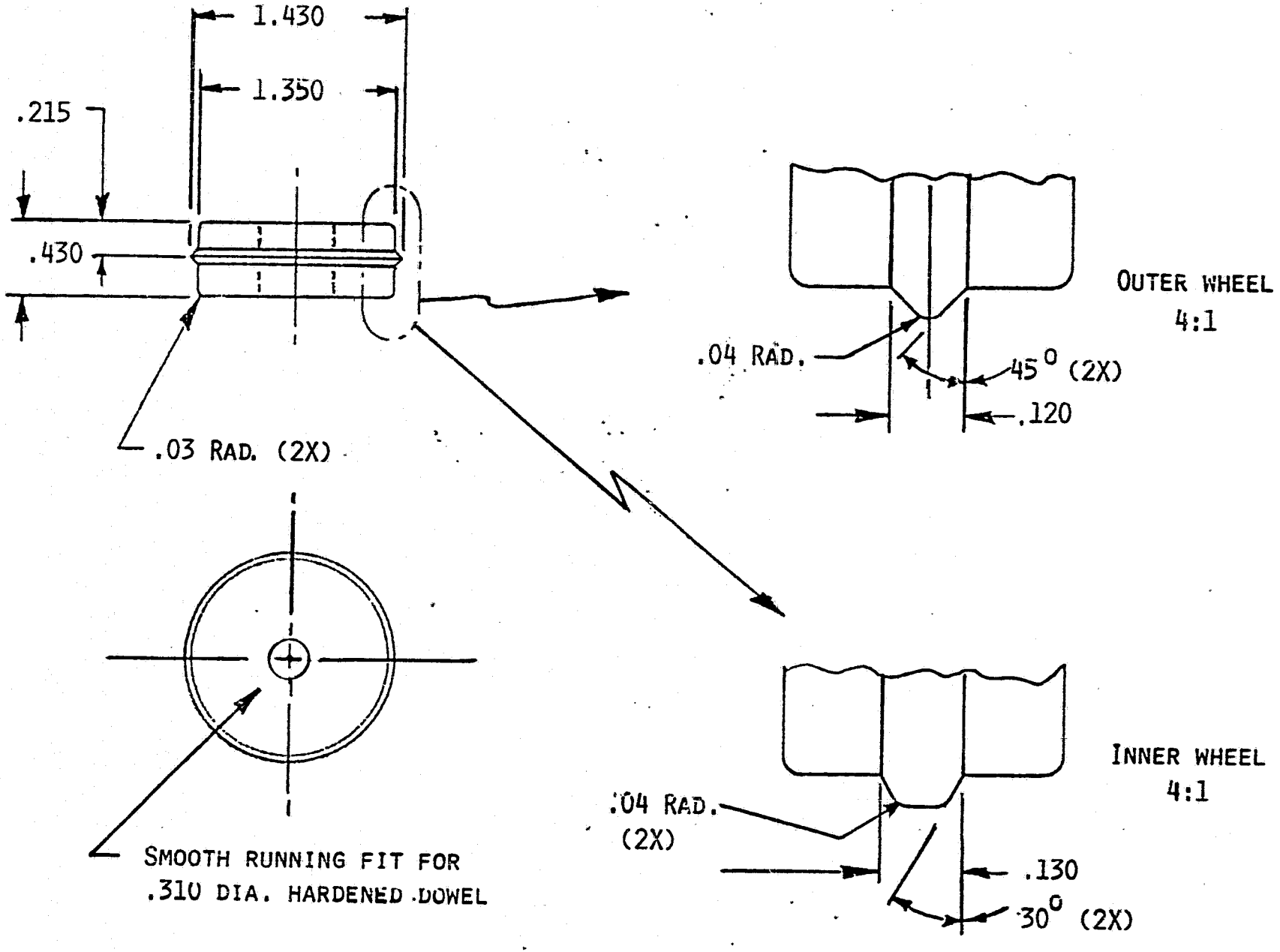

Fig. 8. Forming wheel set.

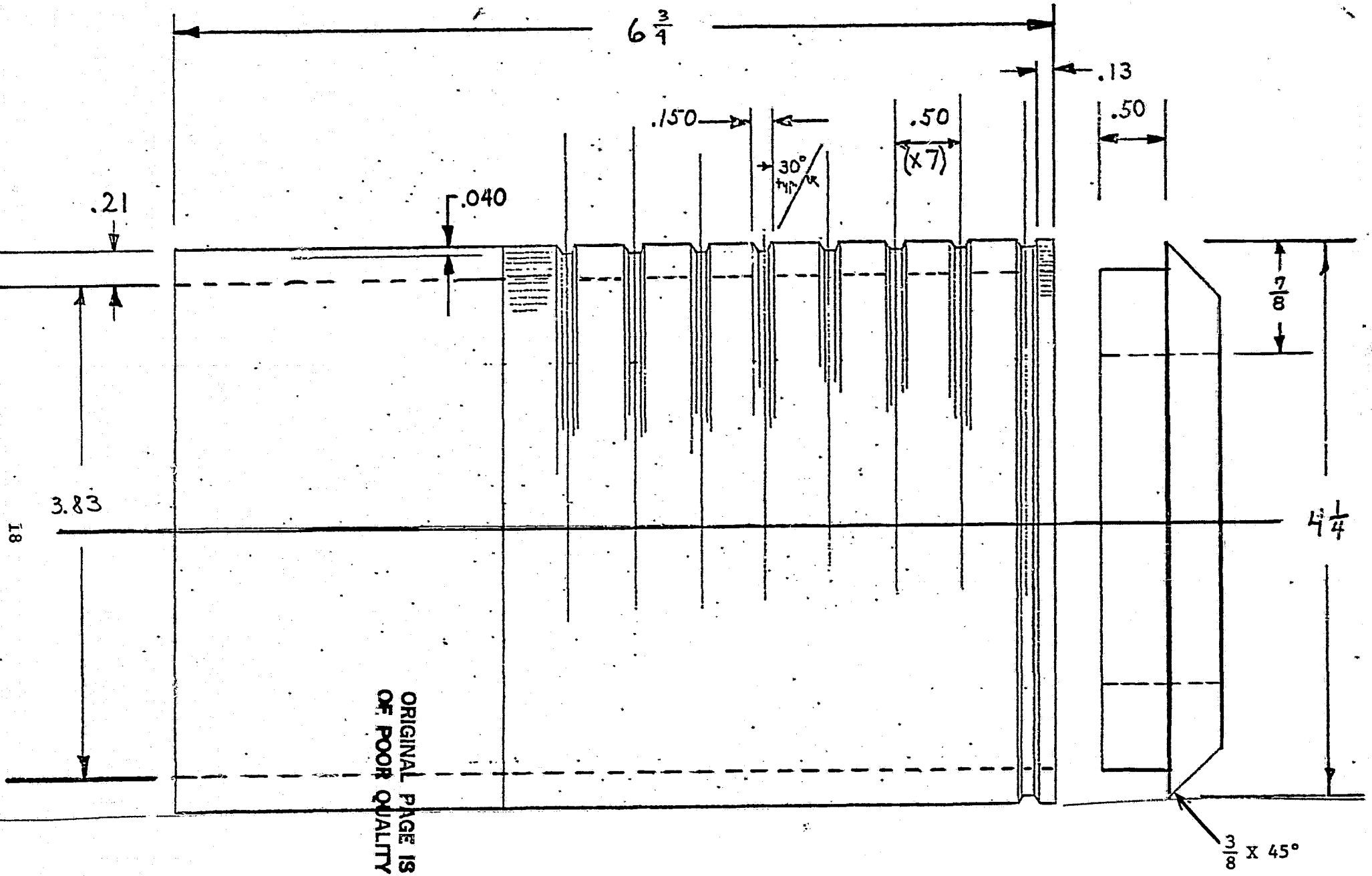

Fig. 9. Inner can support mandrel.

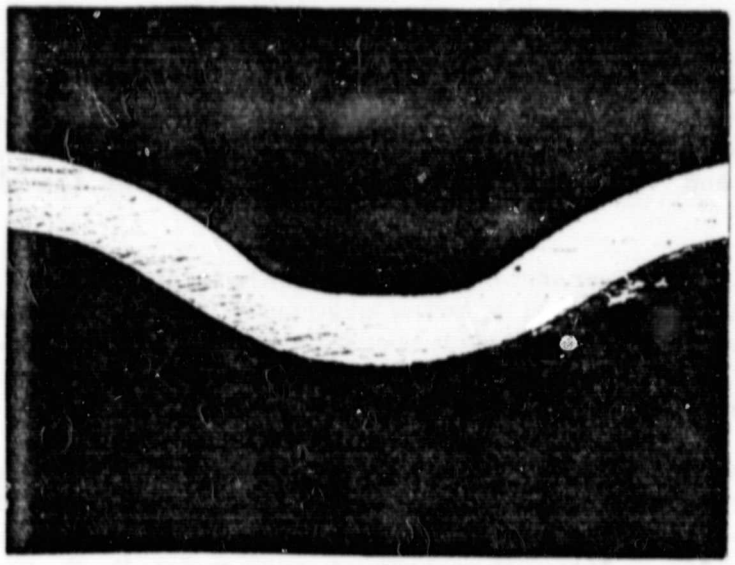

Fig. 10

Fig. 11

Groove cross-sections in cans from Watts baths (X20 enlargement).

larly to the left and right of the groove center (see Fig. 10). In addition, the groove depression is slightly shallower than the groove in the annealed can probably due to elastic rebound after passage of the forming wheel. The grooves in the annealed cans gave cross-sections showing little or no thinning and with dimensions closely duplicating the wheel head profile.

In the thinner parts of the non-annealed cans (14 mil or less) the metal cracked and parted while being grooved. A cross-section showing the initiation of a crack in a 14 mil specimen is shown in Figure 12 and the crack enlarged in Figure 13 (X150). Annealed cans show tearing at approximately half the above thickness at around 6 mil.

Cans plated from a sulfamate bath (A. J. Tuck Co., Brookfield, CT) were evenly formed at a thickness of 22-27 mils. However, they were extremely hard (~ Brinell 210) and showed ~20% thinning in the grooving operation (Fig. 14). After annealing at 800° under N_2-H_2 the cans became quite soft (~ Brinell 70). This material grooved easily and became very rigid as a result of the grooving operation (Fig. 15). This rigidity is due to the combined effect of the groove shape and workhardening of the metal.

During the grooving studies reported above, it was found that annealed cans could be grooved evenly using moderate pressure from the forming wheel. Two cross-sections of the grooves produced are compared to the profile of the forming wheel used, see Figures 16 and 17. The annealed nickel matches the shape of the forming wheel (Fig. 17) better than the unannealed nickel (Fig. 16). This duplication of profile allows the generation of the different possible corrugated seal types based on forming wheel shape.

Experimentation as illustrated above showed the relationship between metal properties, grooving wheel configuration and groove shape and dimension. Annealed nickel from sulfamate plating baths appears to be a suitable substrate.

2.3.2.2 Sealing of Cylinder Sections

After establishing the response of the metal to the varying grooving processes we investigated simulated seals using concentric cylinders. To form the cylinders, two pieces of commercially annealed 0.021" nickel (representative lengths: 11.80" and 12.20") gave cylinders of appropriate diameters to have approximately 0.040" of gap between the cylinders when the smaller one is nested in the larger. The ends of the sheet were joined by spot welding 1/2" strips of 0.005" nickel over the

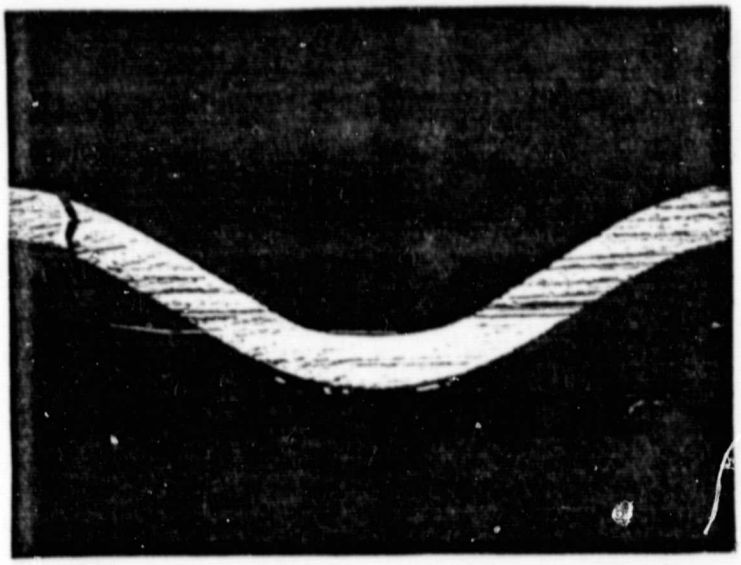

Fig. 12

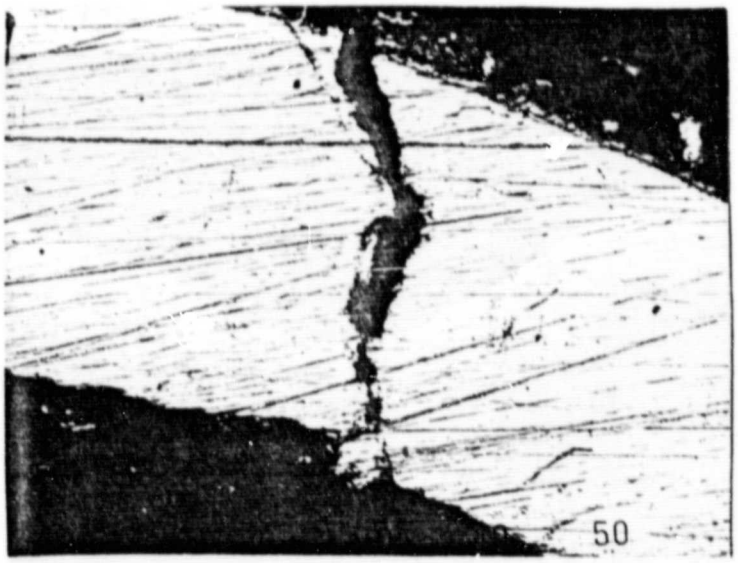

Fig. 13

Crack in grooved can from a Watts plating bath (top X20, bottom X150).

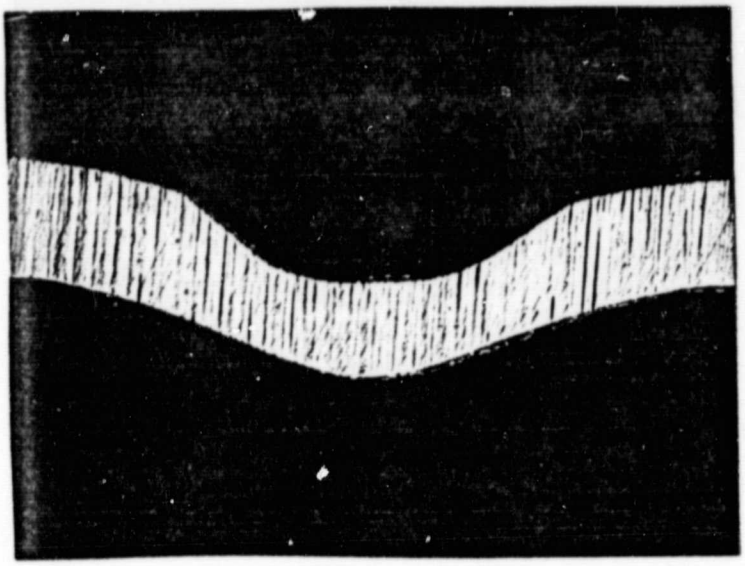

Fig. 14

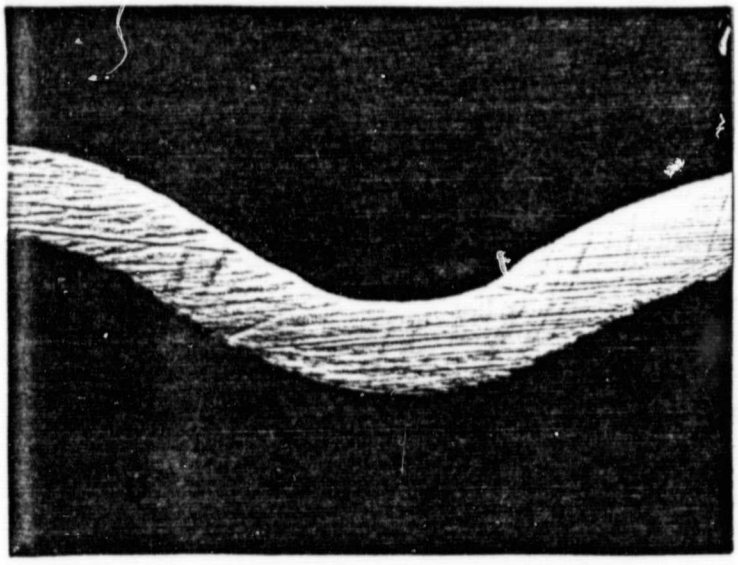

Fig. 15

Cross-sections of swaged cans plated from a sulfamate bath (X20).

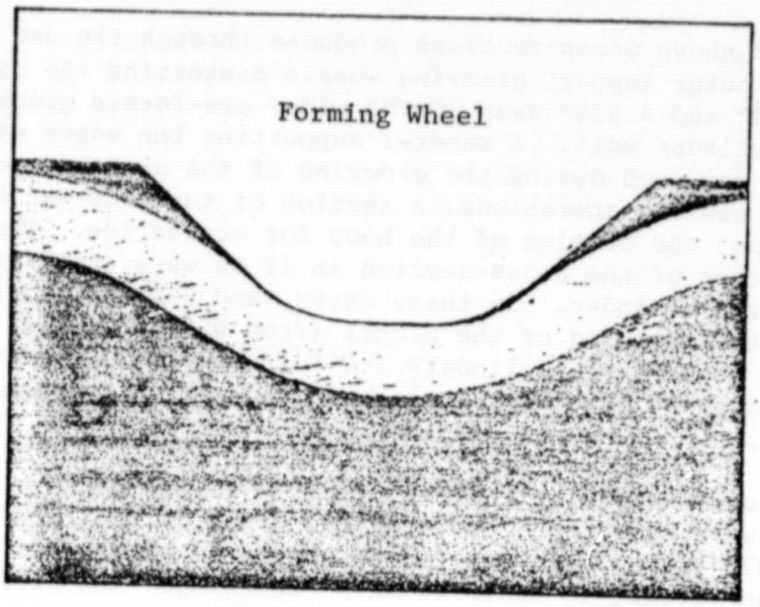

Fig. 16

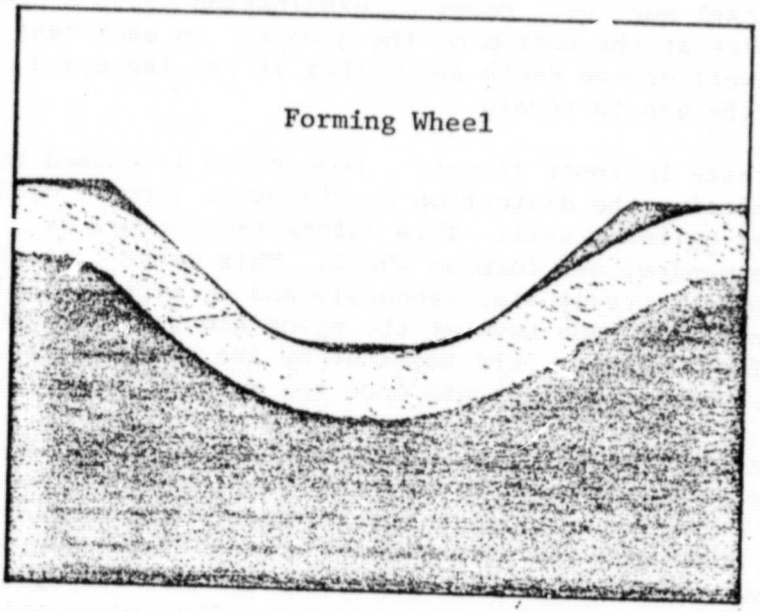

Fig. 17

Cross-sections of grooves in 18 mil nickel (Figs. 10 and 11). Mated with grooving wheel profile.

seam. Figure 18 shows cross-sections produced through the use of 0.040" and 0.050" deep outer (upper) grooving wheels distorting the nylon insulator into 0.040" and 0.035" deep (0.20" wide) pre-formed grooves in the inner (lower) cylinder wall. A mandrel supporting the edges of the inner (lower) grooves was used during the grooving of the outer (upper) cylinder wall. After the sealing operations, a section of the hoop was cast in epoxy before cutting out the section of the hoop for evaluation. The objective was the examination of the cross-section as if it were still subject to the hoop stress of the cylinder. In these cases, and especially the case shown in Figure 18b, the thinning of the nickel (from 0.021" to 0.015") combined with excess gap between the cylinders (~0.010" greater the insulator thickness) allows the nylon insulator to escape compression between the can walls.

To overcome these difficulties, forming wheels capable of making deeper grooves were made. Due to increased depth of the forming wheel head (0.060" and 0.070"), the head was formed with a larger radius (from 0.040" to 0.050") in an attempt to minimize metal thinning. The outer grooving operation was again done over an inner mandrel for support.

Figure 19 shows the cross-section of seals produced using the deeper grooving wheels. These seals are improved with the cross-section in Figure 19b showing a gap of less than 3 mils between the nylon insulator and in inner (lower) nickel surface. However, examination shows a new cause for lack of compression at the bottom of the groove. In each case measurement of the inner (lower) groove depth shows that it has increased and that this increase allows the gap to remain.

This increase in inner (lower) groove depth is caused by the nylon insulator transmitting the distortion in the outer (upper) cylinder wall to the inner (lower) cylinder wall. This deformation occurs as the cylinders pass between the mandrel and forming wheel. This means that the inner and outer groove depths increase simultaneously and by approximately like amounts once contact is made between the nylon and inner cylinder surface. Because the surfaces are not held together by the hoop stresses in the cylinders, the surfaces can separate once the forming wheel has passed.

To better simulate the actual sealing procedure, cylinders (2.5" high) were fabricated, nested, and mounted (separated by a nylon insulator) in shallow (~1/4"), close-fitting wells (fitted to the outside diameter) attached to the headstock and tailstock of a lathe. The deeper forming wheels (0.060" and 0.070") were then used to form the corrugated seal between the cylinders using no internal support. The cross-sections of such seals are shown in Figure 20.

These cross-sections show no increase in inner (lower) groove depth. The outer (upper) grooves are nearly as deep as observed previously with the 0.060" and 0.070" deep forming wheels (0.050" instead of 0.055" for the

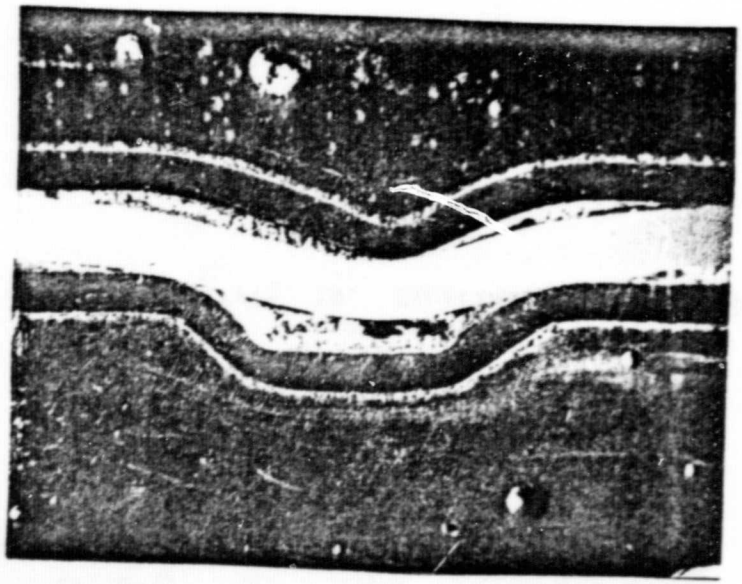

a. 40 mil deep outer wheel
40 mil deep inner wheel (0.20" wide)

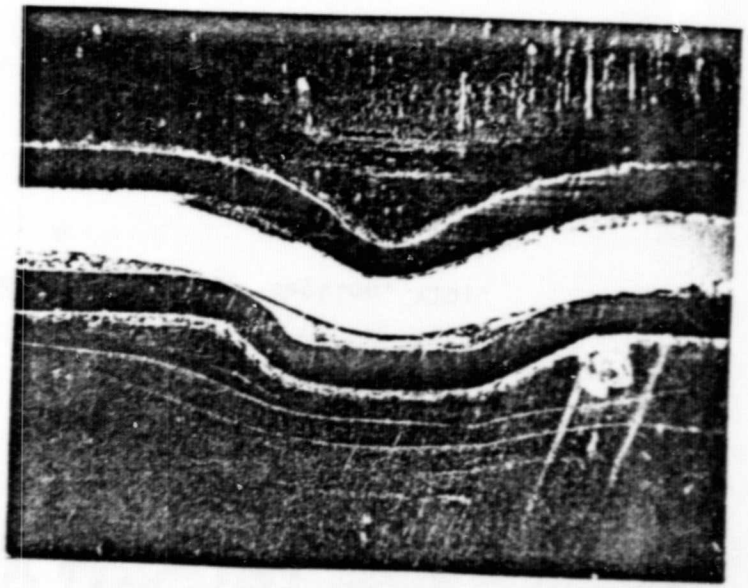

b. 50 mil deep outer wheel
35 mil deep inner wheel (0.20" wide)

Fig. 18. Experimental seals in nickel cylinders (cross-section, X10).

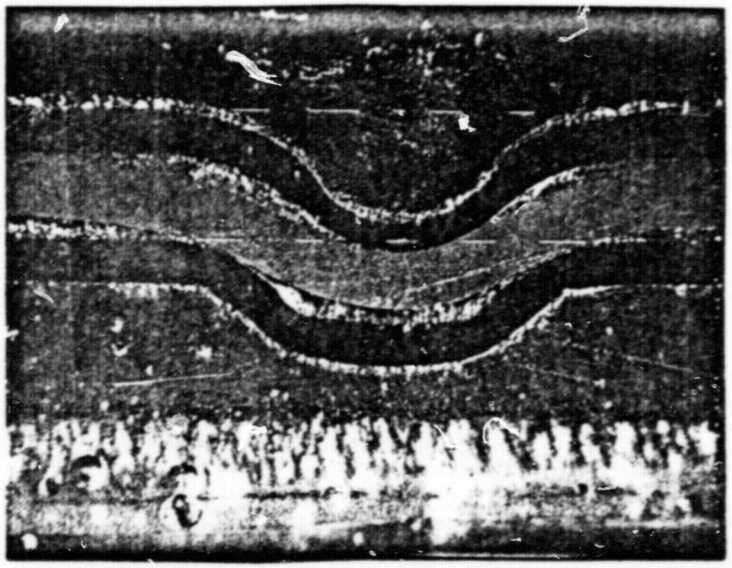

a. 60 mil deep outer wheel
35 mil deep inner wheel (0.20" wide)

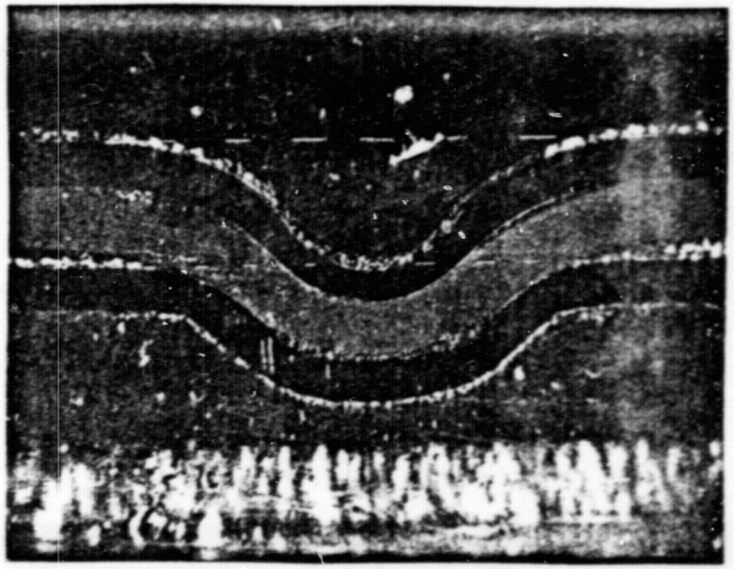

b. 70 mil deep outer wheel
35 mil deep inner wheel (0.20" wide)

Fig. 19. Experimental seals using deeper grooves (cross-section, X10).

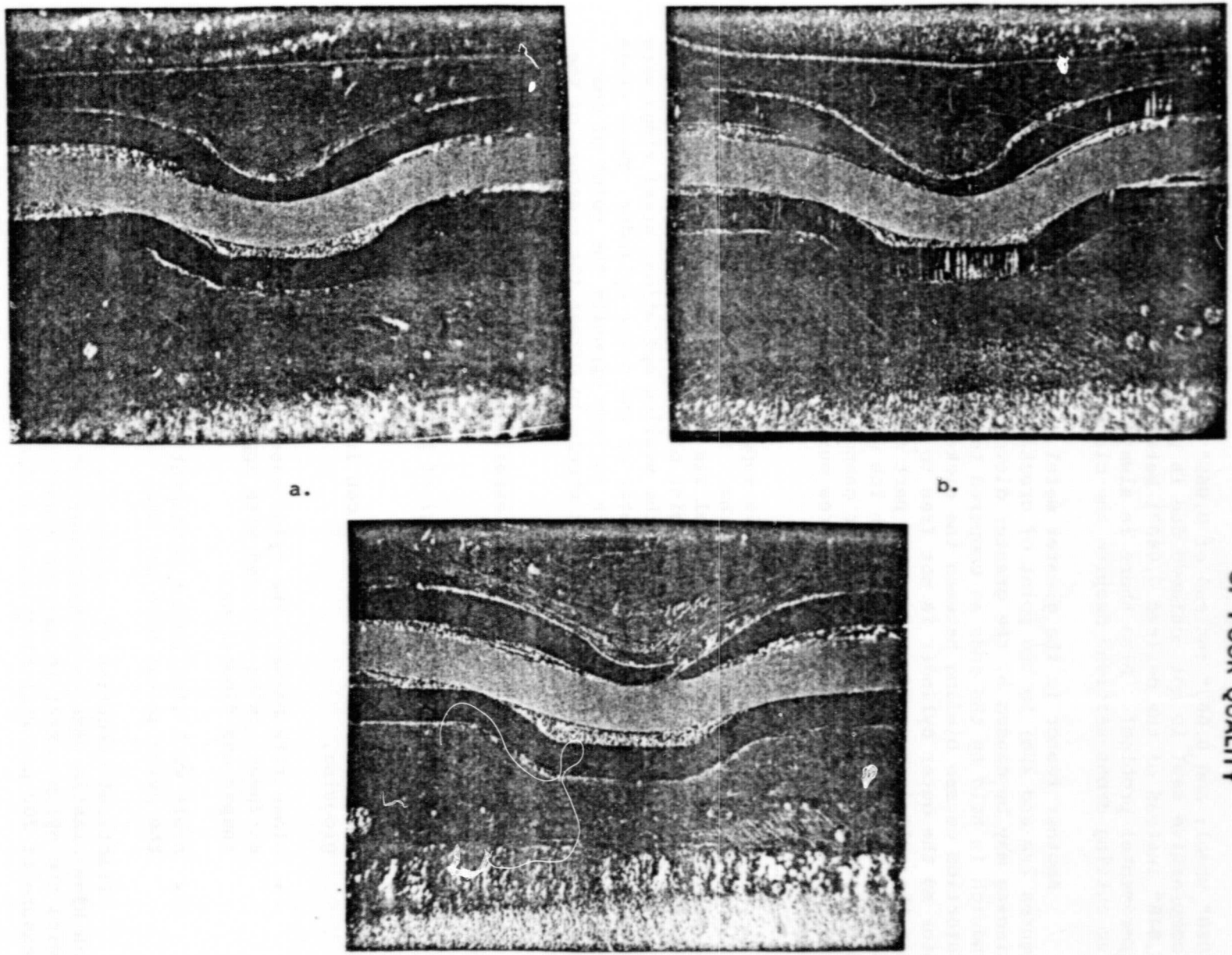

a.

b.

c.

Fig. 20. Experimental seal formed without internal support (cross-section, X10).

0.060" wheel; and 0.060" instead of 0.065" for the 0.070" wheel). However, a compressive seal is not achieved due in part to an apparent oversized gap (0.048" instead of the desired 0.040") between the nickel cylinders (an experimental problem). Also there is always some relaxation of tension when cutting cross-sections despite the clamping and epoxy mounting.

Another factor is the greater metal thinning (0.021" to 0.009", see Figures 20a and 20b) to the point of cracking (Fig. 20c). This greater thinning may be caused by the greater distortion caused when the cylinder sandwich is held by the ends as compared to grooving over a mandrel. This distortion causes binding between the nickel cylinders and the nylon insulator so the outer cylinder is not free to slide over the nylon surface. When the cylinders are free to move, part of the material used to make up the increased surface are required in the groove comes from a decrease in the cylinder length. If the cylinder cannot provide the material by moving into the groove, then the increased area must be formed at the expense of metal thinning.

Outer grooves can be made while supporting the outer seal package by its ends in supports mounted in a lathe. However, a severe distortion of the seal package by the grooving wheel was noted during the grooving operation and thinning of the Ni to the point of cracking was observed. To better support the seal package during the sealing operation, steel rings were made that closely fit the outer diameter of the outer cylinder. These rings hold the cylinders round and provide a surface opposite the point of contact of the forming wheel for support wheels to offset the pressure of the forming wheel (see Fig. 21).

A critical examination of our experimental results has shown the following:

- localized swaging (grooving) of both inner and outer cell surfaces is feasible,
- form stability of the cell can increases greatly with grooving,
- close fits between the nylon gasket and the two cell surfaces can be achieved with appropriate groove tool shapes and dimensions,
- seals with significant permanent compressive force on the nylon gasket have not been realized.

Practical execution of compressive seals with a gasket material of such high elastic modulus as nylon may not be possible. For example, assuming the nylon gasket to have an elastic modulus of 5×10^5 psi, a radial pressure of 200 psi will elastically deform the 30 mil insulator only about

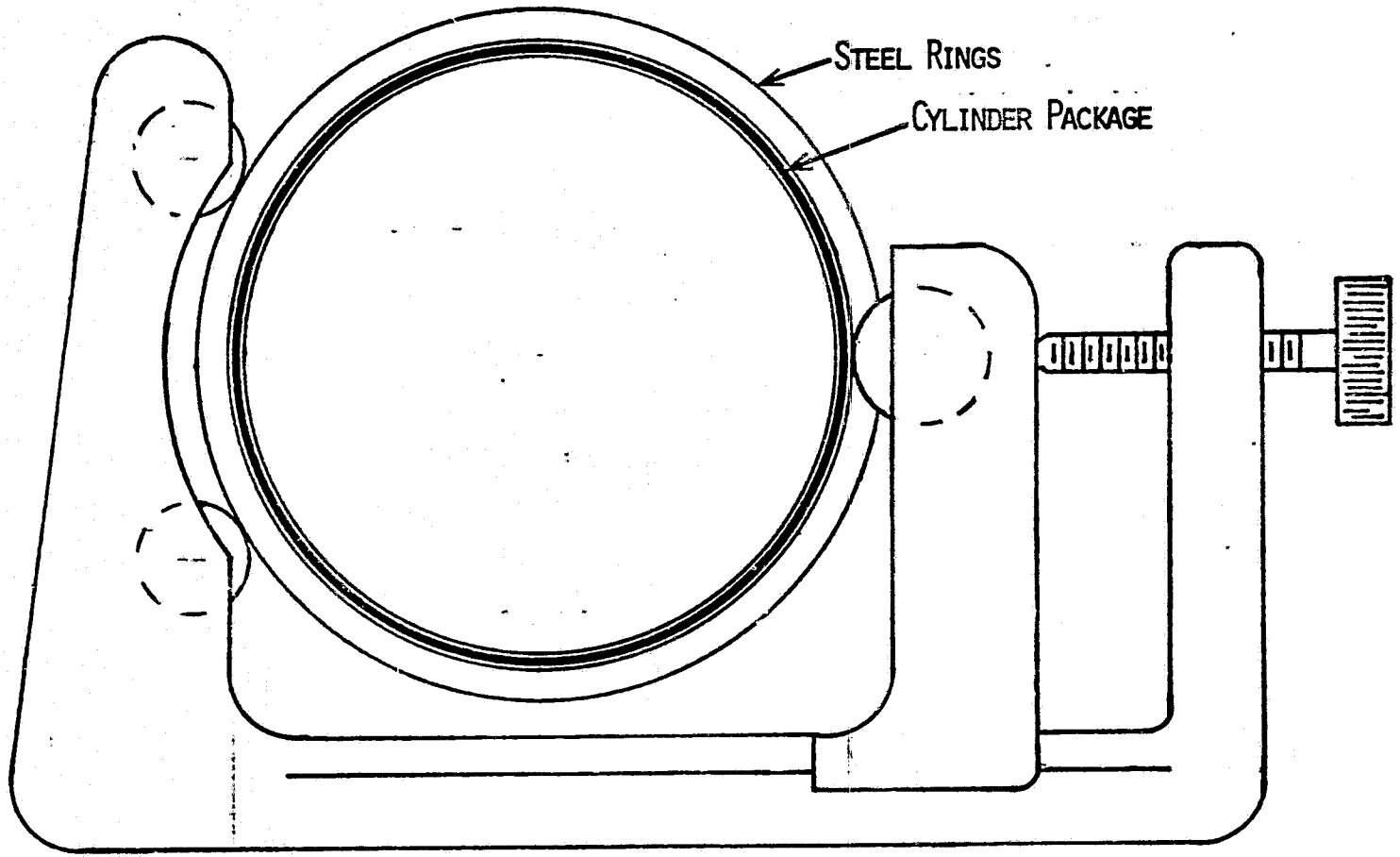

Fig. 21. End view of outer seal formation.

0.012 mil. This means the slight relaxation of the two can walls removes the compressive force from the gasket. To prevent such a small relaxation is particularly difficult in the formation of the outer seal involving plastic deformation of the nickel by compression. Even tightly fitting retaining rings allow a significant amount of can flattening in the area of forming wheel. We therefore investigated also the use of a rubber type gasket instead of nylon. Chemical and thermal stability are additional selection criteria.

To evaluate the ability of elastomers and ethylene-propylene rubber (EPR) in particular to create satisfactory seals, test seals were made as previously with nylon. For example, a cylinder of EPR was fabricated and placed between nickel cylinders. The inner cylinder was pregrooved to 0.030" and 0.040" depth and a portion was not grooved. The outer cylinder was grooved through rubber into the inner grooves and over a portion of the surface without grooves. A cross-section was potted in epoxy, cut from the seal package, polished, and photographed (X10), see Figures 22, 23 and 24.

Figure 22 shows a sealing attempt over a 0.040" deep inner groove. The rubber is under compression on the side of the groove but not on the bottom. This is a result of a slight error (0.10") in outer groove placement. It appears that if the outer grooves were correctly positioned, the outer groove could have been made deeper allowing a compression bottom seal. This indicates that wider bottom grooves might be used in forming the bottom seal in order to compensate for such errors.

Figure 23 shows a seal made over a shallower and wider inner groove (0.030" deep, ~0.150 wide) giving two apparent points of compression (~10% compression on the left side and bottom) implying the existence of a good seal. Figure 24 shows a seal made over a previously ungrooved portion of inner can. The EPR is compressed ~25% and the inner can surface has been grooved to a depth of 0.010". This compressed EPR appears to be a very good seal.

2.3.2.3 Sealing of Cylindrical Cans

Nylon Seal: Nickel cans with ~3.9" diameters were fabricated from nickel 200 sheet and sealed together using a nylon insulator. This seal contained one very small leak and was tested to 25 psi pressure. The leak in the seal was sufficiently small as to allow the use of this container in evaluating the effects of variations in pressure and higher pressure on the seal.

The container was pressurized under water to 50 psi. The ends of the can rounded slightly but no other effects of the pressure were apparent. The pressure was released and container was connected to a vacuum pump. After evacuation the container was repressurized. During five such pressure-vacuum cycles no change in the quality of the seal was observed. Finally

Fig. 23

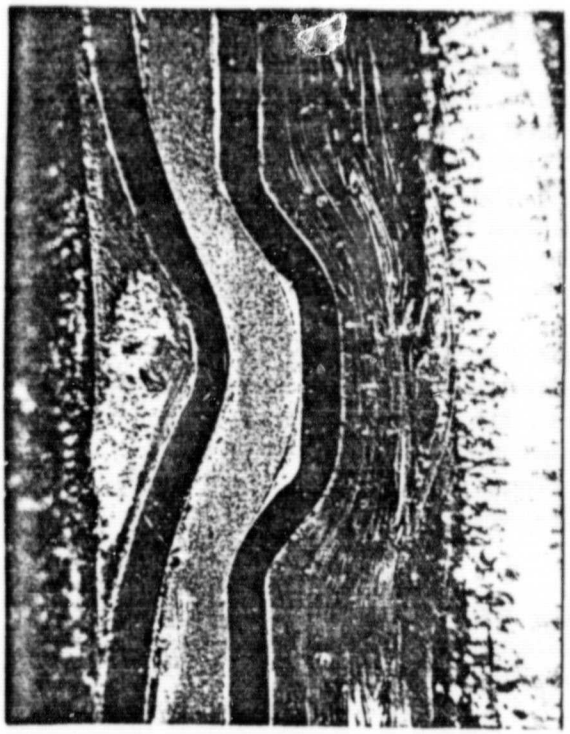

Fig. 22

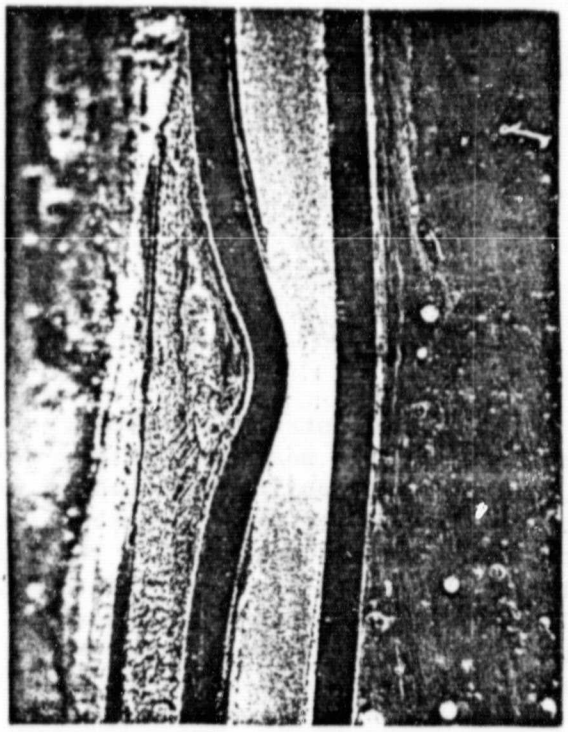

Fig. 24

Cross-sections of EPR seals (X10).

the container was pressurized to 100 psi, and cycled between 50 and 100 psi with the seal showing no change in quality. Inner seals were evaluated in the same manner.

Cans were constructed with the diameter of each corresponding to the inner cylinder diameter of each of the toroidal cell halves. These were nested inside one another (separated by a nylon insulator) so that the bottom of each was at the same end of the nested cylinders (see Fig. 25 below).

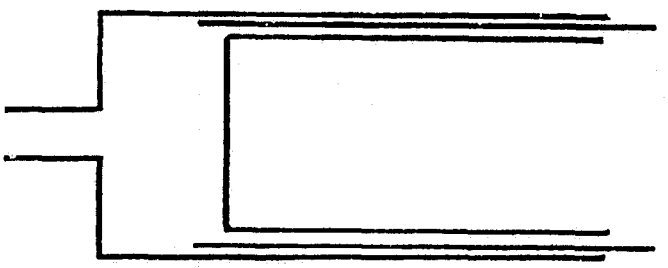

Fig. 25. Cross-section of inner seal test package.

This construction allows a seal to be formed from the inner surface as necessary in sealing the toroidal cell. The outer can was fitted with a gas inlet for testing the seal by pressurizing the space between the ends of the cans. The seal formation sequence involved pregrooving of the outer cylinder of the inner seal. The insulator and inner cylinder are then inserted and the inner cylinder is grooved using the inner grooving tool. This tool contains a grooving wheel which is forced out and into the inner cylinder by an asymmetric cam while the circularity of the cylinder is maintained by bushings on the tool (see Fig. 26).

Inner seal cylinders were sealed and pressure tested. Two grooves created a nearly complete seal when tested to 25 psi. Immersion in water revealed a slight leak (~1 ml/min) between the nylon insulator and the inner can. After reswaging the leak rate actually increased. The reason could be traced to surface irregularities (formed during cylinder construction) which were transmitted through the gasket to the outer cylinder wall.

Elastomer Seals: To evaluate the outer sealing technique, two simple electroformed nickel cans (sulfamate bath) were sealed into a container using a Neoprene seal. The cans have inside diameters of

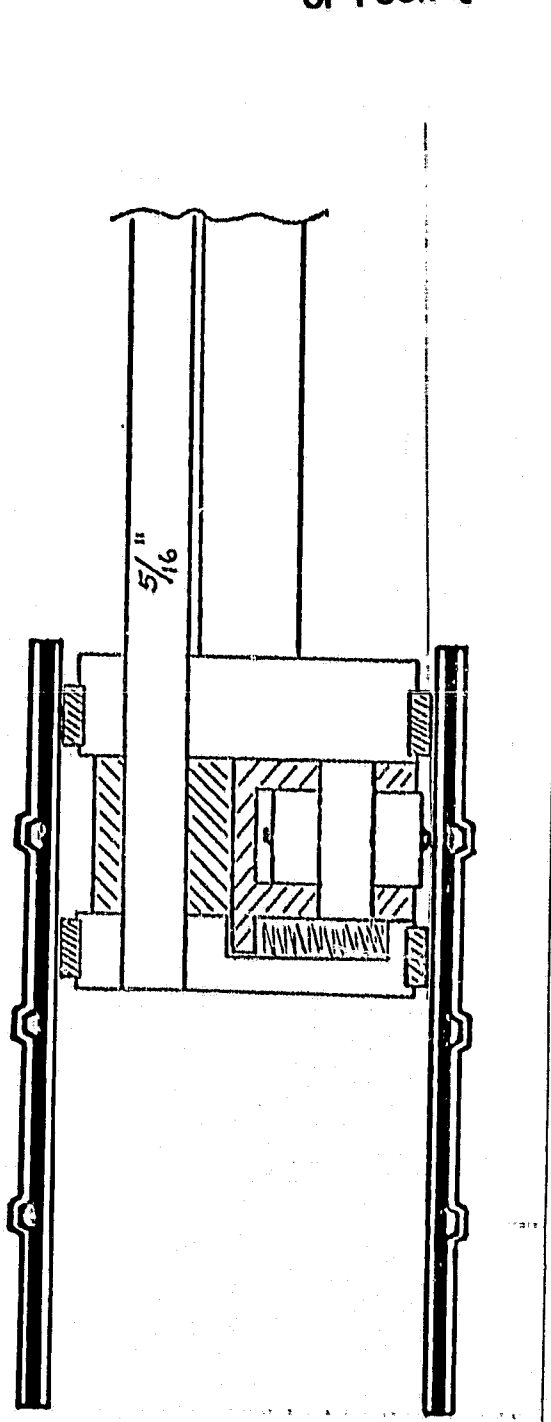

Fig. 26. Cross-section of inner sealing tool inside inner seal package.

4.50" and 4.62", walls of ~0.026" thickness, and heights of 3.38" and 3.75" respectively. The inner can had been machined to an even wall of 0.025-0.027" which leaves a gap between the can walls, when nested one within the other, of ~0.034". Both cans had been annealed. A Neoprene insulator was constructed from 0.030" Neoprene sheet. The inner can was pregrooved at 0.5" intervals to a depth of 0.030" over a 0.25" mandrel, fitted with the Neoprene insulator, and fitted into the outer can. A single sealing groove was made. The sealing groove was ~0.50" deep with a 0.050" radius.

The seal made by the single band of compression was tested by pressuring the container to 10 psi under water. No leaks were apparent. For three days the sealed container showed no pressure drop. The container was then tested to 25 psi and cycled five times between 25 psi pressure and a vacuum with no leaks apparent.

To further test the sealing procedure, two additional sealing grooves were added and the pressure raised to 50 psi giving a 0.22" bulge in can bottom. Again the container was cycled five times between pressure (50 psi) and vacuum while maintaining a complete seal. The container was then pressurized to 100 psi with no leaks or wall deformation (bulging in the bottom to 0.36" measured after pressure release). The desired seal is achieved. The sealed container is shown in Figure 27.

2.2.3 Discussion and Conclusion

In the preceeding sections we have shown that localized swaging (grooving) of inner and outer toroid surfaces can be carried out and leads to strong interlocking closures. The groove shape depends on the configuration and dimensions of the grooving wheel and also on the metal properties of the cans to be deformed. Soft annealed nickel for example follows very closely the grooving tool shape. Hardened metal cans show less accurate shape reproduction, more spring back and ultimately tearing and cracking. The number and nature of the sealing contacts depends on the relative shape and depth of the two grooves, the pregroove and the final closure groove. Pregrooving is essential at least on the outer can wall to obtain sufficient can rigidity.

To achieve not only a strong closure but a hermetic seal with a nylon insulator is more difficult and even though possible, probably not feasible in practice. To maintain the necessary compression uniformly over the whole seal with a gasket material of such high elastic compressibility requires extremely close process control. For example, tightly fitting inner and outer guide rings are essential to prevent can eccentricity during the swaging process. Also a very smooth surface finish on both metal surfaces facing the nylon insulator is necessary. To force the nylon gas-

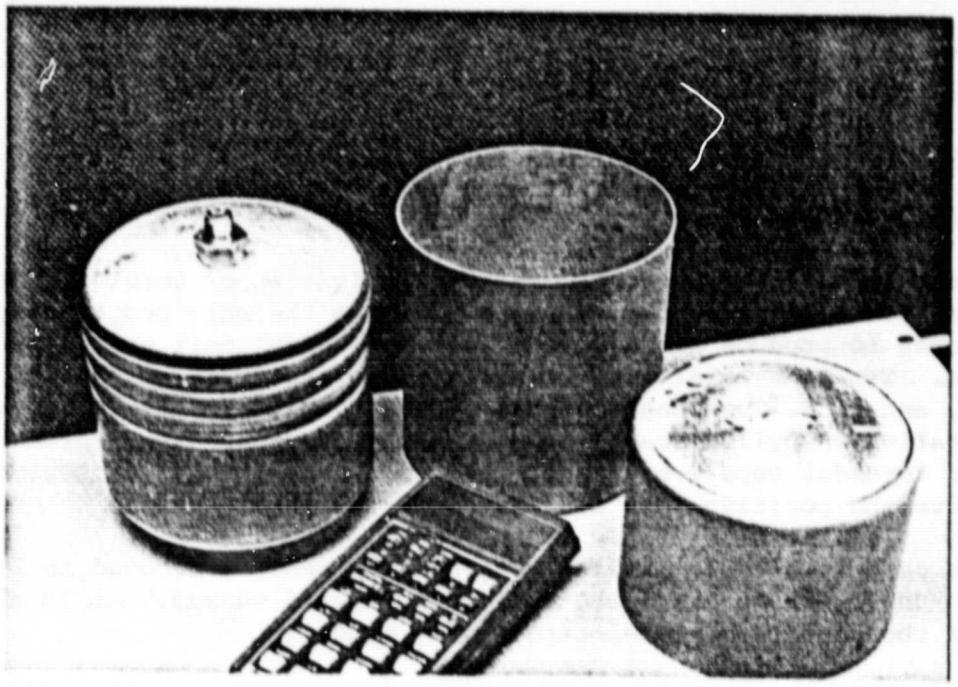

Fig. 27. Sealed electroformed container with unassembled parts.

ket, which is quite hard, into small scratches requires more force than can be tolerated especially by the outer cylinder wall. This problem can be overcome by the use of a more resilient gasket material, e.g., various elastometric insulators.

In summary, hermetic and strong closure seals can be achieved by local swaging of grooves using elastomeric insulators.

3. Prototype Cell Construction

3.1 Cell Cans

Various processes for the possible fabrication of toroidal cell cans were reviewed. Electroforming was identified as the only practically feasible process to produce small quantities of toroidal cell parts as integral units. Two commercial vendors were identified (Optical Radiation Co., Azusa, CA, and A. J. Tuck Engineering, Brookfield, CT). After initial experimentation on cylindrical electroformed components (see Section 2.3) orders for toroidal cups wre placed. The configuration and dimensions of the negative and positive cups are shown in Figures 28 and 29.

The cans have 0.020" walls. The can bottoms are grooved to lessen distortion under pressure and the walls are tapered ~1 mil/inch to allow removal of the cans from the electroforming mandrel.

Externally the cans appeared acceptable showing, however, some surface roughness and pitting. The uniformity was less than desired. Typical measurements are summarized in Table 2 and Figure 30 shows an overall view of the cans. After formation the cans were very hard (172 Bhn). After annealing (800°C, 5% H_2 in Ar) they became very soft (78 Bhn) yet cracked easily when deformed. From literature information and conversations with other electroplaters we concluded that sulfur inclusions were probably responsible for the brittleness. Frederick Lowenheim states in Modern Electroplating that the presence of sulfur in excess of 0.002% results in embrittlement when the temperature of the nickel electroplate is raised above 500°F. If clean plating baths are used there should be no problem with the sulfur contamination.

It was hoped that the sulfur contamination might be a random problem affecting only a few cans and that the majority of the cans would be free of contaminants. Using a lower annealing temperature satisfactory working properties were obtained in an experimental can. This material was noticeably harder (108 Bhn) but could be grooved satisfactorily.

3.2 Electrode Core

The electrode core consisted of spirally wound nickel and cadmium electrodes (General Electric Co., Gainsville, FL) with non woven nylon

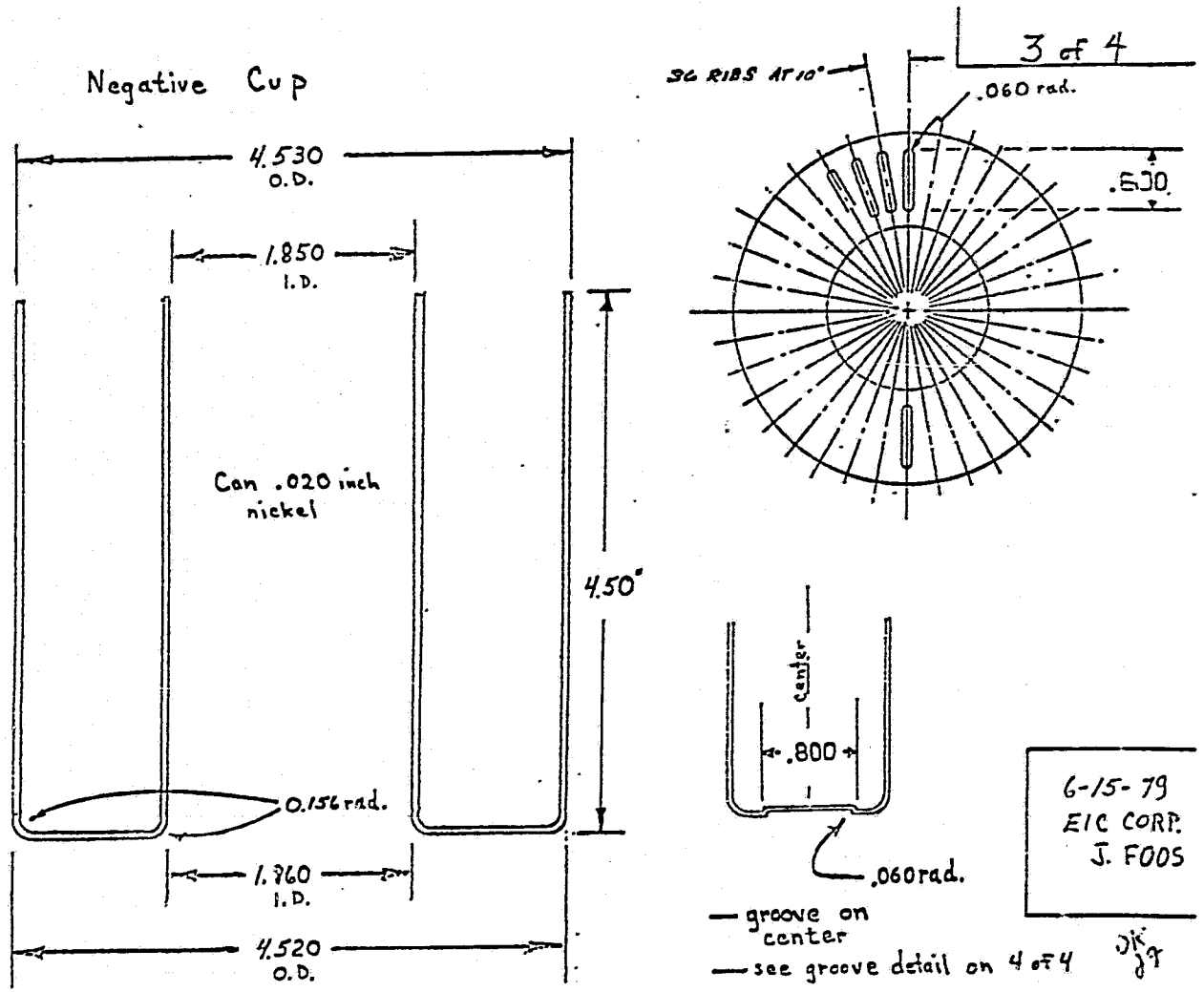

Fig. 28. Negative cup.

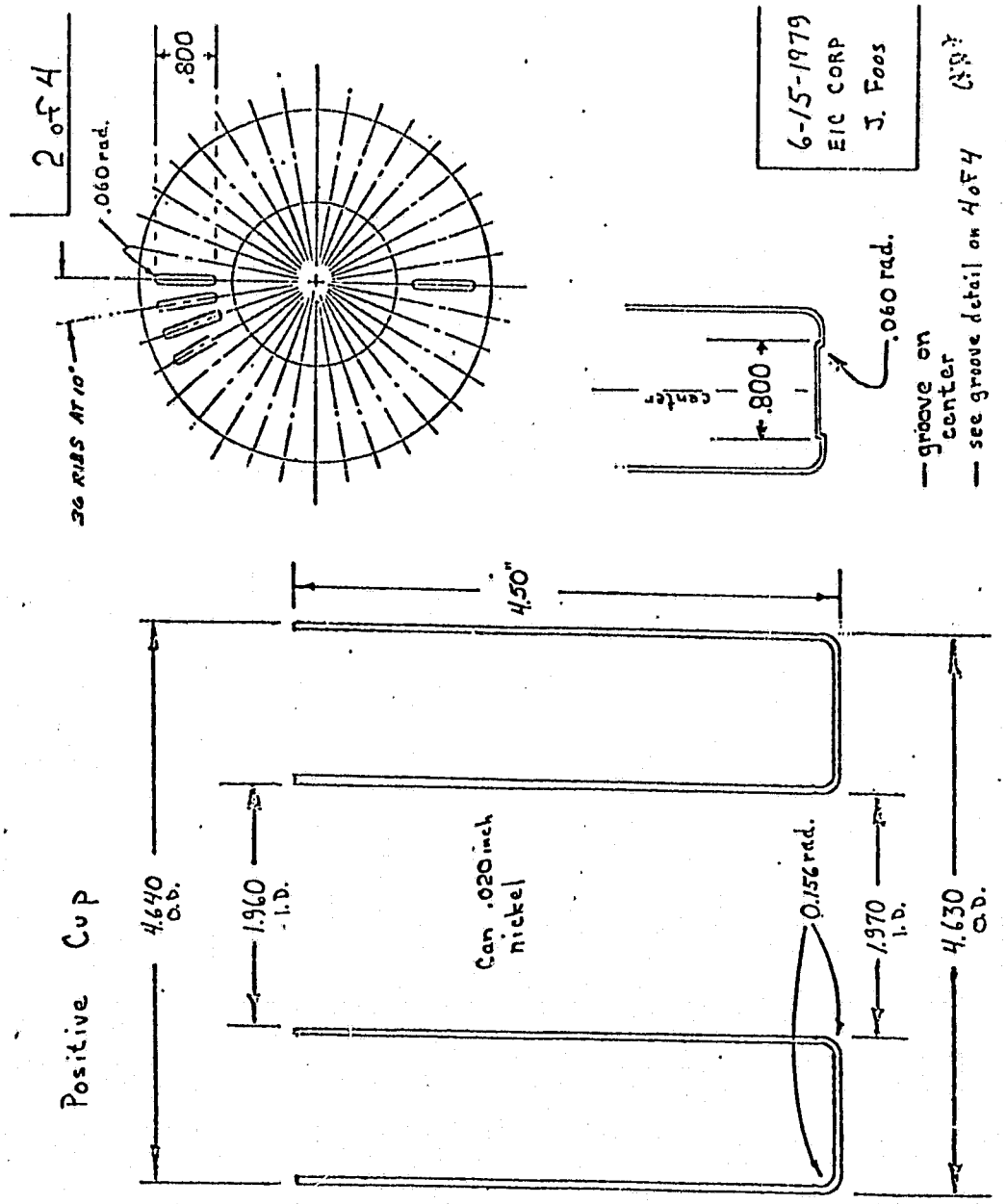

Fig. 29. Positive cup.

Table 2

Wall Thickness of Toroidal Cans in Thousandths of an Inch

	Inner Cylinder			Outer Cylinder		
Can	Bottom*	Middle	Top*	Bottom*	Middle	Top*
Positive 1	20	25	22	20	19	24
Negative 1	37	30	35	25	21	21
Positive 2	23	19	24	17	13	16
Negative 2	19	18	18	18	19	21
Positive 3	40	42	34	21	20	20
Negative 3	22	23	25	25	20	20

*Measured 0.5" from end.

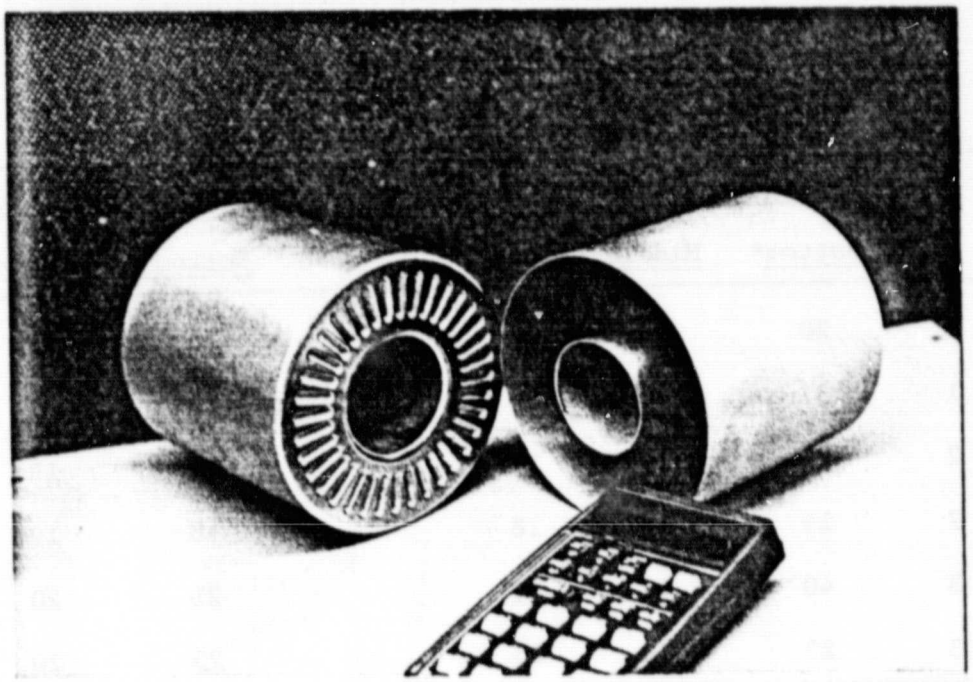

Fig. 30. Toroidal cans.

(Pellon 2505) separator. The electrode package was wound around an inner cylinder. Specifically, the core preparation involved the following steps:

- A cylinder (2.16" OD, 4.0" high) is formed from 0.021 nickel 200 sheet, using a welded seam, for use as the core winding mandrel. Four hardened nickel strips are welded inside and to one end of the cylinder so as to bow out in the middle. These are for making electrical contact with the positive can. This is placed on the expanding arbor of the core winding jig (Fig. 31).

- Strips of positive and negative electrode material are cut (4.5" wide x ~11' long) and strips of Pellon insulator are cut (5.0" wide x 12' long).

- The electrodes and Pellon are stacked with Pellon on the bottom, then the negative, Pellon again, then the positive on top. The package is placed in the winding fixture (Fig. 32).

- The positive is spot welded to the winding mandrel and the package wound until slightly less than 4.50" in diameter (tight fit in the negative cup).

- The electrodes are trimmed and ends of the spiral secured. The expanding arbor is removed from the fixture and the core removed from the arbor.

3.3 Swaged Cell Assembly

3.3.1 Can Preparation

In order to establish a proper electrolyte charge and to monitor cell pressure during cycle testing a fill tube was mounted into one of the cell halves. During welding of the fill tubes into the electroformed toroids we experienced severe cracking of the toroids along the perimeter of the weld. Variation of the weld conditions over a wide range did not prevent this complication. We decided therefore, in order that we may use the electroformed toroids with minimum risk, to install an O-ring sealed fill tube. This design is shown in Figure 33.

The cans were sized to dimensions and the sealing surfaces polished. Then the outer cylinder of the negative cup was pregrooved over 0.25 in. wide mandrel grooves, 0.030 in. deep using a lathe mounted grooving tool. Similarly the inner cylinder of the positive cup was also pregrooved over 0.25 in. wide mandrel grooves, 0.030 in. deep (Fig. 34) using an inside pregrooving tool (Fig. 35). Pregrooved cans and insulators are shown in Figure 36.

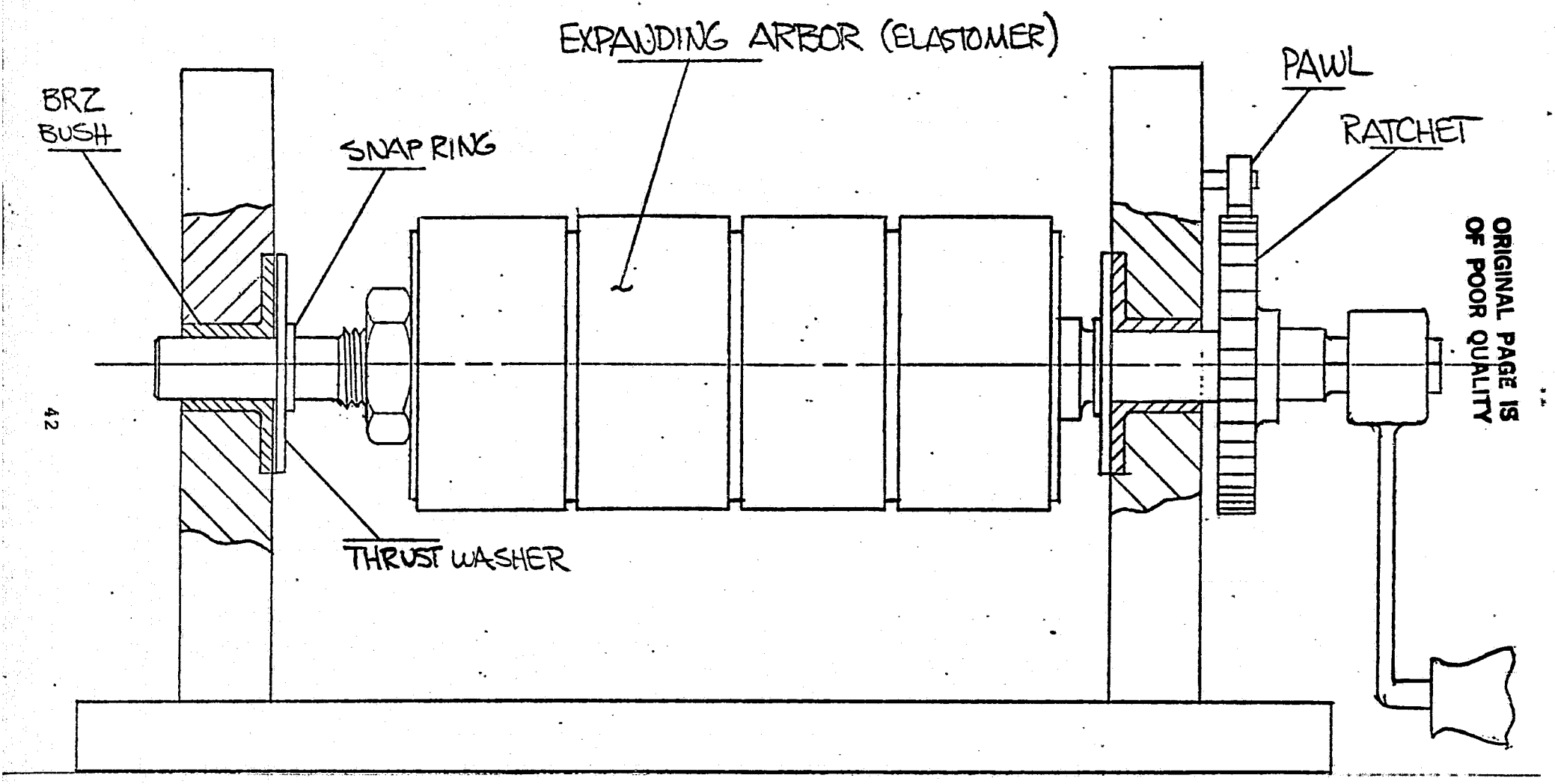

Fig. 31. Core winding jig.

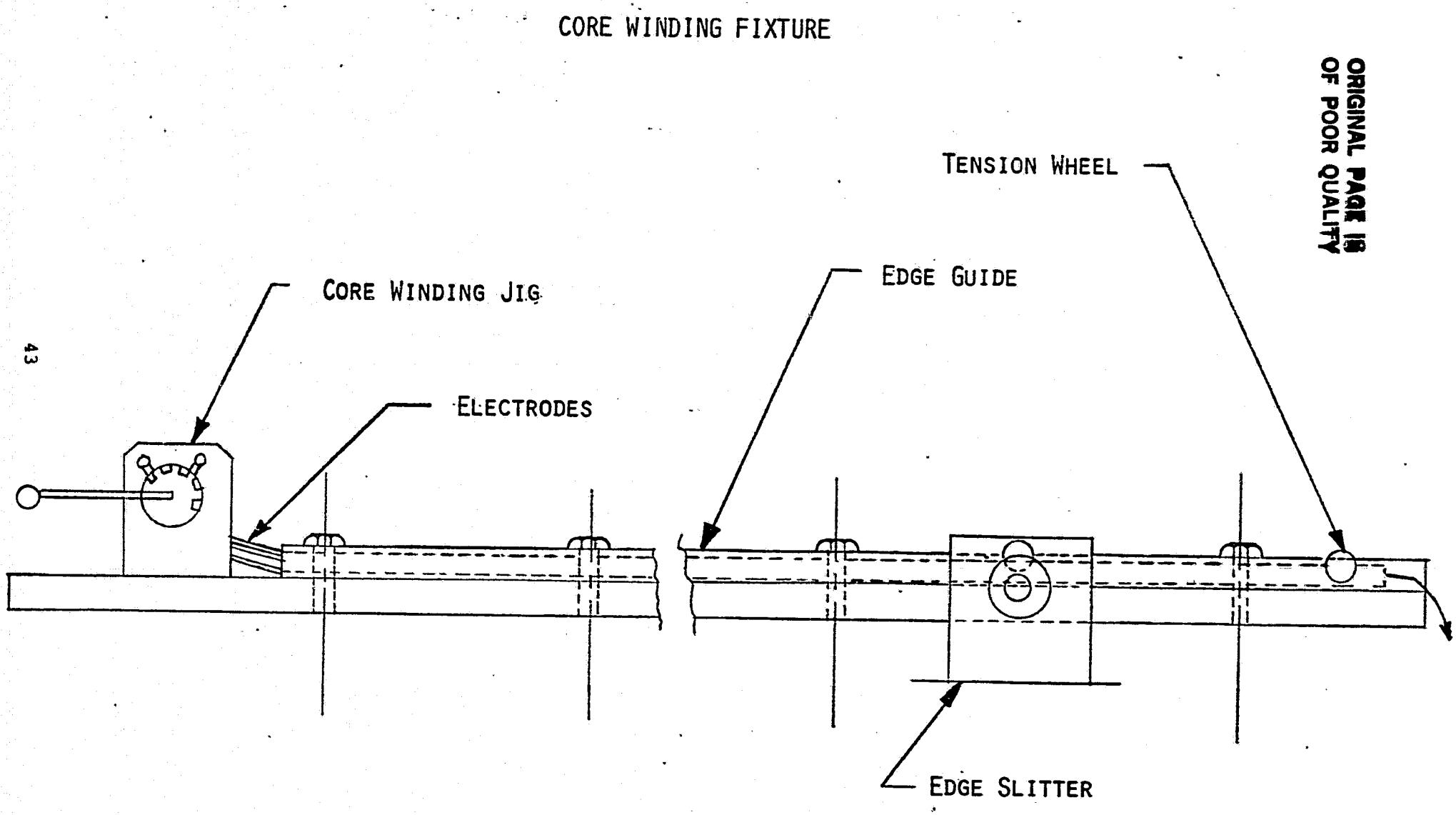

Fig. 32. Electrode winding fixture.

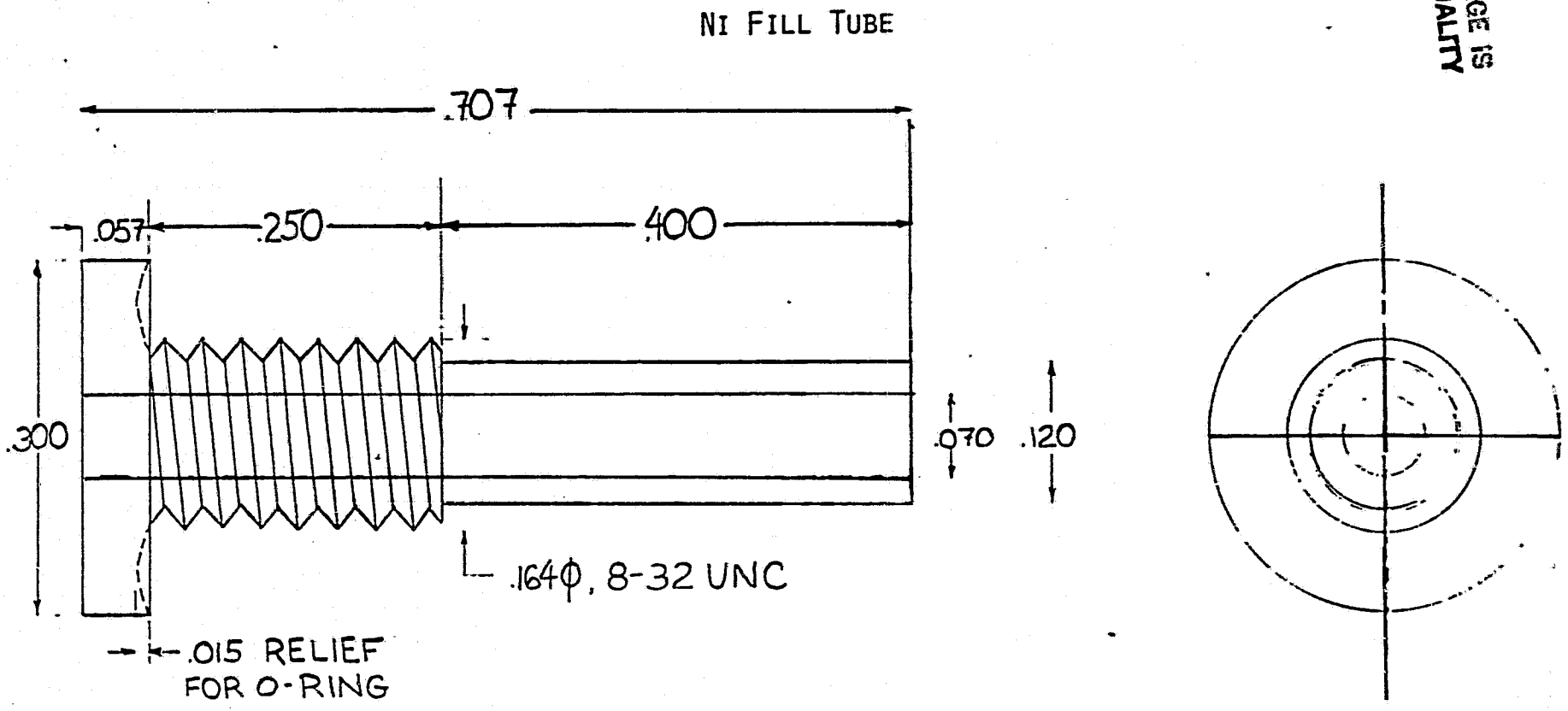

Fig. 33. Threaded type fill tube.

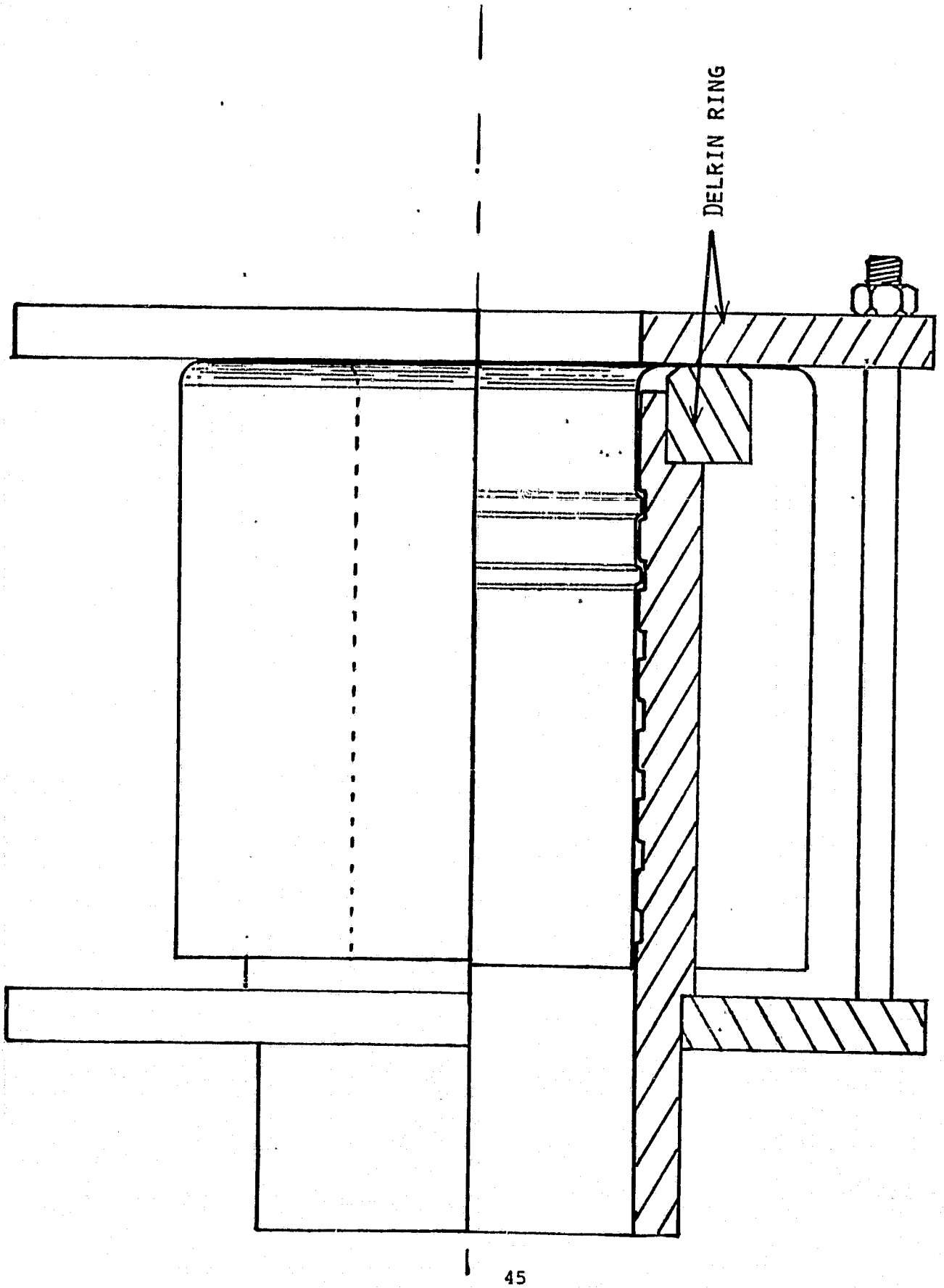

Fig. 34. Inner grooving mandrel holding positive cup (quarter section).

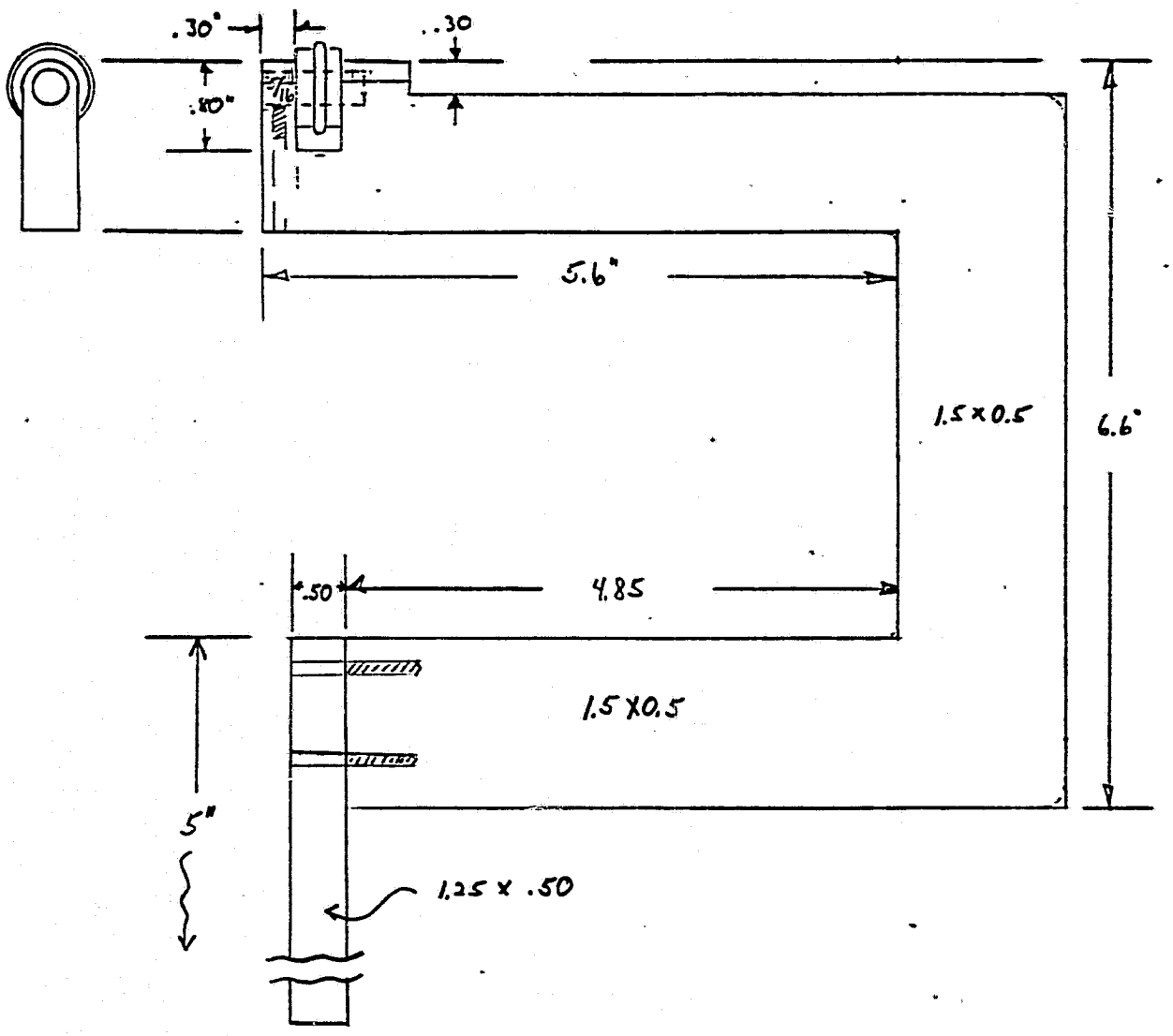

Fig. 35. Inside grooving wheel holder.

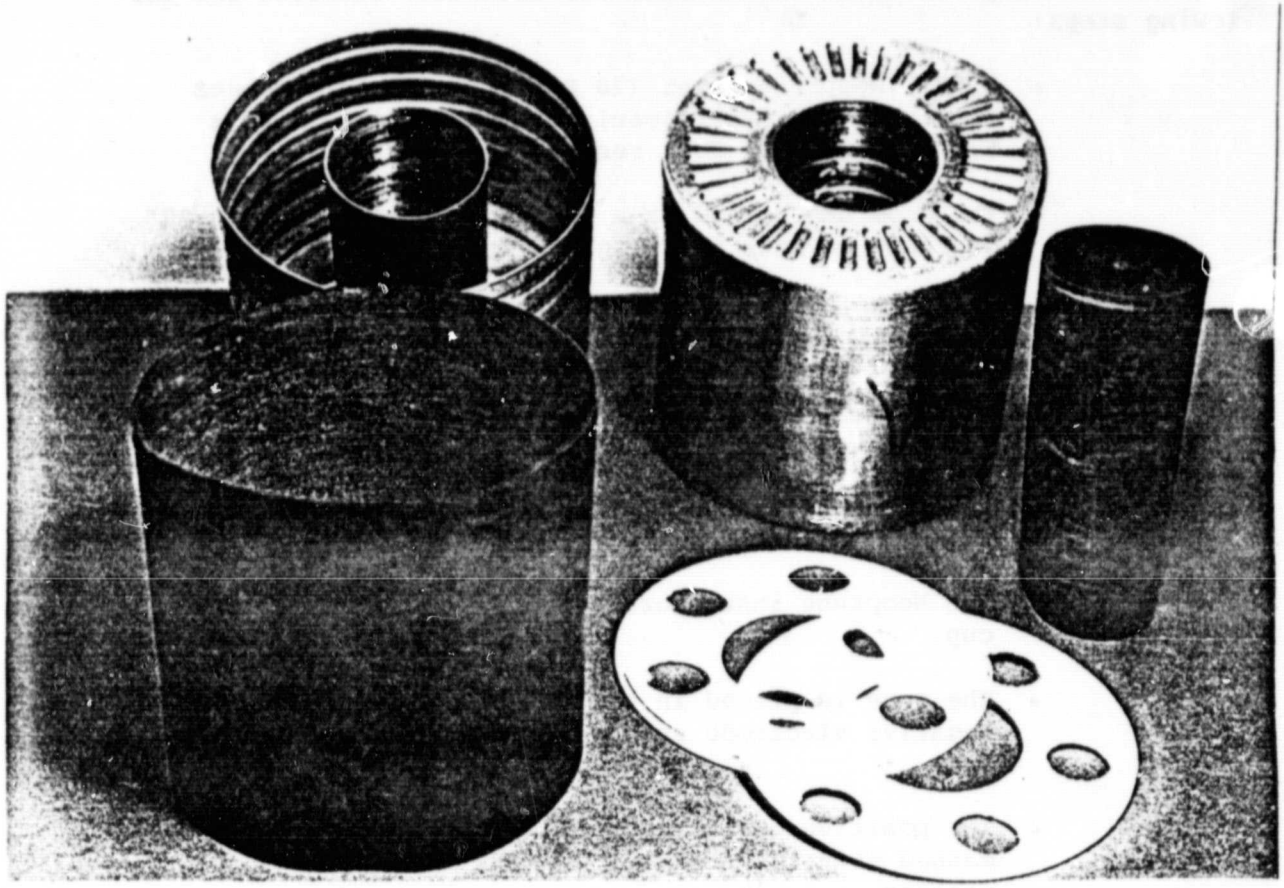

Fig. 36. Neoprene and nylon insulators - swaged cell.

3.3.2 Insulator

Preparation of the elastomeric insulator involved the following steps:

- 0.031" Neoprene sheet (70 Duro) is cut into sheets for inner and outer insulator fabrication, 6.2" x 6.0" and 14.3" x 6.0" respectively.
- The ends are joined in a lapped, adhesive seal (0.30" overlap) to make 6.0" high cylinders.
- After curing, the seal area is smoothed using a small sanding drum and cylinders trimmed to 4.5".

3.3.3 Cell Assembly

- A spacer fabricated from 1/8" nylon sheet is placed in the negative cup. This insulates the core edges from the cup bottom.
- The Neoprene insulators are placed on the negative cup.
- The core is placed in the negative cup and the negative electrode spot welded to the edge of the cup.
- The positive cup (along with the nylon spacer) is meshed with the negative cup containing the cell package.
- The package is fitted with support rings and mounted in a sealing support (Fig. 37) while the outer surface is grooved into the preformed inner grooves using the outer sealing tool.
- The seal on the inside surface is formed using the inner sealing tool while the cell package is supported in the sealing support (Fig. 38).

4. Prototype Cell Evaluation

We were able to completely assemble two toroidal Ni/Cd cells despite the poor quality of the electroformed cell cans. The main problem consisted of brittle fracture during grooving. The completed cells were leak tested with pressurized argon. Despite occasional cracking along some groove sections no leaks were found along either the inner or

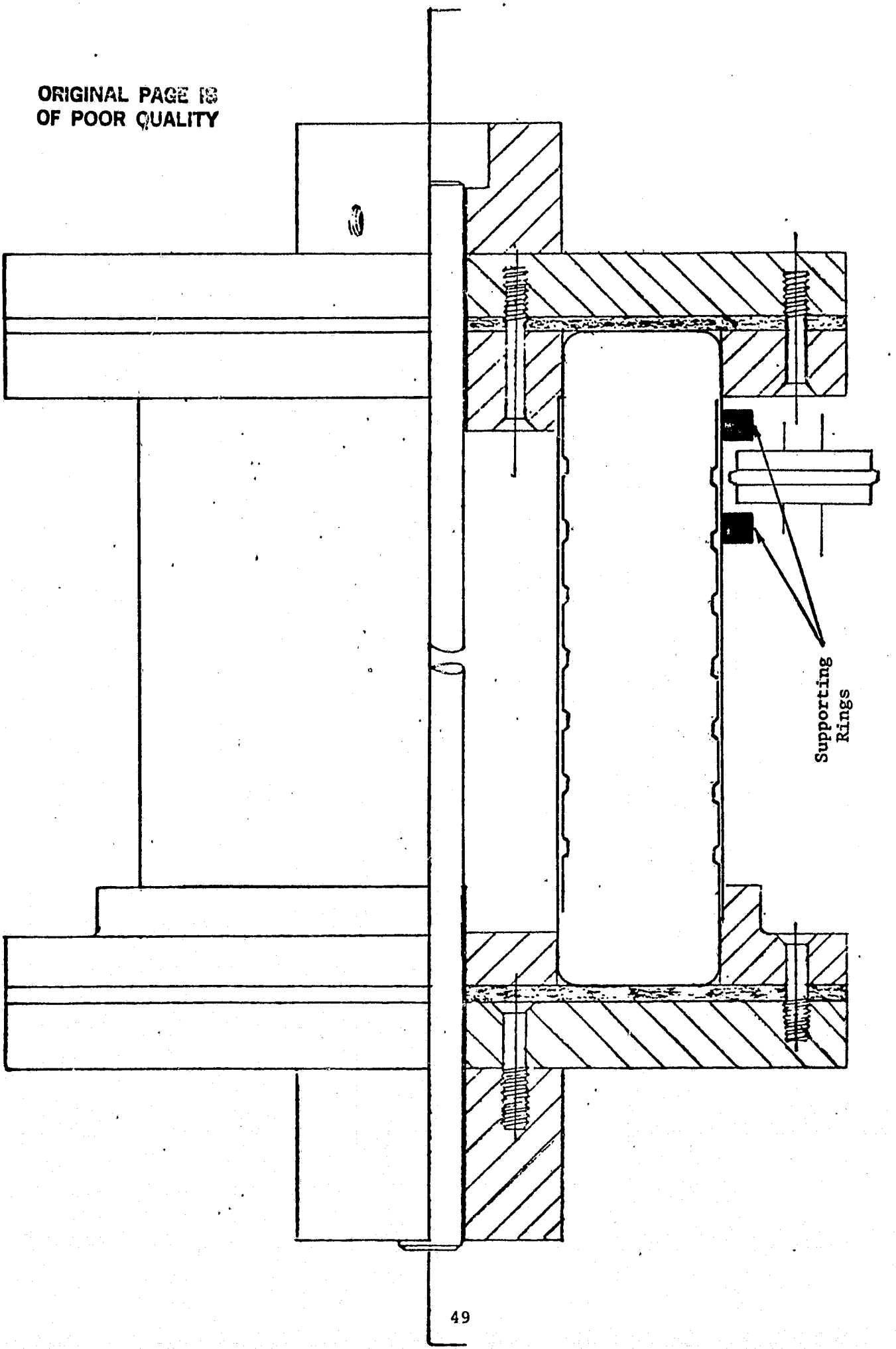

Fig. 37. Sealing support holding battery for making outer seal (quarter section).

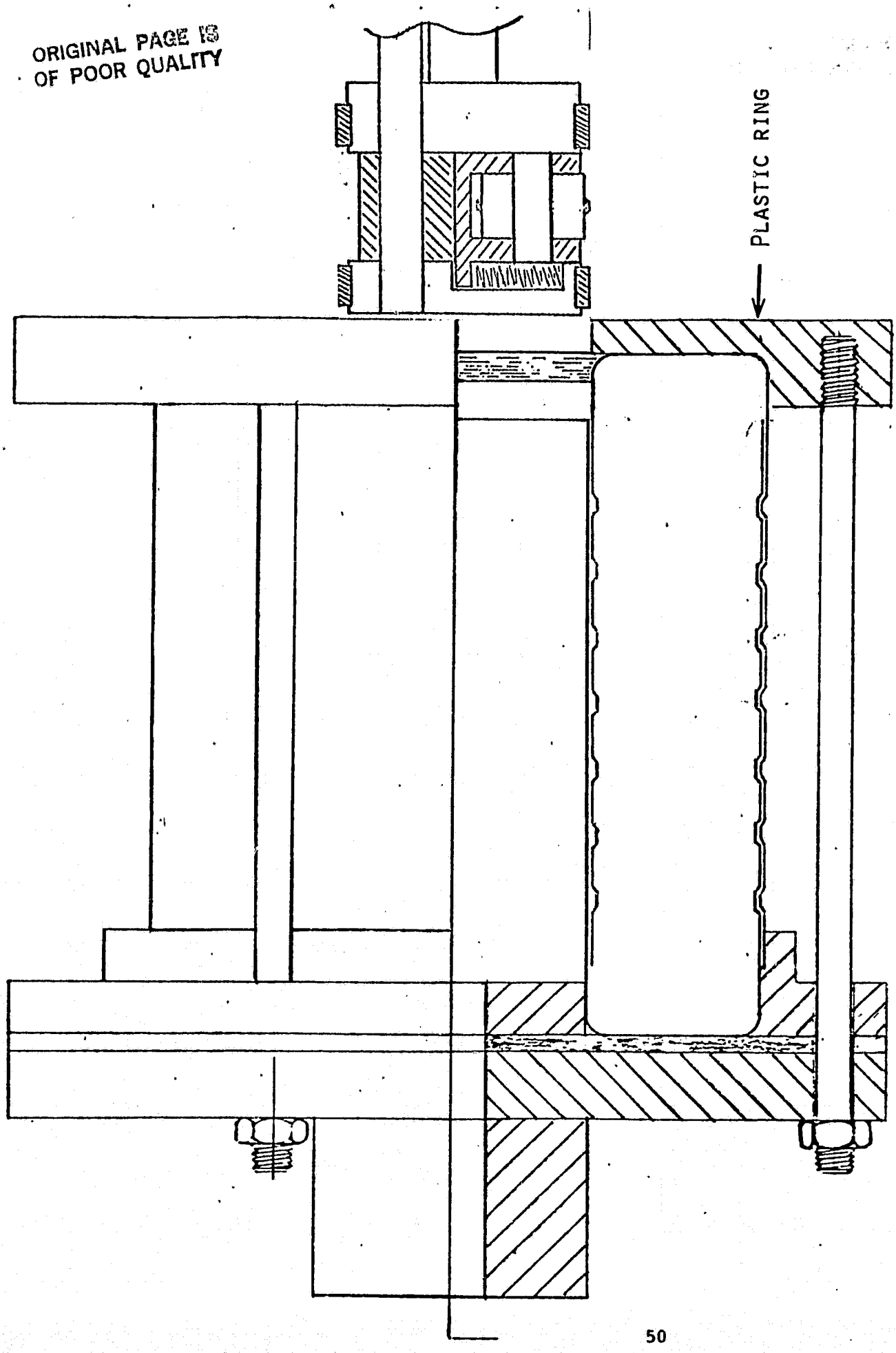

Fig. 38. Sealing support for making inner seal (quarter section).

outer swaged closure seals. However, the can parts themselves had multiple pin holes along the ribbed bottom and top surfaces. In view of this we did not conduct electrochemical cycle testing on these cells.

In summary we find that hermetic sealing of toroidal cans by localized swaging of grooves is feasible. The fabrication of suitable toroidal cans by electroforming proved to be quite difficult. No feasible alternative procedure for the manufacture of small quantities of complete toroidal cups with the desired dimensions could be identified. Based on the results of this effort we developed an modified swaged-welded cell design which offers significant advantages while retaining the basic toroidal concept. It is described in the following section.

III. DEVELOPMENT OF A SWAGED-WELDED TOROIDAL Ni/Cd CELL

1. Swaged-Welded Cell Design

We have demonstrated that a completely swaged cell closure can be achieved. However, with increasing cell diameter the outer closure becomes increasingly more difficult and requires stronger cans to prevent buckling failure. We therefore developed an alternative toroidal cell design which does not require a compressive outer seal. This design is illustrated in Figure 39. It uses a seam weld on the larger diameter cell closure and a double plastic compression seal at the smaller inner wall of the toroidal cell can. The electrode stack, the method of contacting, and all other important features of the NASA design are maintained. The large area, low curvature outside plastic seal is eliminated and replaced by an easily controllable seam weld. The inner seal is formed by swaged grooves as discussed earlier. The use of such corrugation not only seals the cell can but interlocks the pressure vessel making separation by internal pressure almost impossible. For cell stacking, an insulating disk will be used on the cell top. Additional advantages are: (1) weight savings by eliminating the double wall at the high-surface-area outer cell border; (2) elimination of the buckling and sealing problems at the outer, low curvature side of the toroidal vessel; (3) simplification of the cell case; and (4) improved heat transfer at the outer cell can.

2. Prototype Cell Construction

2.1 Cell Cans

Initial cell prototypes were constructed using electroformed half cans with electroformed covers and inner sealing tubes. The restrictions posed by the electroformed cans (see Section II.3) prompted us to search for alternatives. A review of possible fabrication techniques showed that custom manufacture of a limited quantity of one-piece toroidal cans was impractical. We therefore directed our efforts towards utilizing stock items wherever possible. We obtained deep drawn 316 stainless steel cans with 0.024" wall thickness (Polar Ware, Inc., Sheboygan, WI). A hole is punched into the bottom and the sides flared as shown in Figure 40. A 2.00 in. diameter, 0.020 in. wall thickness 321 stainless steel tube (Tube Sales, Inc., Los Angeles, CA) is welded into the can to form the toroidal cup part. The top parts, Figure 41, were spun from one piece of stainless steel sheet (R. W. Jacques & Sons, Attleboro, MA). The cylindrical part was made as long as the initial spinning technique allowed. For the inner sealing tube we have selected a stainless steel tubing 1.875" OD x 0.035" wall. This was the thinnest wall tubing available

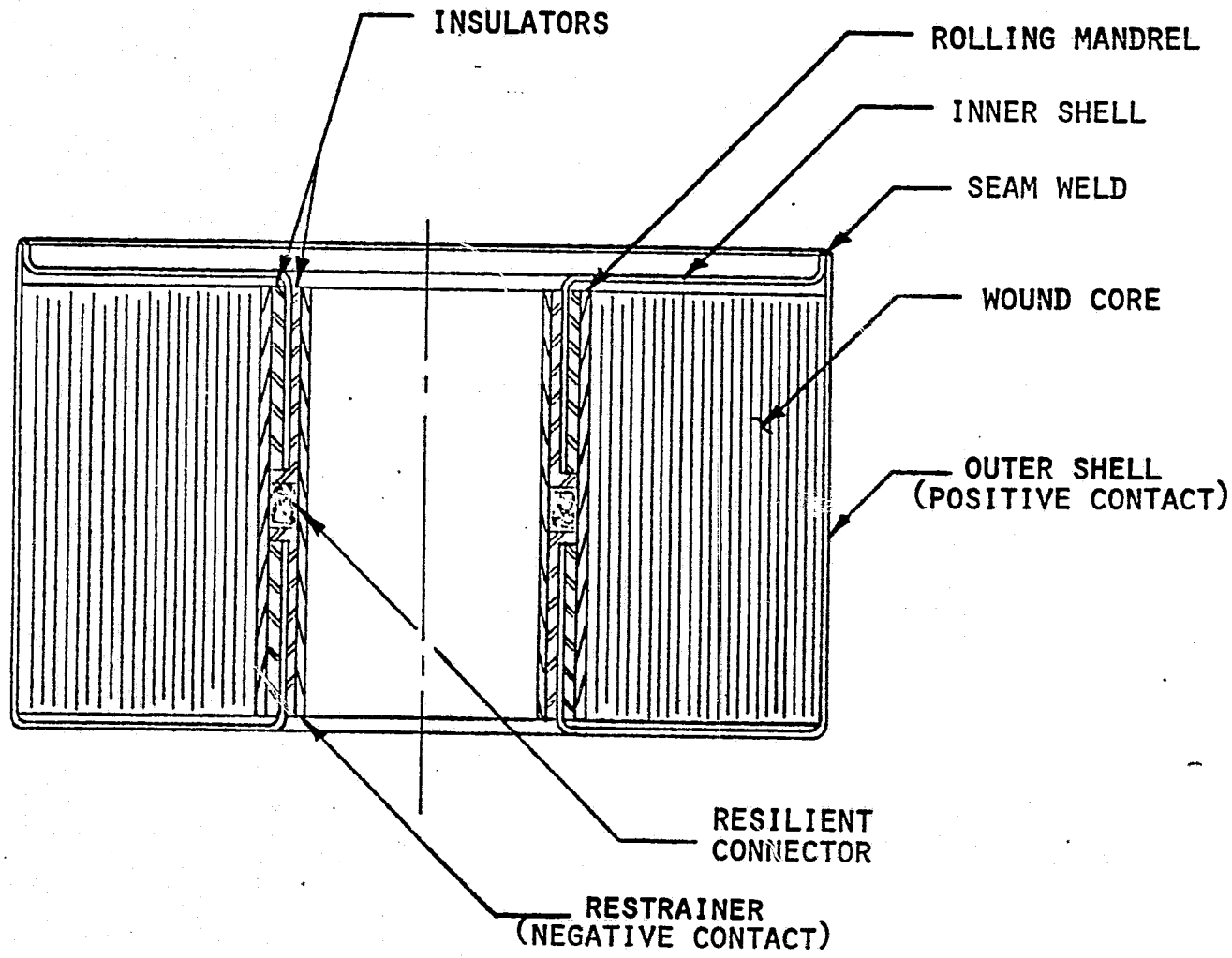

Fig. 39. Swaged-welded toroidal Ni/Cd cell design.

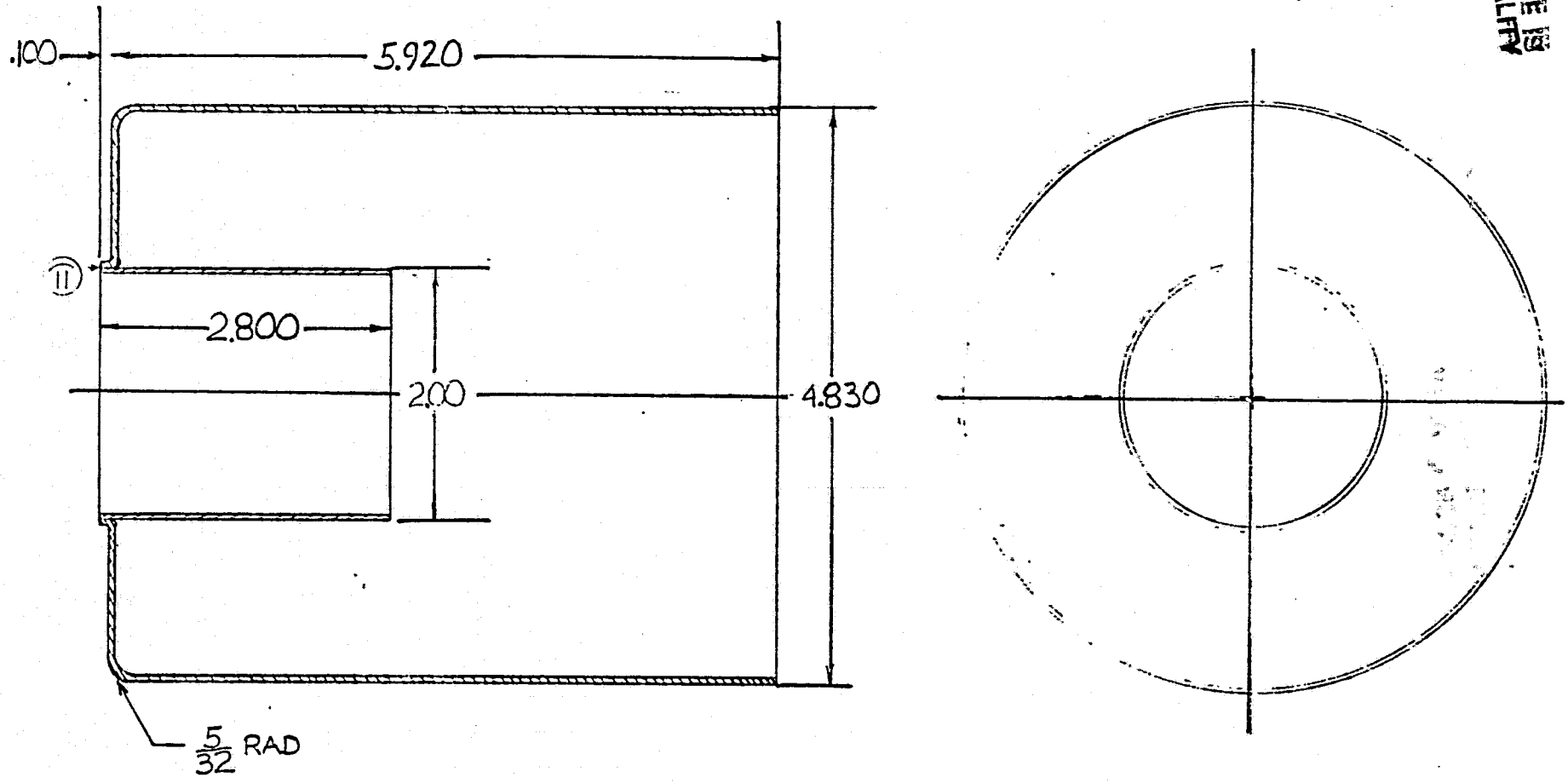

Fig. 40. Two-piece cell bottom.

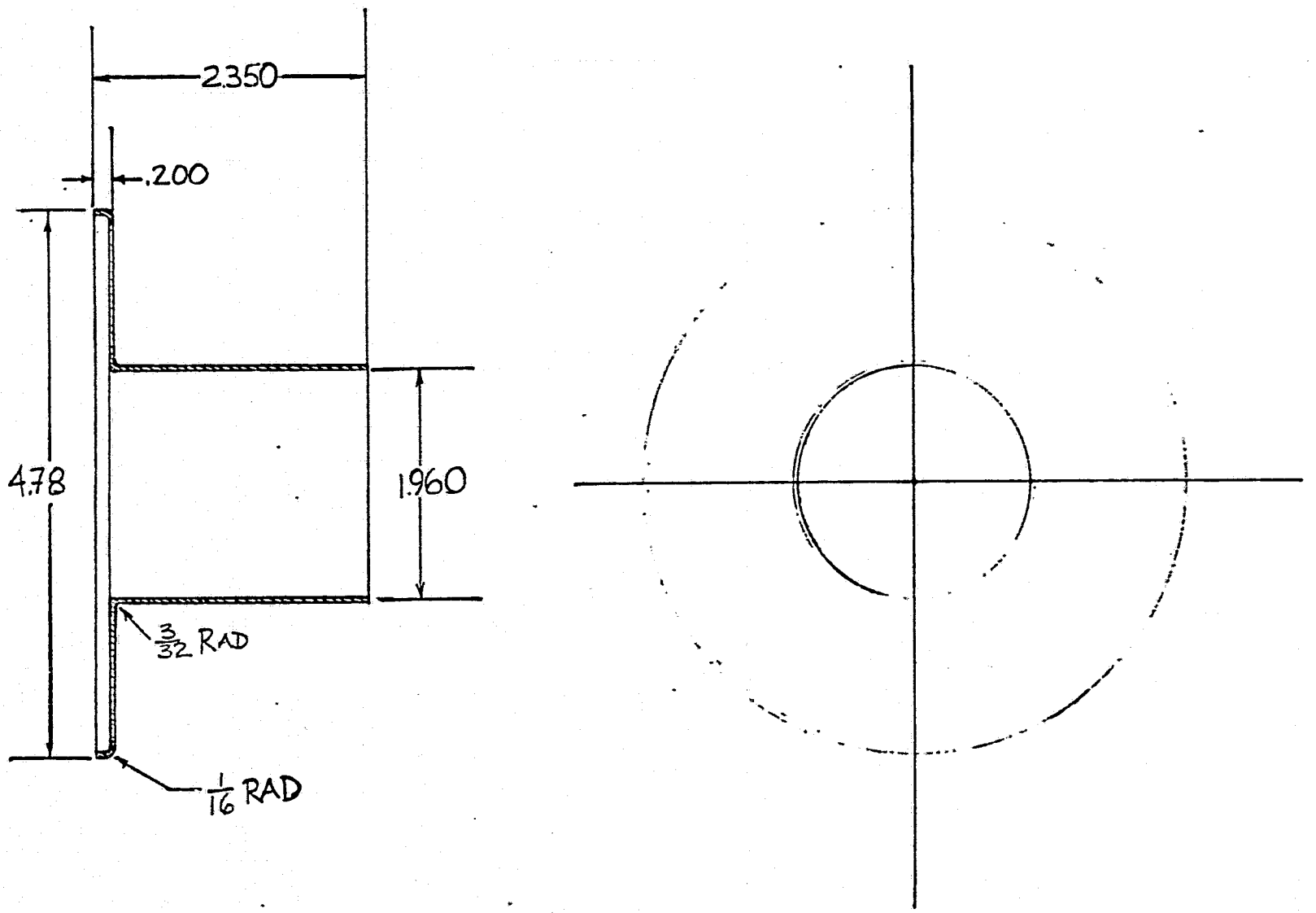

Fig. 41. Cell top.

in the required diameter. An electrolyte fill tube, as described earlier, was mounted into the bottom of the can.

2.2 Electrode Core

The electrode core was prepared by tightly rolling the electrodes and nonwoven nylon separators around a nickel cylinder as described in Section II.3.2. The height of the electrode core was increased slightly to use the full 4.75 in. coated width of the electrodes. The available electrode strips consisted of a 7 in. wide metal substrate which was perforated over a width of 4.75 in. Only the perforated center portion was coated with the nickel sinter. Prior to rolling we trimmed the excess metal border using a rotary cutter. Care was taken to avoid curling of the cut edges. During and after the winding, the core is checked for possible short circuits. For edge contact configuration the electrodes were wound offset with respect to each other. The metal edge was cut 0.2 in. deep in every 0.3 in.; after the package was wound these "tabs" were folded over at right angles to the core.

2.3 Electrical Connections

Of particular concern were the electrical connections to the two electrodes and from the rolling mandrel to the inner sealing tube. The initial cells contained one long nickel and cadmium electrode each connected only at the ends. Such an arrangement is satisfactory only for low rate applications because of the relatively large resistance in the electrode strips ($\sim 2.10^{-4}\Omega$/in.). We explored therefore various connections from multiple tabs to continuous edge contacts. The rolling mandrel-sealing tube contact too proved to be a critical component significantly affecting cell performance. A variety of configurations were explored.

Specific electrode contacts are shown in Figures 42 through 45. Figure 46 shows the bus plates for welded electrode tabs. The negative terminals (Cd electrode) are connected to the winding mandrel and the positive tabs (nickel electrode) are connected to the can. One tab is provided for each full electrode turn. Thus the longest distance between tabs occurs close to the external circumference of the electrode roll. To reduce this spacing we used a modified double buss plate which allows two tab connections which are almost opposite each other close to the outer circumference of the electrode roll. An edge contact configuration is illustrated in Figure 42. To increase the contact area slots were cut into the metal rim and the edge folded over as shown in Figure 43. The contact between can or tab and the folded edge was achieved via metal mesh or special spring configurations. Such a spring is shown in Figure 44. To reduce contact resistances contact members in certain cells were electroplated with copper, silver or gold. For this we used commercial plating solutions (Technics, Inc., Providence, RI) and standard cleaning, etching, strike and plating procedures.

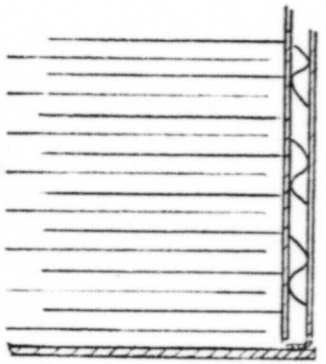

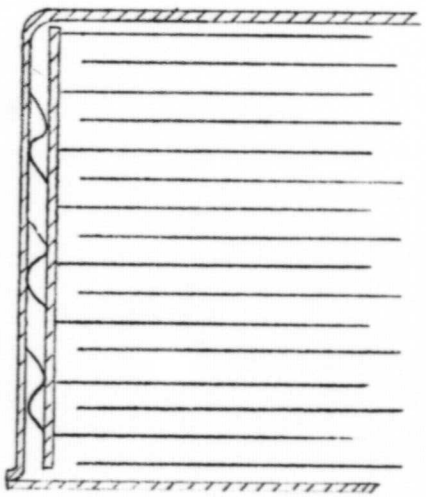

EDGE CONTACT, NICKEL MESH RINGS, TOP VIEW

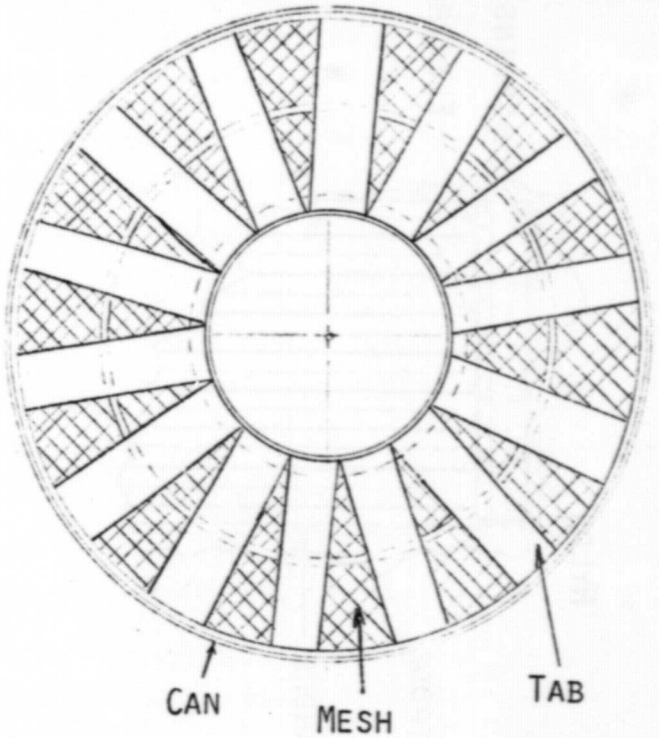

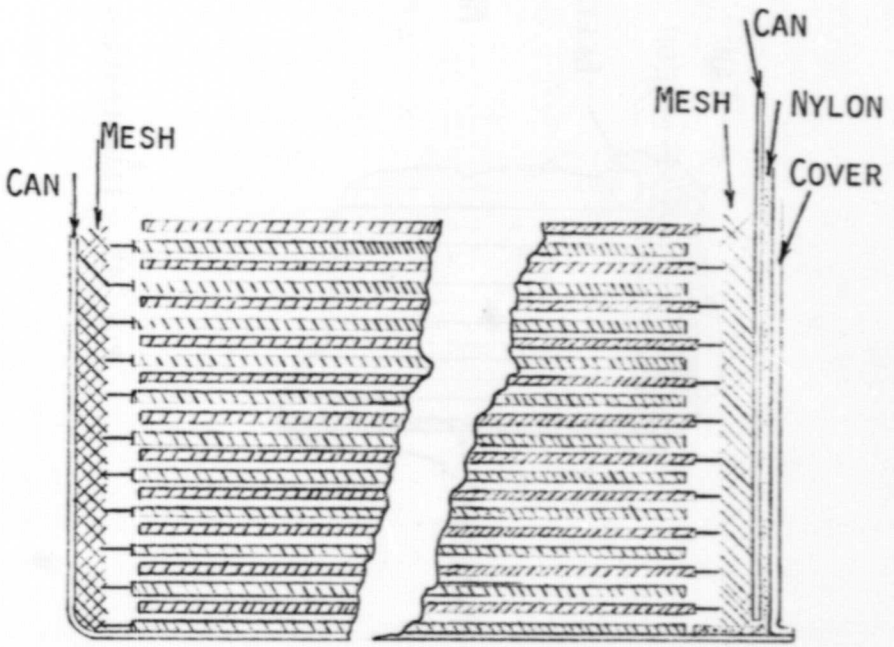

EDGE CONTACT, NICKEL MESH RINGS, SIDE VIEW

Fig. 42. Illustration of typical edge contact arrangement.

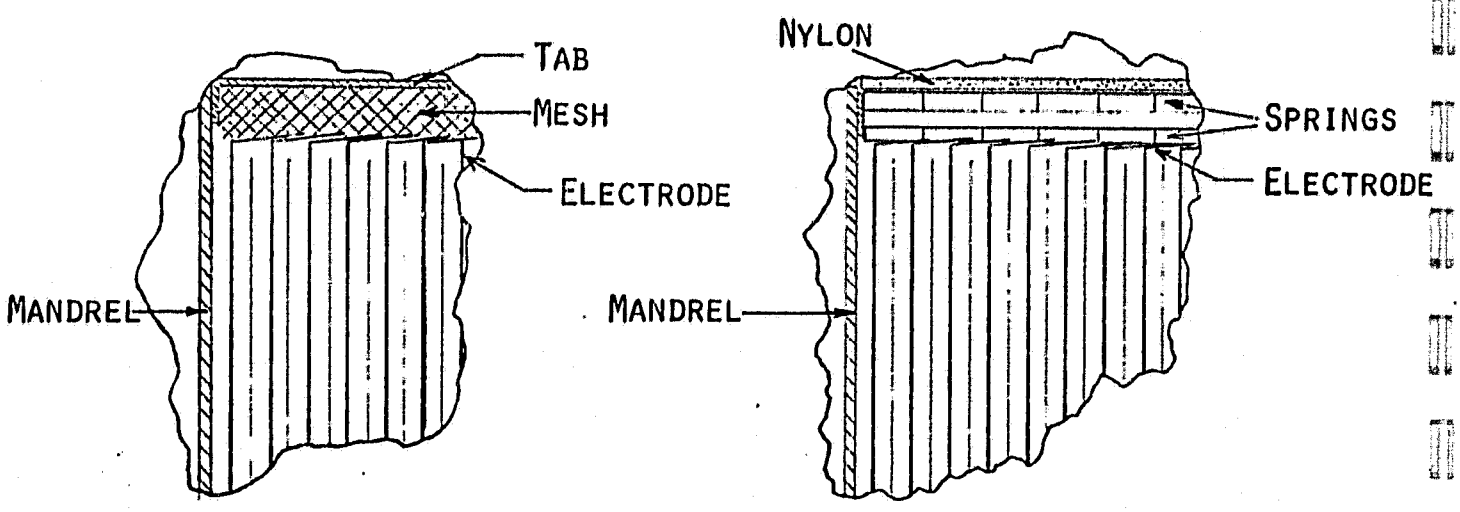

Fig. 43. Illustration of various edge contacts.

Fig. 44. Contact spring, 0.005" thick stainless.

PLAIN NICKEL MESH

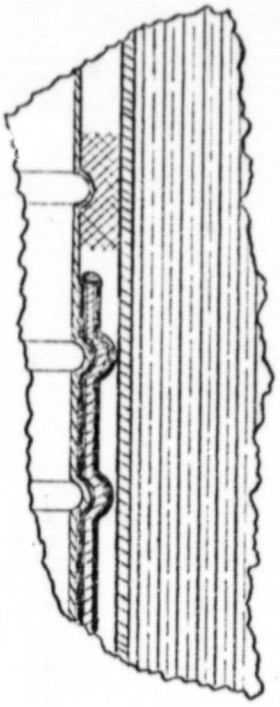

A

NICKEL MESH W/NEOPRENE CORE

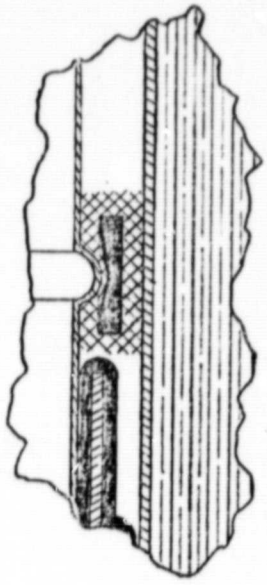

B

NICKEL SHEET WRAPPED AROUND
NEOPRENE CORE

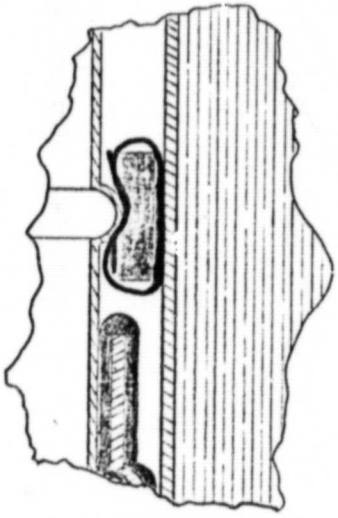

D

FOLDED NICKEL SHEET

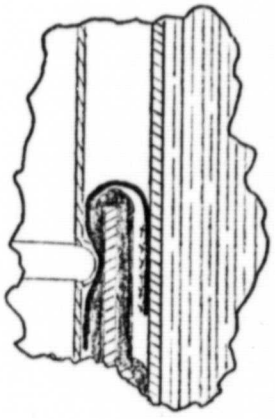

E

Fig. 45. Illustration of various winding-mandrel-sealing tube contacts.

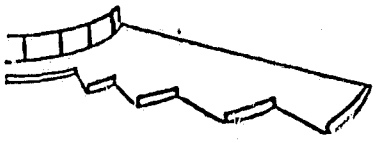

STAGGERED BUSS-NEG.

STAGGERED BUSS-POS.

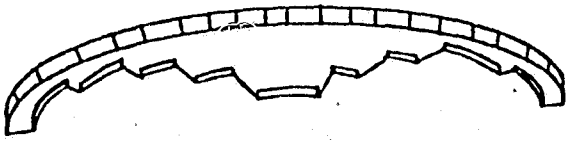

DOUBLE BUSS-POS.

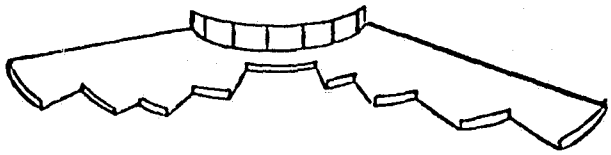

DOUBLE BUSS-NEG.

Fig. 46. Illustration of buss plates for welded tab electrode connections.

Variations in the winding mandrel inner sealing tube contact are shown in Figure 45. They included contacts of metal mesh and metal sheet and different arrangements to maintain intimate contact. Configuration d shows a slotted nickel sheet which is welded to the winding mandrel and then folded over the gasket surrounding the core tube of the can. During swaging of the inner sealing grooves the sheet is pressed into intimate contact with the sealing tube. Here too surface resistances were modified by electroplating all contacting interfaces.

2.4 Cell Assembly Procedure

Cell assembly included the following general steps:

- Electroplating of all parts and surfaces were derived (can bottom, sealing cylinder, winding mandrel, contact springs).
- Pregrooving of the inner cylindrical part of the toroidal cell can in a two step process using the pregroove wheels shown in Figures 47 and 48. Grooves are placed every 0.4 inch.
- Preparation of a Neoprene insulating cylinder (2.00 in. ID) formed from 0.031 in. sheet. The insulator is folded over the inner can tube so that both the inside and outside surfaces are covered.
- For edge contact configurations the bottom contact was inserted. For tabbed configurations a nylon insulator was placed in the can bottom.
- Pressing of the wound electrode core into the cell can.
- Insertion of the winding mandrel-sealing tube contact. If preattached to winding mandrel bend tabs over lower Neoprene insulator.
- For edge contact place contact springs on top of wound core.
- Weld bus plates to winding mandrel and cell can. For edge contact weld radial tabs or contact plate to winding mandrel.
- Insert inner sealing tube.
- Pregroove cylindrical part of cover (see cell can).

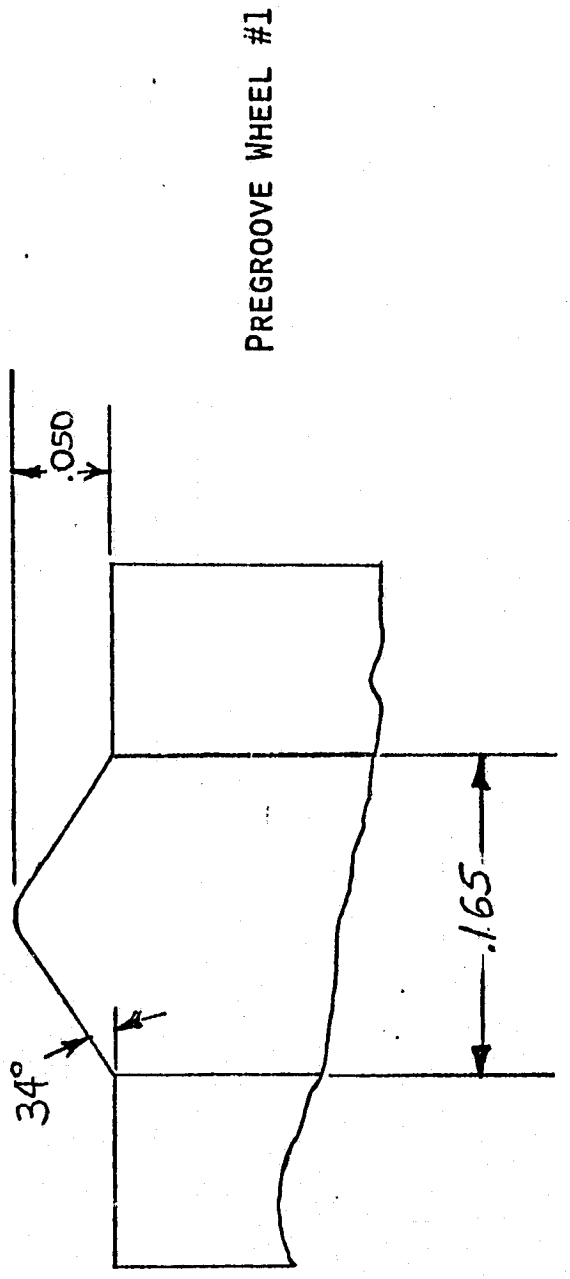

Fig. 47.. Pregroove wheel.

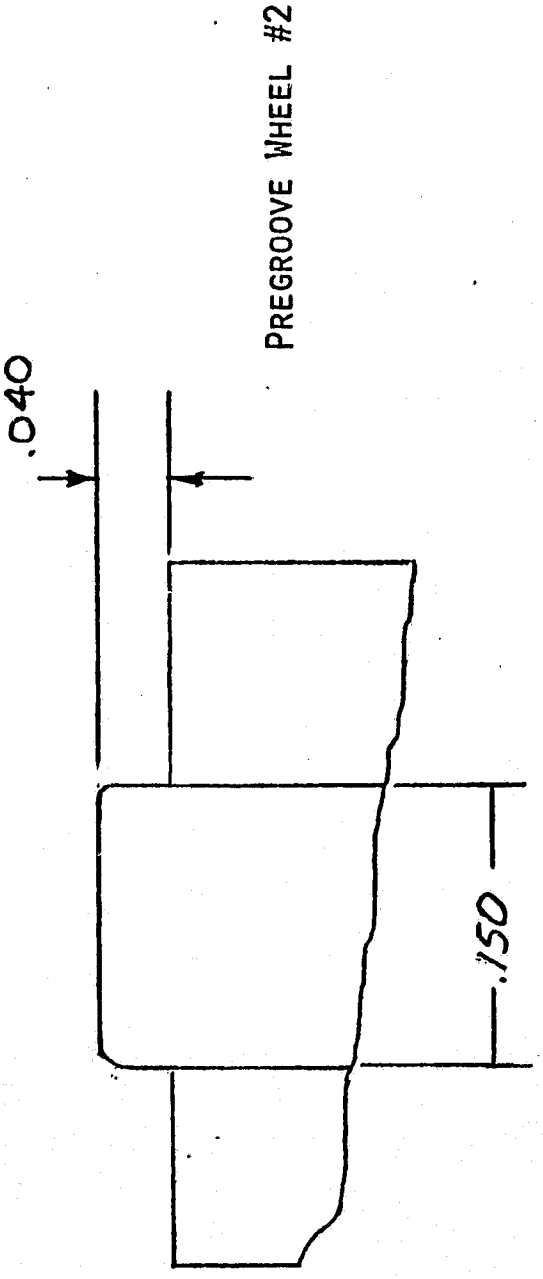

Fig. 48.· Pregroove wheel.

- Fold Neoprene insulator cylinder over both sides of cylindrical section of cover.
- For edge contact cells place a nylon insulating ring into top of can to prevent contact of negative terminal with cell can.
- Place nylon insulator disc on top of cell assembly.
- Insert cover, provide desired compression, spot weld cover in place.
- TIG weld cover.
- Perform final closure swaging starting with the can part using internal grooving tool and grooving wheel shown in Figure 49. The final groove will be 0.060 in. deep. Grooves in initial cells (1-12) were somewhat shallower due to limited travel of the grooving tool.

3. Evaluation of Prototype Cell Iterations

3.1 Pressure Test

To establish safe operating limits we pressure tested two cells using water as hydraulic fluid. Between 5, 6.4 atm (60 to 80 psig) the cell cover started to bulge and at 14.6, 16.3 atm (200 psig and 225 psig) respectively, the swaged seal between the cover and the inner sealing tube started to slip. With deeper grooves this pressure limit can easily be increased.

3.2 Cell Activation

The cells were equipped with a valve and a pressure gauge (vacuum to 60 psig, Ashcroft SS, 316). For some cells we used also pressure transducers (Data Instruments Model AB, Lexington, MA) allowing continuous recording of cell pressure. For activation the cells were evacuated, then back filled with 400 cm^3 of 31% KOH followed by standing time for equilibration. This amount of electrolyte was approximated by calculation of the core void volume such that the electrodes would be completely saturated and the separator pores filled to approximately 75% of capacity. Several experiments with various amounts of electrolyte around this value were carried out to experimentally confirm its appropriateness. In most cases the cells were evacuated prior to cycle testing to enhance oxygen recombination during cycle testing. The initial charge of the cells was at 15A. Nominal cell capcity was 90 Ah.

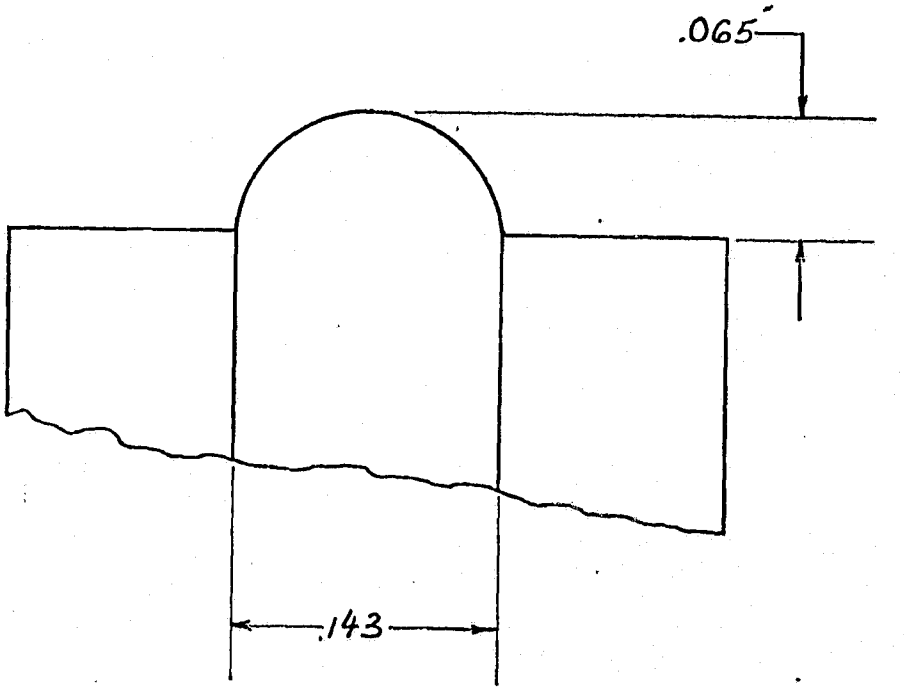

Fig. 49. Grooving wheel for the final cell closure swaging.

3.3 General Test Procedure

The general test procedure involved cycle testing at various rates. A typical regime consisted of charge at 50A and discharge at 90A (~C rate) to 0.6V. Typically we used a recharge ratio of 1:1. Cell voltage pressure and cell temperature mostly at two places were monitored. Cell charging was interrupted if cell pressure exceeded 35 psig in the early cells and 60 psig in the later cells or if cell temperature exceeded 75°C. This occurred occasionally during overcharge at higher rates especially with high contact resistance cells. In addition we periodically measured cell impedance via galvanostatic steps. For this a discharge current was interrupted and the voltage change monitored in the millisecond range. A typical voltage time trace is shown in Figure 50.

The cycler and cell test stand is shown in Figure 51. Contact to the cells was made in the center via slightly tapered copper plugs and externally via a 2 in. wide band of 0.05 in. copper (see Fig. 52). Voltage measurements were made via separate sensing leads connected directly to the cell. The data was recorded with a Bascom-Turner Data Acquisition System (Series 8000).

3.4 Results and Discussion

The results of the prototype cell testing are summarized in Table 3. Early cells showed high polarization. Cell No. 5 was cut open and analyzed with respect to all voltage drops. The results are shown in Table 4. The main resistance was located in the rolling mandrel-sealing tube contact. Therefore, in subsequent cells we concentrated on improving this area. The cycle test results showed also that the cell resistance was generally quite moderate during the first charge and then gradually increased. Initially it appeared that this may be the result of a relaxation in the compressive tension on the contact mesh and resilient Neoprene cores were used in an attempt to counter it. Cell resistances were markedly decreased but remained still higher than desired and increased upon cycling especially after extended overcharge. To provide a lower contact resistance nickel sheet was used instead of the thin wire mesh. This further decreased the resistance but did not completely stabilize it upon repetitive cycling. All evidence pointed to a gradual deterioration of the interface contact resistance in the oxygen atmosphere of the cell during the later parts of charge and on overcharge. Electrochemical oxidation must be excluded in this particular case since the inner contact is connected to the cadmium electrode. We therefore experimented with various surface coatings of Cu, Ag and Au. In these cases all contact areas, e.g., contact region of the winding mandrel, contact mesh or sheet, and the contact region of the sealing tube were electroplated. The stable resistance upon cycling of, for example, cells 15 and 16, demonstrate that indeed the deterioration of the contact surface was the problem and that silver plating can overcome it. Two typical charge/discharge curves are shown in Figures 53 and 54.

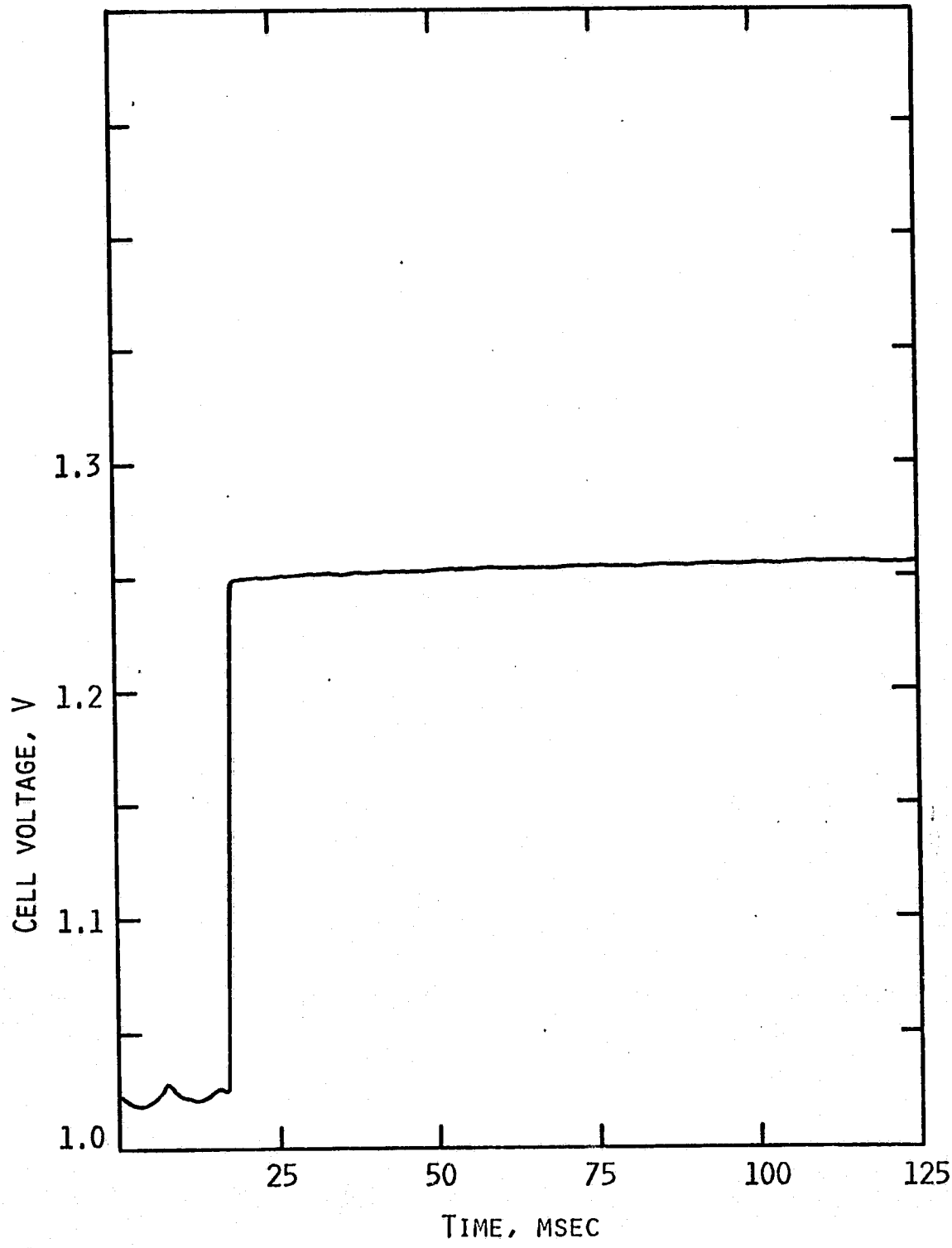

Fig. 50. Typical voltage-time trace upon current interruption (Bascom-Turner Electronic Recorder). Cell 12 during 90A discharge → open circuit.

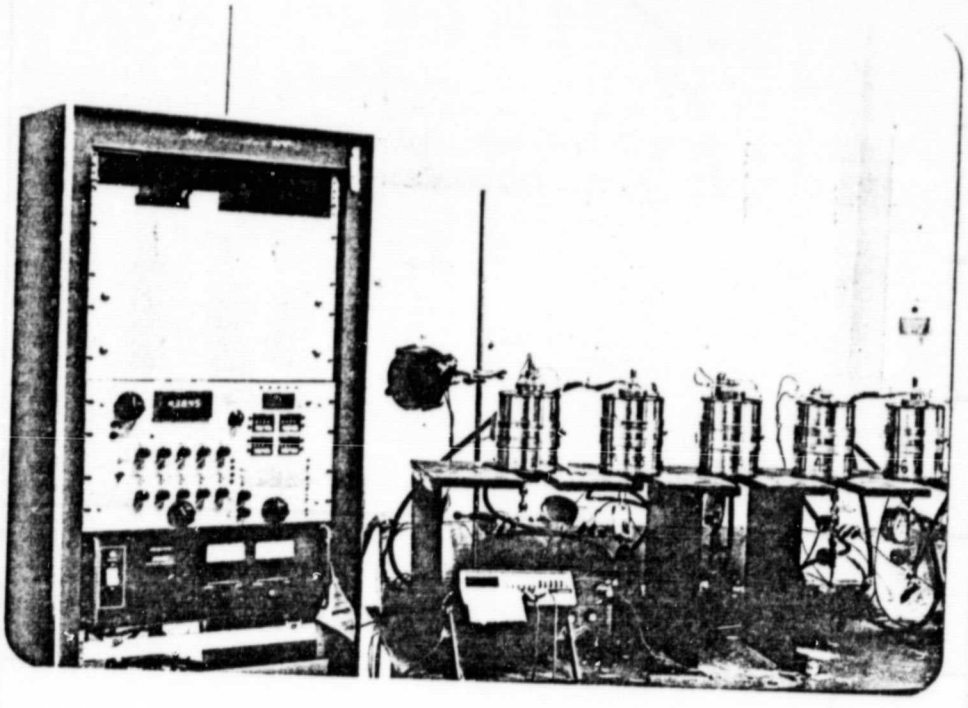

Fig. 51. Cell cycler and test stand.

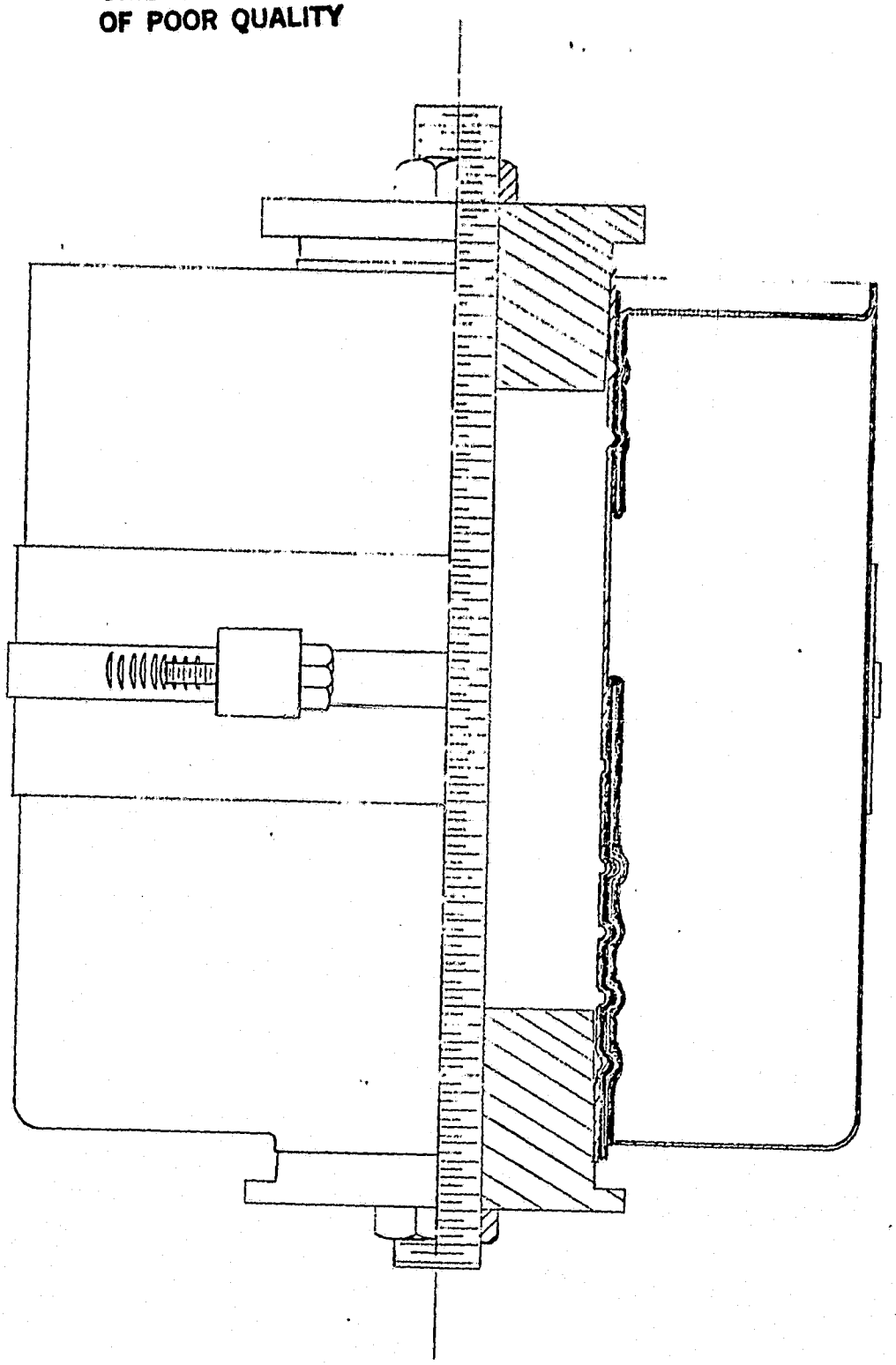

Fig. 52. Connections to cells.

Table 3

Summary of Prototype Cell Configurations and Test Performance

Cell No.	Type of Contacts: Electrode	Type of Contacts: Tube-Mandrel	Cycle No.	Charge: i (A)	Charge: Input (Ah)	Charge: MCV (V)	Charge: End Pressure (atm)	Discharge: i (A)	Discharge: Cap. (Ah)	Discharge: MDV (V)	Discharge: Resistance (mΩ)	Comments
1	Welded	Ni mesh grooved	1	4.7	84.5	1.6	0.33	0.75				Polarization increased on cycling.
			2	7		2.1	5.08					
2	Welded	Ni mesh grooved	1	4.7	9.8	1.6	1.54	0.54		0.5		
			2[1]	10			3.40					
5	Welded	Ni mesh grooved	1	27	180	1.750	2.50	27	92.2	0.6		Heating in tube-mandrel contact area (>100°C)
			2	27[2]	38	2.490	1.0	5	~1.2	0.23		
			3	27[3]	20	2.680	0.67	1	~2	0.17	59.0	
			4	45	105	1.529	1.0	50	82	1.05		
6	Welded	Ni sheet with Neoprene core grooved	1	25	99.5	1.506	0.50	50	76	1.070	5.5	Regrooved contact area after Cycles 2 and 4.
			2	30	90	1.702	0.68	50	85	0.819	8.8	
			3	30	90	1.675	1.54	50	80.2	0.793	10.0	
			4a	30		1.837						
			b	30		1.978						
			c	30	100	1.833	2.09	50	86.8	0.740	15.5	
			5	50	96.5	1.950	2.50	50	85.8	0.80		
			6	25	100	1.950	1.0	30	89.2	0.60	20.0	
8	Welded	Ni mesh and Neoprene core, welded core, grooved	1	15	100	1.500	1.41	50	65.0	1.06	5.4	
			2	50	80	1.630	1.27	50	72.5	0.98	5.8	
			3	50	85	1.650	2.36	50	79.0	1.03	5.6	
			4	50	85	1.640	0.66	50	67.5	0.97	6.6	
			5	50	85	1.630	2.22	50	80.8	1.00	6.2	
			6[3]	50	191.2	1.660	3.31	50	94.2	0.82	8.1	
			7	50	100	1.910	3.04	50	85.1	0.68	10.6	
9	Welded	As No. 8 plus Ni sheet with Neoprene core, grooved	1	15	110	1.480	0.33	60	80.4	1.02	4.8	Case temperature 70°C.
			2	60	126	1.620	2.63	50	103	1.05	4.4	
			3[3]	60	142	1.610	1.54	80	100	0.85	5.6	
			4	60	113	1.620	3.04	60	88	1.03	4.7	
			5	60	100	1.620	2.36	50	97.5	1.05	4.4	
			6	60	100	1.630	0.80	50	91.5	1.07		
			7	50	100	1.600	0.43	120	74.0	0.753	4.6	
			8	50		1.550	1.54	120	60	0.77	4.6	

[1]Cell reached 3.4 atm pressure limit before fully charged.

[2]Cell reached 70°C temperature limit before fully charged.

[3]Overcharge study.

Table 3
(continued)

Cell No.	Type of Contacts: Electrode	Type of Contacts: Tube-Mandrel	Cycle No.	Charge: i (A)	Charge: Input (Ah)	Charge: MCV (V)	Charge: End Pressure (atm)	Discharge: i (A)	Discharge: Cap. (Ah)	Discharge: MDV (V)	Discharge: Resistance (mΩ)	Comments
10	Welded	Ni mesh Neoprene core, welded, grooved	1	15	104	1.470	0.83	50	86	1.130	3.2	
			2	15	102	1.431	0.50	50	56.5	1.110	3.5	
			3	50	100	1.567	1.68	50	96	1.125	3.1	
			4	50	100	1.516	1.14	80	92	1.039	2.6	
			5	15	100	1.432	0.70	50	90.9	1.134		
			6	50	100	1.527	2.22	50	99.2	1.124		
			7[4]	50	100	1.539	0.43	120	64.0	0.919	3.3	
			8	50	100	1.555	3.18	120	88	0.905	3.1	
			9	50	101	1.570		90	82.9	0.940	3.8	
11	Welded	Ni sheet, Neoprene core, grooved, welded to sealing tube	1	15	102	1.450	1.00	50	54.2	1.133	2.8	
			2	50	100	1.529	1.61	50	91.6	1.159	2.2	
			3	50	100	1.481	1.34	80	90.4	1.124	1.8	
			4	15	100	1.418	0.53	50	85.9	1.176	2.7	
			5	50	100	1.504	2.36	50	97.5	1.161		
			6[4]	50	100	1.474	0.37	120	62	1.073	2.0	
			7	50	100	1.486	2.36	120	88	1.067	1.8	
			8	50	101	1.565		90	91.1	1.020	2.4	
			9	90	100	1.70		90	65.6	0.99		
12	Welded	Ni sheet, Neoprene core, grooved, welded to sealing tube	1	15	100	1.379	0.40	50	68.3	1.133	2.8	
			2	50	100	1.490	1.27	50	87.5	1.150	3.3	
			3	15	102	1.338	0.40	60	65	1.078		
			4	90	102	1.484	2.43	100	15			
			5	15	100	1.371	0.30	60	50	1.055		
			6	100	100	1.460	2.09	120	52	0.992	2.3	
			7	90	103	1.581	2.87	120	78	0.994	2.4	
			8	90	100	1.575	2.97	120	90	0.966	2.3	
			9	60	100	1.505	3.04	90	90	1.062	2.5	
			10[4]	50	102	1.512		90	83.5	1.088		
			11	90	100	1.630		90	58.0	1.080		
			12	90	100			90	94.5			
13	Welded	Cu plated Ni mesh, Neoprene core - one side welded	1	15	100	1.466	0.33	60	77	1.117		
			2	90	102	1.640	1.07	60	77	0.989		
			3	15	100	1.469	0.87	60	78	0.908		
			4	100	100	1.948	2.63	50	66.5	0.825	8.1	
			5	90	58.5	2.16	1.07					

[4]Cell sat idle for several weeks between cycles.

Table 3
(continued)

Cell No.	Type of Contacts: Electrode	Type of Contacts: Tube-Mandrel	Cycle No.	Charge: i (A)	Charge: Input (Ah)	Charge: MCV (V)	Charge: End Pressure (atm)	Discharge: I (A)	Discharge: Cap. (Ah)	Discharge: MDV (V)	Discharge: Resistance (mΩ)	Comments
14	Welded	Cu plated Ni sheet welded to sealing tube, Neoprene core, grooved	1	15	100	1.439	0.33	50	76.5	1.170	2.4	
			2	50	100	1.502	1.14	50	95	1.157		
			3	15	100	1.432	0.67	60	93	1.148		
			4	90	105	1.539	1.08	60	77	1.122	2.2	
			5	15	100	1.412	0.77	60	89	1.156		
			6	100	100	1.556	2.70	120	84	0.981	2.1	
			7	90	102	1.582	2.77	120	76	0.975	2.5	
			8	90	100	1.609	3.18	120	90	0.939	2.9	
			9	60	100	1.505	2.29	90	90	1.008	3.2	
			10[4]	50	101	1.540		90	87	1.060		
15	Welded	Ag plated Ni mesh, Neoprene core - one side welded, grooved	1	15	100	1.451	0.26	60	75	1.141		
			2	90	105	1.535	2.50	60	83	1.125	2.3	
			3	15	100	1.428	0.53	60	86	1.143		
			4	100	100	1.570	1.82	120	52	1.004	2.1	
			5	90	100	1.575	0.47	120	78	1.024	2.3	
			6	90	100	1.565	3.04	120	90	0.983	2.2	
			7	60	100	1.500	1.68	90	90	1.067	2.4	
			8	15	100		0.60	60	87	1.139	2.6	
			9	90	100	1.554	2.90	120	72	1.018	2.3	
			10	90	100	1.564	2.90	120	80	1.00	2.2	
			11	50	100	1.505	1.95	120	92	1.101	2.2	
			12[4]	50	101	1.510		90	93.7	1.120		
			13	90	98.4	1.578		90	89.4	1.110		
16	Welded	Ag plated Ni sheet, Neoprene core, welded to sealing mandrel, grooved	1	15	100	1.455	0.16	60	70	1.143	1.9	
			2	100	100	1.570		120	76	1.056	2.0	
			3	90	100	1.558	2.84	120	78	1.066	2.0	
			4	90	100	1.557	2.77	120	92	1.042	2.1	
			5	60		1.472	0.83	90	88.5	1.108	2.1	
			6	15	100		0.53	60	79	1.159		
			7	90	100	1.540	2.77	120	72	1.054		
			8	90	100	1.553	3.04	120	96	1.027	1.9	
			9	50	100	1.501	1.68	120	92	1.039	2.2	
			10[4]	50	101	1.520		90	92.4	1.130		
			11	90	98.4	1.580		90	87	1.130		

[4]Cell sat idle for several weeks between cycles.

Table 3
(continued)

Cell No.	Type of Contacts: Electrode	Type of Contacts: Tube-Mandrel	Cycle No.	Charge: i (A)	Charge: Input (Ah)	Charge: MCV (V)	Charge: End Pressure (atm)	Discharge: i (A)	Discharge: Cap. (Ah)	Discharge: MDV (V)	Discharge: Resistance (mΩ)	Comments
17	Welded	Ni sheet folded over can bottom, grooved	1	15	100	1.473	0.67	60	70	1.090	2.7	
			2	90	100	1.684	2.02	120	82	0.764	4.2	
			3	90	118	1.657	1.14	120	114	0.878		
			4	50	102	1.626	1.14	120	88	0.810	3.8	
			5	50	100	1.520		120	89.2			
			6	90	98	1.595		90	93.6	0.920		
18	Welded	As above plus spacer ring	1	15	100	1.460	1.00	60	69	1.125	2.5	
			2	90	100	1.572	2.56	120	72	1.033	2.1	
			3	90	100	1.562	2.77	120	94	1.013	2.1	
			4	50	102	1.500	2.29	120	92	1.013	2.1	
			5[4]	50	100			120	79			
			6	90	99	1.610		90	86	1.079		
19	Welded	Ni sheet welded to winding mandrel, folded over can, grooved	1	15	100	1.455	0.33	60	69	1.127	2.4	
			2	90	100	1.574	2.09	120	72	1.027	2.2	
			3	90	100	1.555	1.82	120	94	1.017	2.0	
			4	50	102	1.498	1.61	120	92	1.024	2.2	
			5	50	100	1.494	0.87	120	84	0.996	2.4	
			6[4]	50	100				81.2			
			7	90	99	1.560		90	88	1.090		
20	Straight edge, wave spring	Ag plated, configuration as No. 19	1	50	100	1.616		30	42	0.890		Temperature in top-bottom contact area 93°C.
			2[1]	90	21	2.295	3.40	90	7.5	0.547	8.2	
21	Straight edge, Ni mesh	As above	1	50	101	1.635		90	56	0.800	9.1	High temperature in contact area.
			2[1]	90	58.5	2.431	3.40	90	35	0.262		
			3[1]	90	69		3.40	90	56			
28	Edge folded, Ni mesh	As above	1	50	100	1.640		90	65.5	0.920	4.8	
			2	90	87	1.810		90	58	0.720		
29	Edge folded, SS mesh	As No. 20	1	15	50	1.526	0.20	90	33	0.586	7.6	
			2	50	100	1.962	2.63	90	4.5	0.150	12.6	
			3	50	12.5	2.272	1.00	90	0	0.100	16.7	

[1]Cell reached 3.4 atm pressure limit before fully charged.

[4]Cell sat idle for several weeks between cycles.

Table 3
(continued)

Cell No.	Type of Contacts: Electrode	Type of Contacts: Tube-Mandrel	Cycle No.	Charge: i (A)	Charge: Input (Ah)	Charge: MCV (V)	Charge: End Pressure (atm)	Discharge: i (A)	Discharge: Cap. (Ah)	Discharge: MDV (V)	Discharge: Resistance (mΩ)	Comments
30	Edge folded, Ag plated, Cu mesh	As No. 20	1	25	100	1.475		50	90	1.120	3.2	
			2	15	104	1.440		70	87	0.940		
			3	50	100	1.615		90	92	0.650	5.7	
31	Edge folded, Ag plated, SS mesh	As No. 20	1	15	100	1.475		70	69.8	0.992	4.3	
			2	50	100	1.605		90	77	0.0895	5.2	
42	Edge folded, Au plated, SS springs	As No. 20	1	25	124	1.529	1.1	50	80.7	1.077	2.8	
			2	90	99	1.717	4.5	164	34.9	0.630		
			3	90	93	1.700	4.7	162	28.7	0.642		

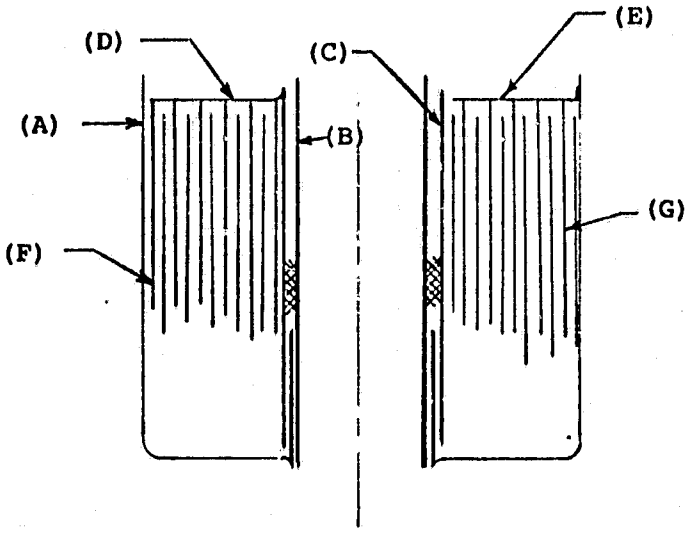

Table 4

Voltage Drops Across Various Points

Measurement Pt	Cell 5 during 27A Charge ΔE, V	Cell 5 during 27A Charge R, Ω	Cell 9 during 50A Charge ΔE, V	Cell 9 during 50A Charge R, Ω
Can (A) - Sealing Tube (B)	2.91	-	1.699	-
Neg. Buss (D) - Pos. Buss (E)	1.33	-	1.432	-
Sealing Tube (B) - Mandrel (C)	1.32	0.0489	0.216	0.0043
Neg. Buss (D) - Mandrel (C)	0.12	0.0044	0.016	0.0003
Pos. Buss (E) - Can (A)	0.00	0.0000	0.032	0.0006
Pos. Buss (E) - Pos. Electrode (G)	-	-	0.019 max	0.0004
Neg. Buss (D) - Neg. Electrode (F)	-	-	0.016 max	0.0003

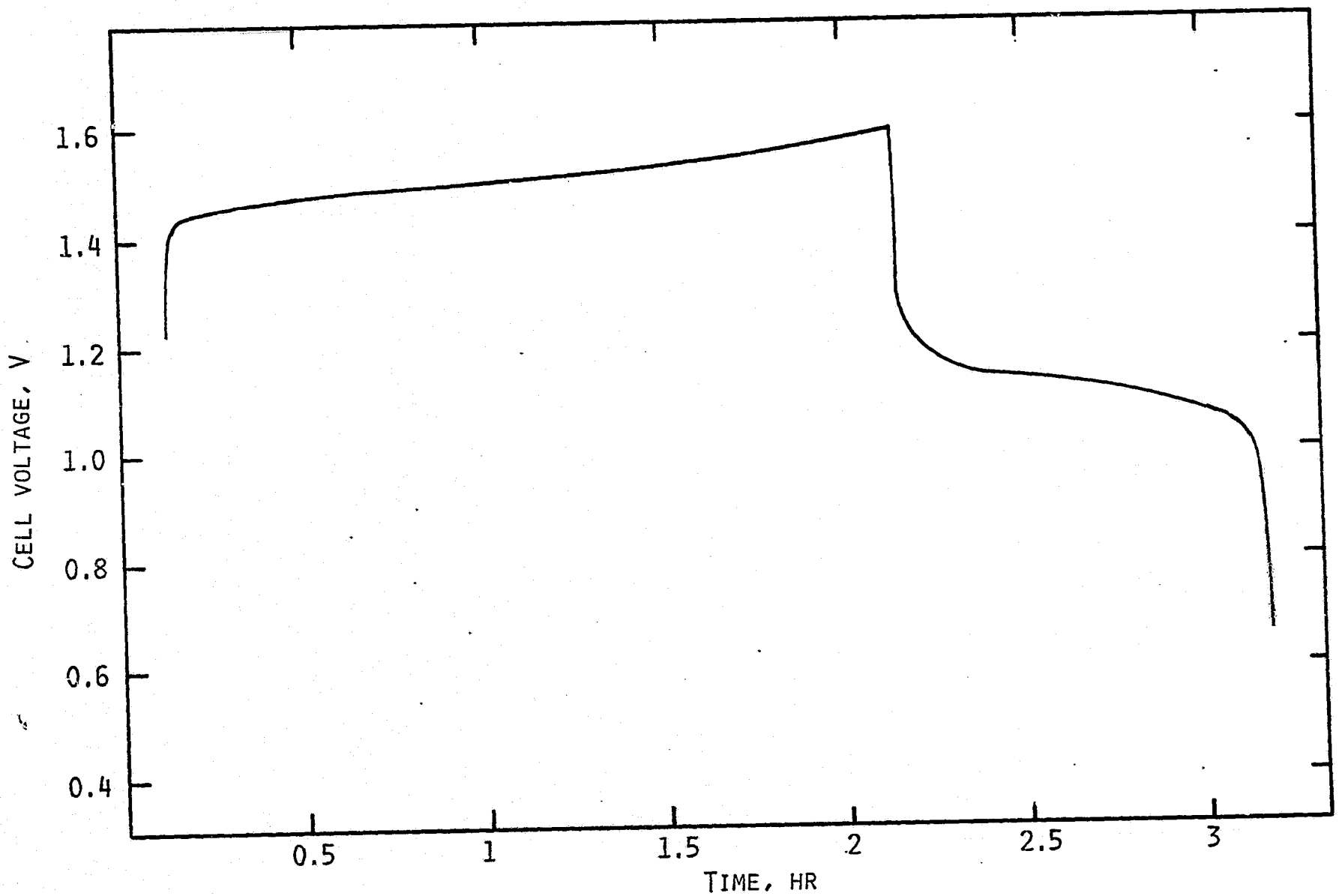

Fig. 53. Voltage profile of cell 16, cycle 10; 50A charge, 90A discharge.

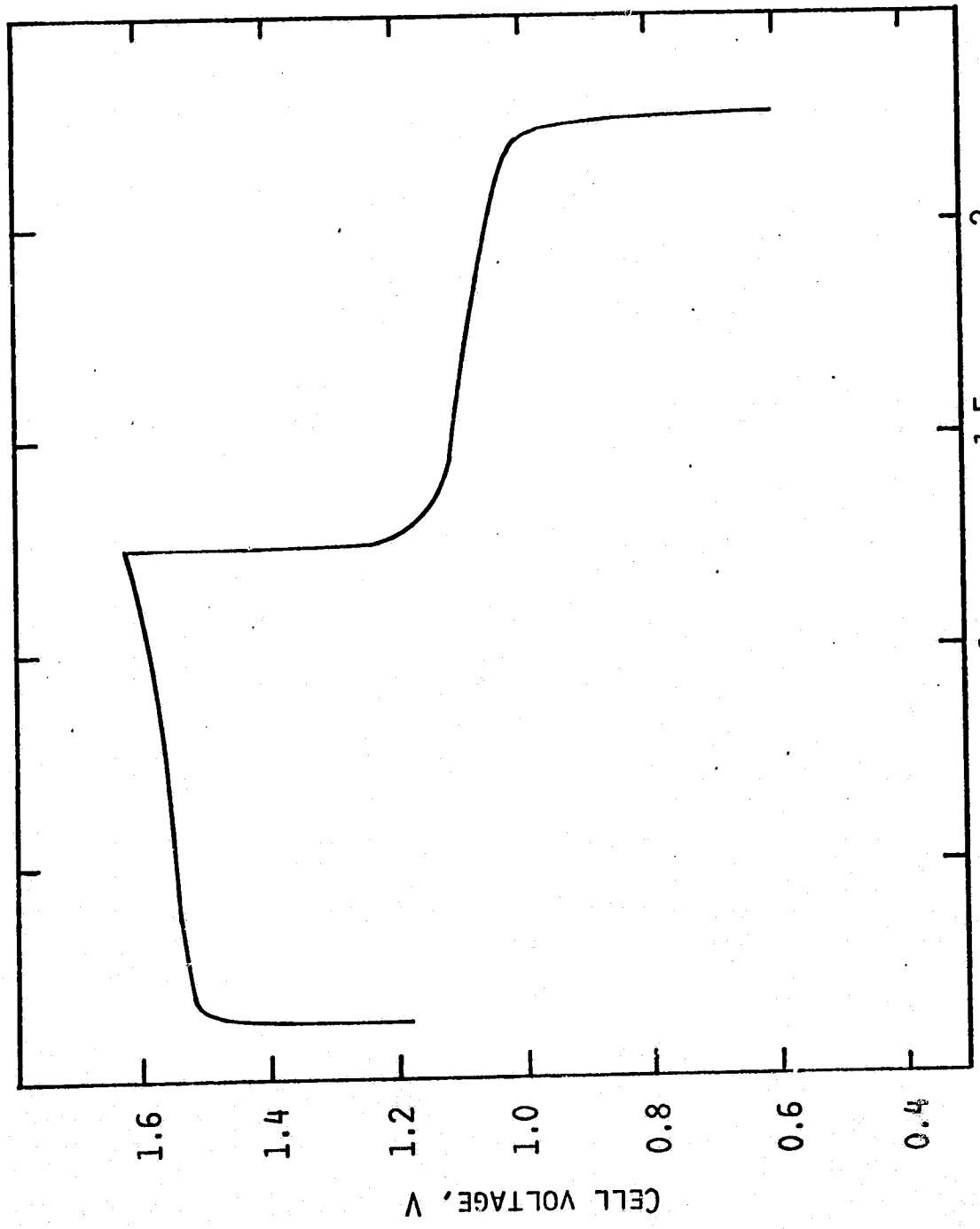

Fig. 34. Voltage profile of cell 19, cycle 7; 90A charge, 90A discharge.

A nickel sheet contact consisting of nickel tabs welded to the rolling mandrel and folded over the Neoprene jacket of the inner can tube with silver plating at the contact with the inner sealing tube became our preferred inner contact. It was retained during experimentation with edge contacts to the electrode core. Conceptually a continuous edge contact is very attractive. During implementation we encountered the same problems as discussed above. The contact resistance in particular at the nickel oxide electrode side increased relatively rapidly upon cycling. A drastic example are the mid charge voltages of cell 29 which increased from 1.5V in the first cycle to 2.3V in the third cycle. Upon disassembly strong surface oxidation of the contact springs was evident. Bending of the electrode substrate edge to increase contact area, special contact spring configurations, and surface plating can alleviate the problem. While plating of the contact springs and of the vessel is straightforward, plating of the substrate of a finished electrode is very difficult without contamination of the sinter region with the plating bath. Two characteristic charge/discharge curves of edge contact cells are shown in Figures 55 and 56.

In summary, contact resistances and their increase with time were identified as major problem areas. They can be minimized by appropriate contact design and by surface treatments especially plating with more noble metals.

4. Toroidal Ni/Cd Demonstration Cells

Based on our experience with the individual test cells described previously we built four different sets of five cells, each set utilizing a different internal configuration. All cells were subjected to an identical test regime designed to examine cell resistance, rate characteristics, overcharge and overdischarge performance. After completion of the test regime cells were connected to a five-channel cycler designed to simulate a low-earth orbit regime (C/2 charge for one hour, C discharge for 0.5 hour).

4.1 Demonstration of Cell Configuration

4.1.1 Set 1

The cells in Set 1 (Cells 23-27) incorporated a welded tab configuration. Electrode contact was achieved by welding nickel tabs (0.400 in. wide x 0.005 in. thick) to the trimmed electrode edge once per revolution as the core was wound. Distance between contact points thus ranged from ~3.2 in. at the inside of the core to ~14.9 in. at the outside of the core. After the core was pressed into the cell case nickel buss plates 0.010 in. thick were used to connect the positive tabs to the case and negative tabs to the winding mandrel (Fig. 57). Contact between the winding mandrel and sealing tube was made by a nickel sheet, welded to the inside diameter of the winding mandrel and folded over the edge of the Neoprene insulating sleeve. Pressing the sealing tube into place provided

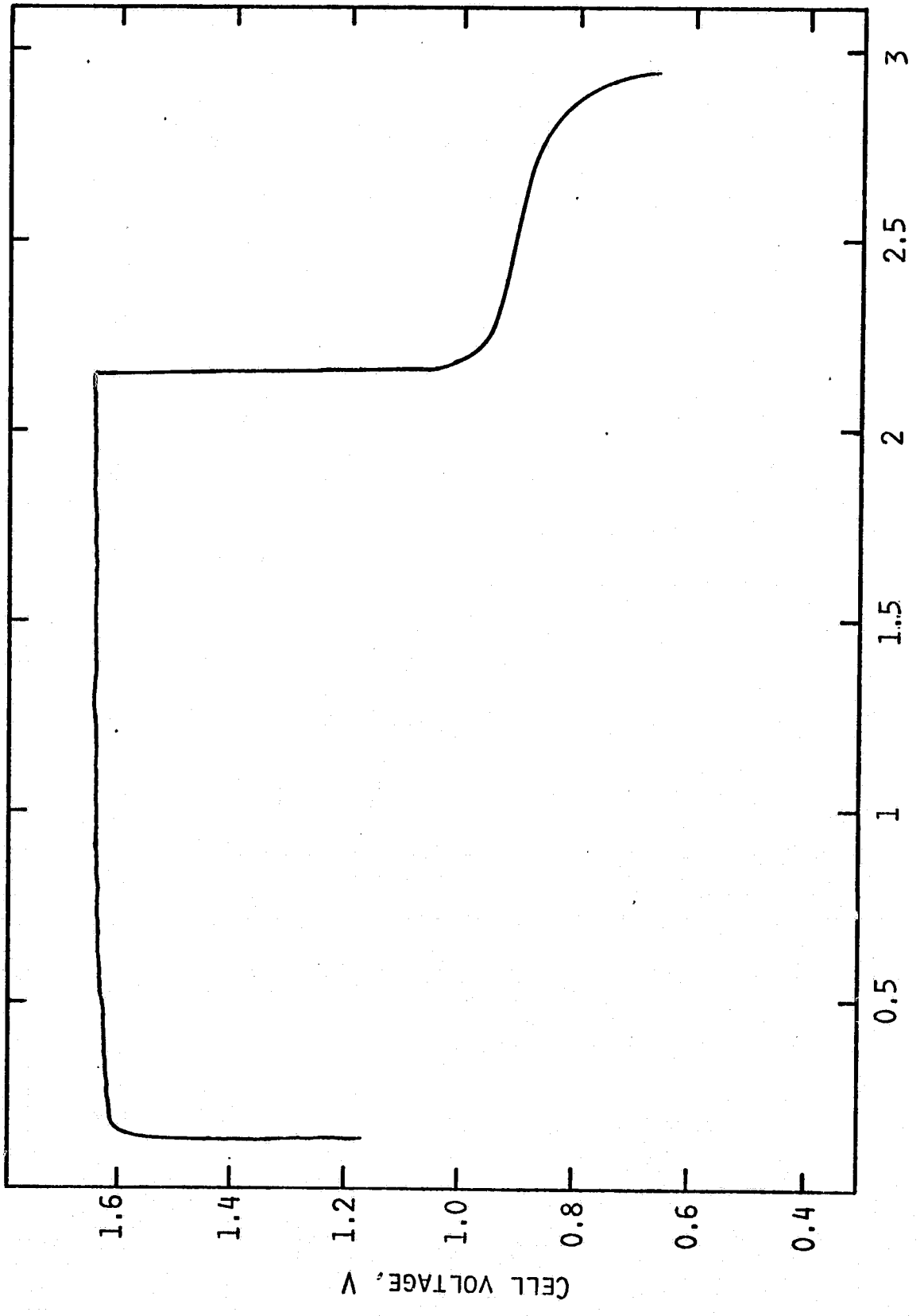

Fig. 55. Voltage profile of cell 28, cycle 1; 50A charge, 90A discharge.

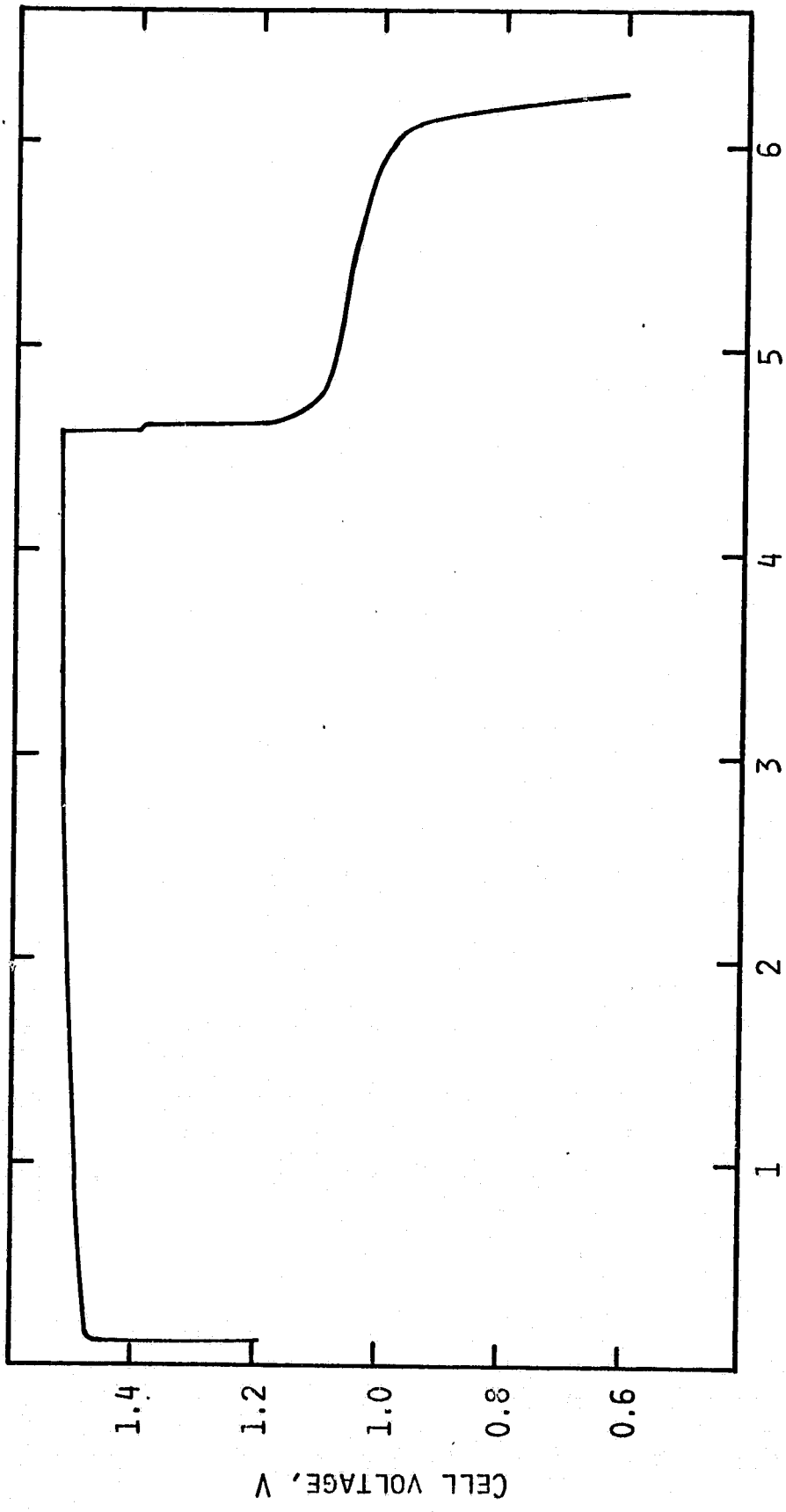

Fig. 56. Voltage profile of cell 42, cycle 1. 25A charge, 50A discharge.

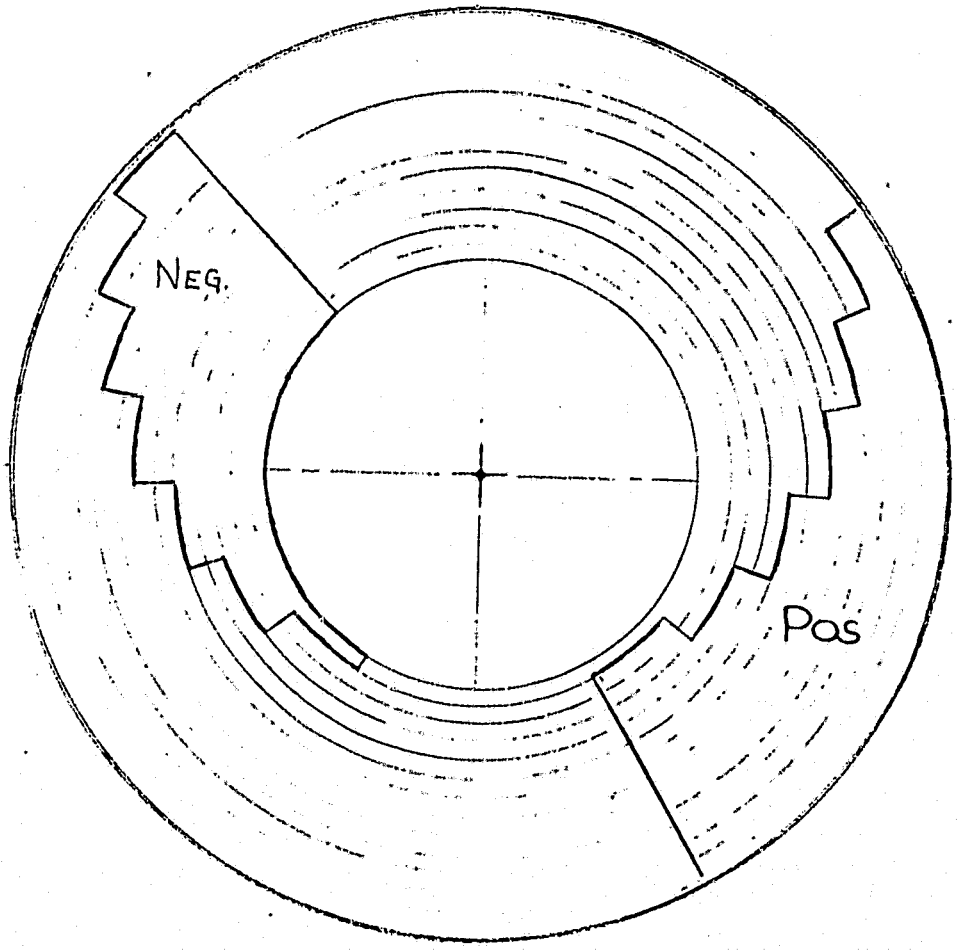

Fig. 57. Buss plates.

contact between the sheet and tube; contact pressure was increased by placing a groove in the contact area during the swaging-sealing process. Surface passivation was avoided by silver plating the winding mandrel, sealing tube, and nickel sheet in the contact area.

4.1.2 Set 2

Set 2 (Cells 32-36) utilized a welded tab contact but we used two tabs per revolution in order to decrease the distance between contacts (Fig. 58). Sealing tube-winding mandrel contact was identical to that of Set 1.

4.1.3 Set 3

The third set of cells (37-41) employed edge contact via flexible copper mesh similar to Cell 30. The electrodes are trimmed flush along one edge of the sintered plaque, along the other edge the substrate is trimmed to within 0.250" of the plaque. This excess substrate strip is cut every 0.350 in. down the length of the electrode. The electrode stack is then laid out so that the excess substrate protrudes beyond the end of the core, positive on one side and negative on the other. After the core is wound the cut tabs are folded over perpendicular to the core axis (Fig. 59). These tabs overlap and provide a rigid, high surface contact area; they also prevent contact between the opposing electrode and the flexible mesh. To prevent surface passivation the copper mesh and the contacting can or take-off plate surfaces were gold plated. Figure 60 shows Cell 39 prior to cover installation. Sealing tube-mandrel contact was identical to that of Set 1.

4.1.4 Set 4

Set 4 (Cells 42-46) had an offset electrode core. Stainless steel springs (Fig. 61) were used to provide edge contact. Core construction was identical to that of Set 3; however, a narrow strip of gold-plated nickel sheet was spot-welded along the edge of the nickel electrode to aid in preservation of surface contact. The springs were welded directly to the winding mandrel. The springs and the inside of the case were gold plated, springs were placed in the bottom of the case and the core was pressed down on the springs, providing positive contact. Sealing tube-winding mandrel contact was identical to Set 1.

4.2 Test Program

After vacuum filling with 400 cc electrolyte and reevacuation, all cells were charged 125 Ah at 25A. The charge cycle was interrupted after 12.5 Ah to determine initial cell resistance. This was measured by interrupting current to the cell and measuring the voltage drop vs. time in the millisecond range. After full charge the cells were discharged at 50A for

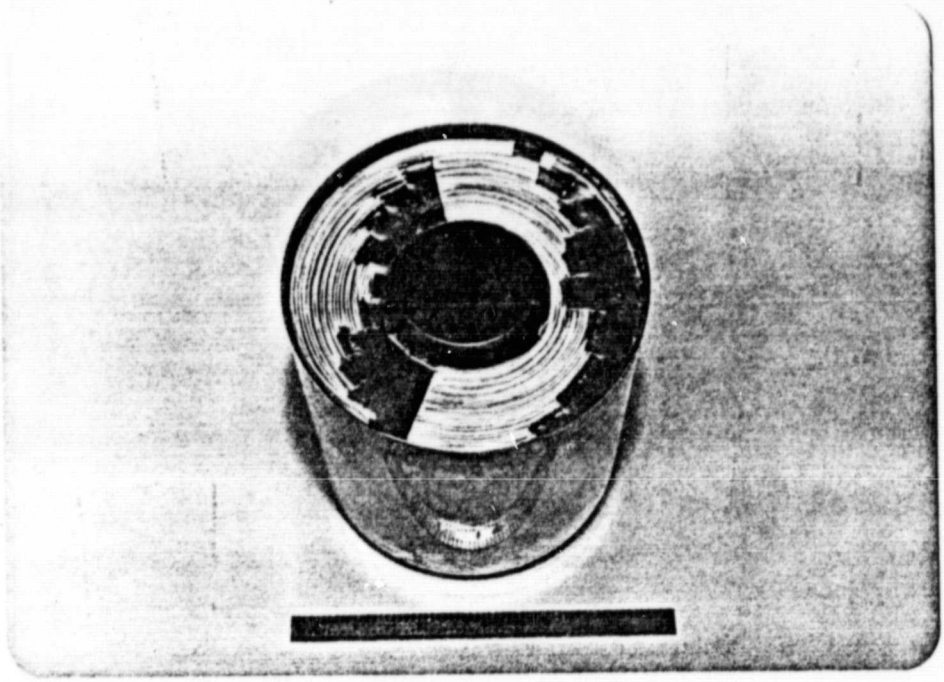

Fig. 58. Cell 35 showing double buss plates.

Fig. 59. Cell 40 showing offset electrodes with folded edge tabs; before insertion of cover.

Fig. 60. Cell 39 prior to cover installation.

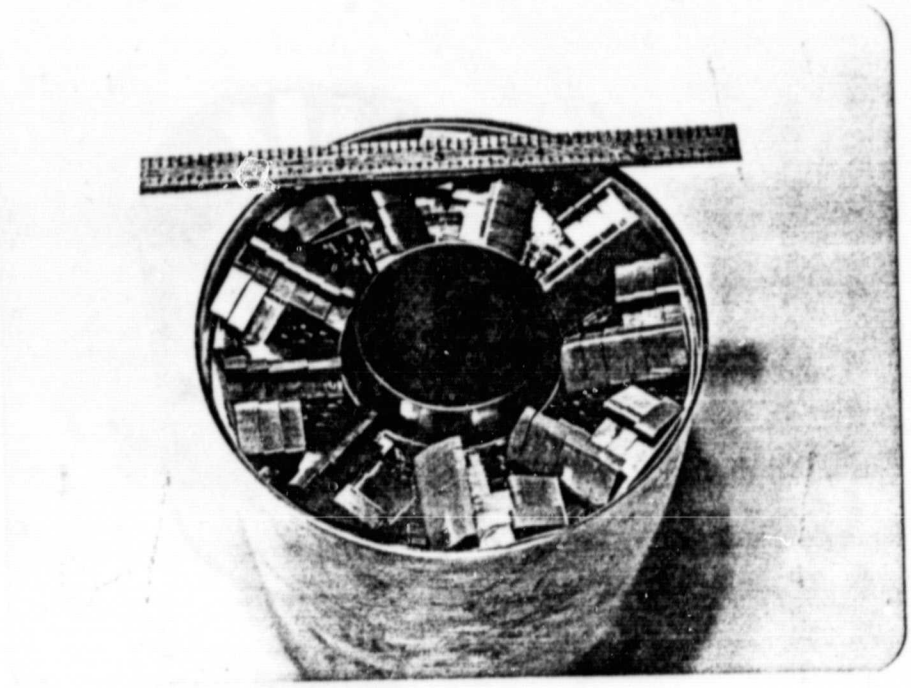

Fig. 61. Stainless steel contact springs in Cell 42.

48 min. at which time the discharge was shortly interrupted to determine cell resistance. Discharging was then resumed to a 0.8V cutoff.

The following charge/discharge cycles were carried out at various rates. Cell potential, cell pressure and cell temperature at two locations were monitored. One cell of each set was equipped with a pressure transducer (Data Instruments, 0-100 psig, 1-8 atm) for continuous pressure recording. The remaining cells had pressure gauges (Ashcroft 316 SS, vacuum to 60 psig). Temperatures were measured with chromel alumel thermocouples placed on the side of the cell case, one near the bottom edge and the other near the top edge.

For data recording we used a Bascom-Turner Series 8000 Data Management System. This system converts input data to digital form and stores it on a magnetic disk. This data may be retrieved and placed in a RAM, where numerical operations may be performed on it (compression, expansion, addition, integration, etc.) and then transformed to analog output for a visual record. The Bascom-Turner recorder has eight input channels. It also allows data acquisition at high speed (0.5 msec/point) which was used for the cell resistance determinations.

For very high rate discharge we used a resistive load. The current was measured via the voltage drop across a 300A precision shunt. A 300A knife switch was used to close the circuit.

Overcharge characteristics of the cells were examined as follows: The cells were charged at 50A for 1.5 hr (70 Ah) followed by continued charge at 25A for two hours at which time the current was increased to 50A until the internal pressure exceeded 5 atm (60 psig). Voltage, temperature and cell pressure were recorded as a function of time.

After the rate and overcharge testing internal cell resistance was measured by current interruption during charge and discharge as described earlier. Finally the cells were overdischarged at 90A until the voltage reached -1.0V or pressure reached 40 psig whichever occurred first. Cell voltage pressure and temperature were recorded.

Subsequent to the test program described above representative cells from each set were subjected to a more extensive cycle test at simulated near earth orbit conditions (50A charge for one hour, 90A discharge for 1/2 hour).

4.3 Test Results

Characteristic recordings of cell voltage, pressure and temperature with time for the various tests employed are shown in Figures 62 to 66. The results for each set and each cell are summarized in Tables 5 to 8.

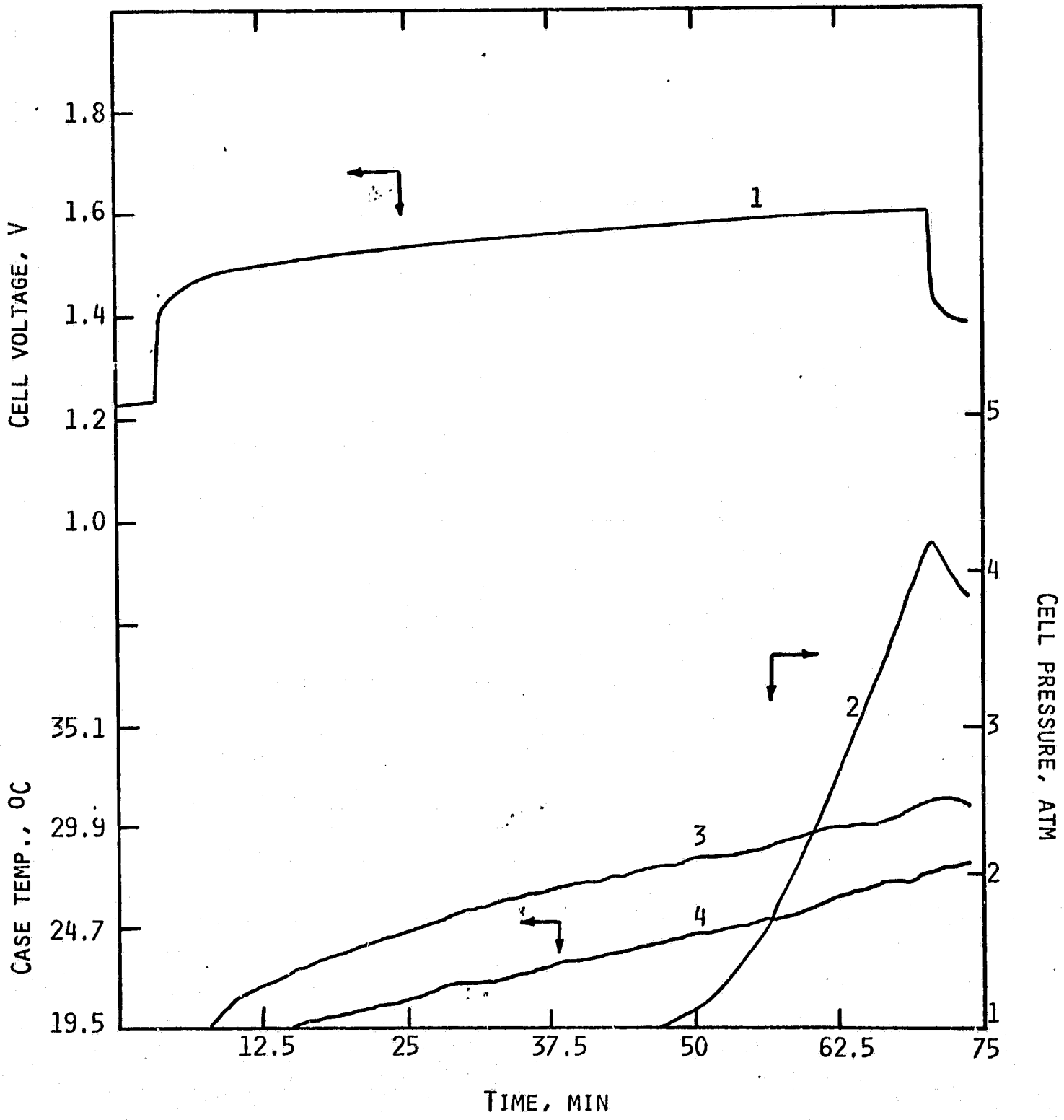

Fig. 62. Characteristics of Cell 26 during 90A charge. (1) voltage profile, (2) pressure profile, (3) temperature profile, top of case and (4) temperature profile, bottom of case.

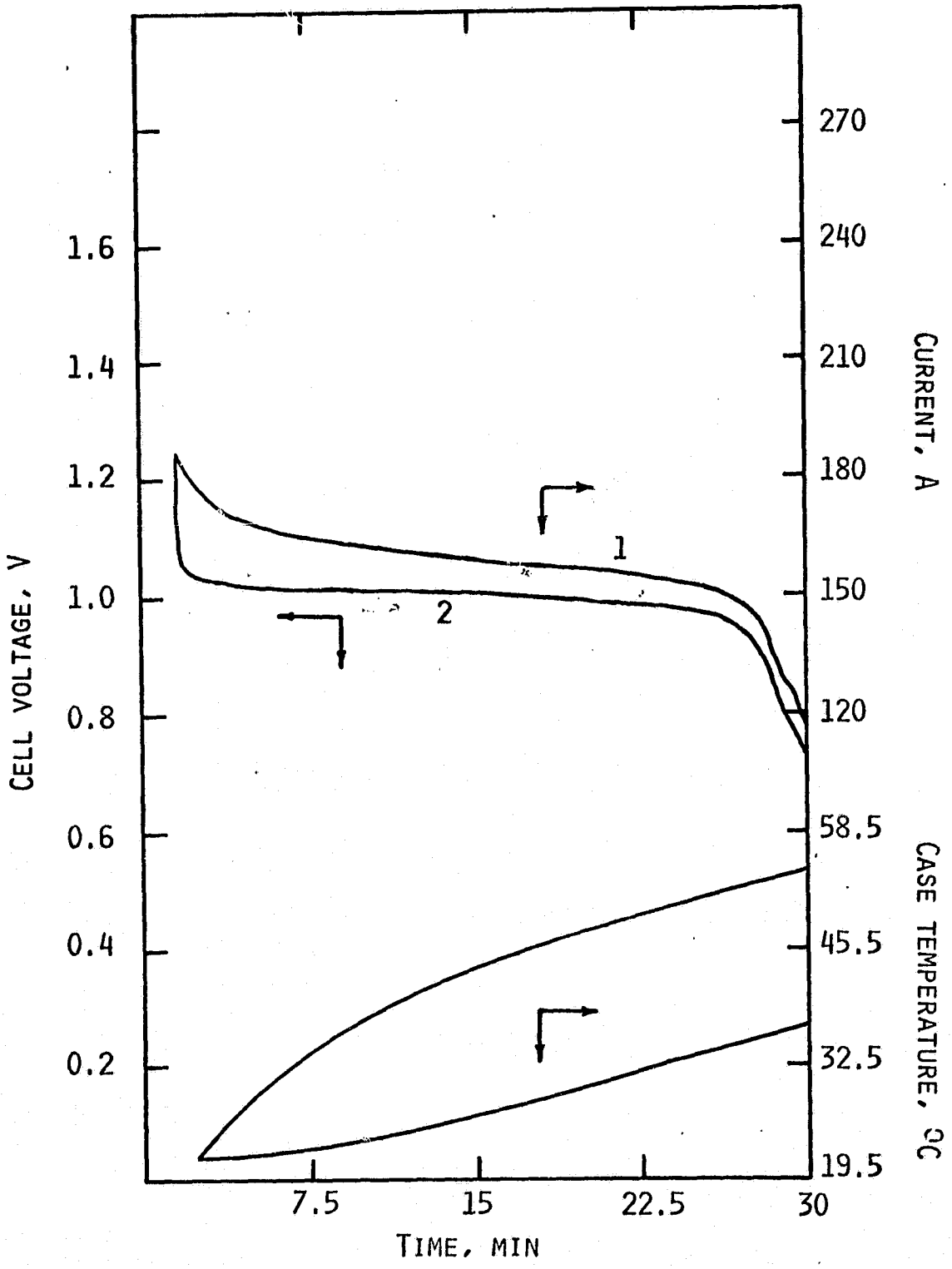

Fig. 63 Characteristics of Cell 26 during resistive discharge. (1) current profile, (2) voltage profile, (3) temperature profile, top of case, (4) temperature profile, bottom of case.

C-2

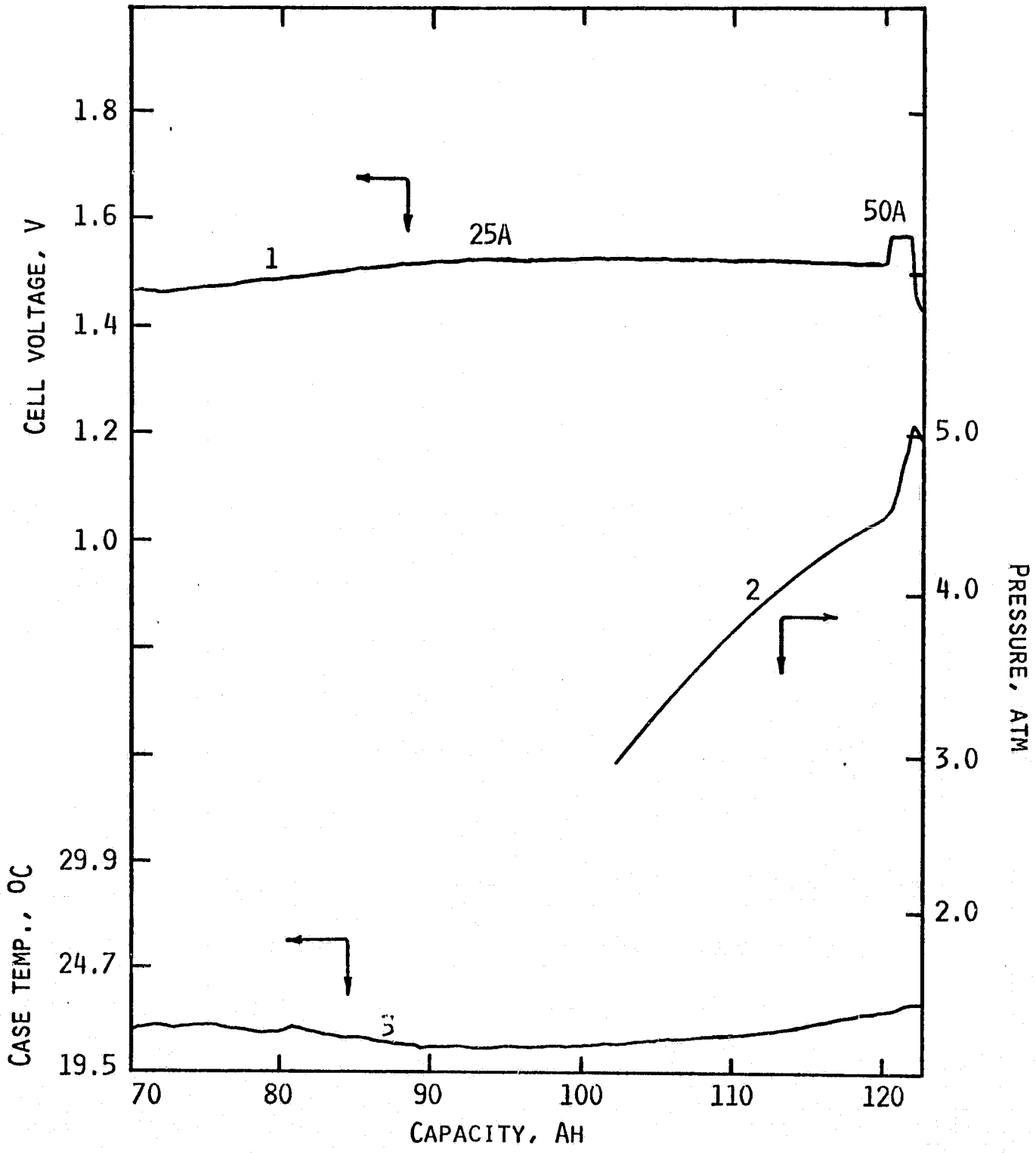

Fig. 64. Profiles of cell 24 during overcharge. Began recording at ~100 Ah. Voltage (1), pressure (2) and temperature (3).

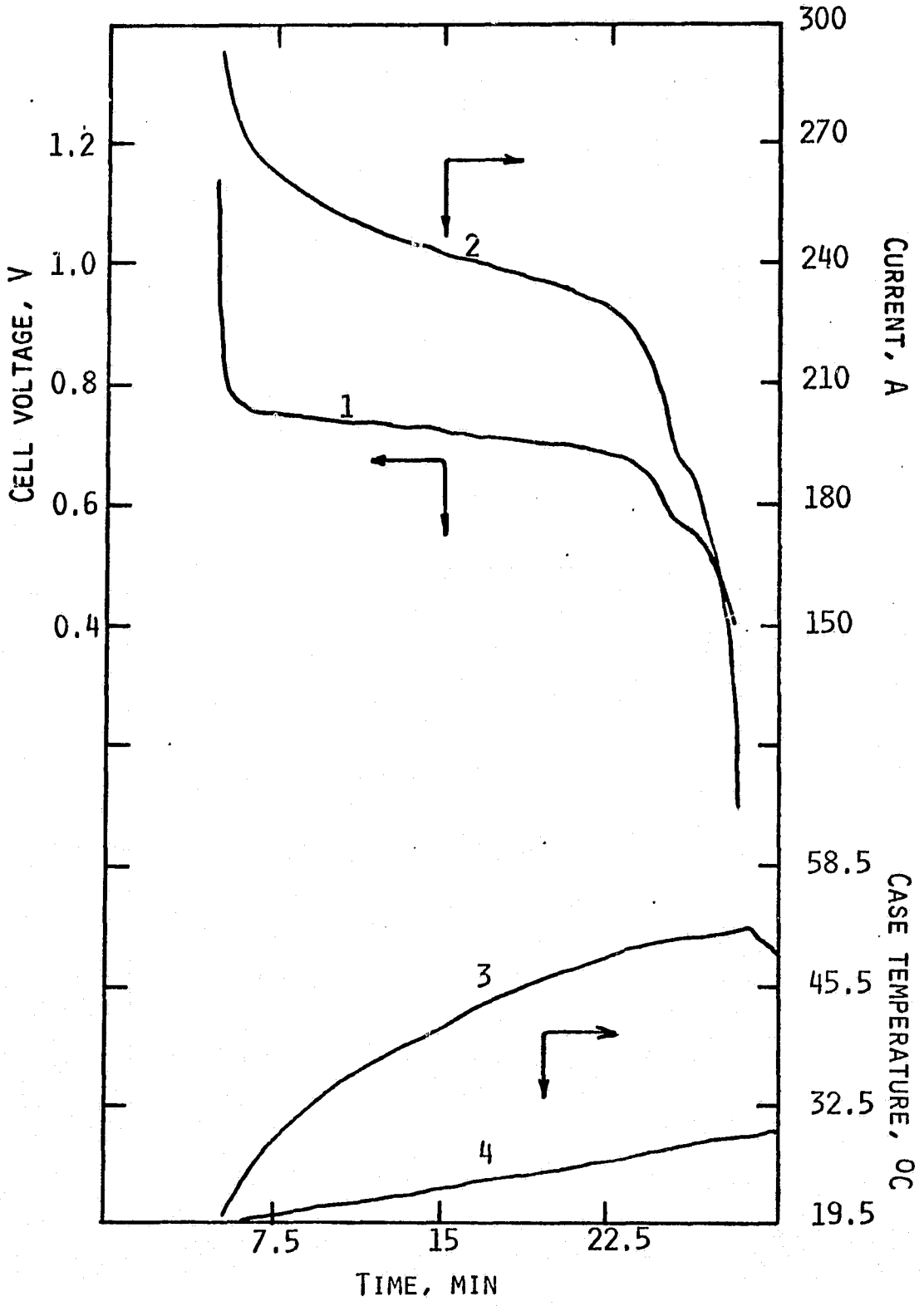

Fig. 65. Case temperature profiles of cell 26 during resistive discharge. Voltage (1), current (2), top (3) and bottom (4).

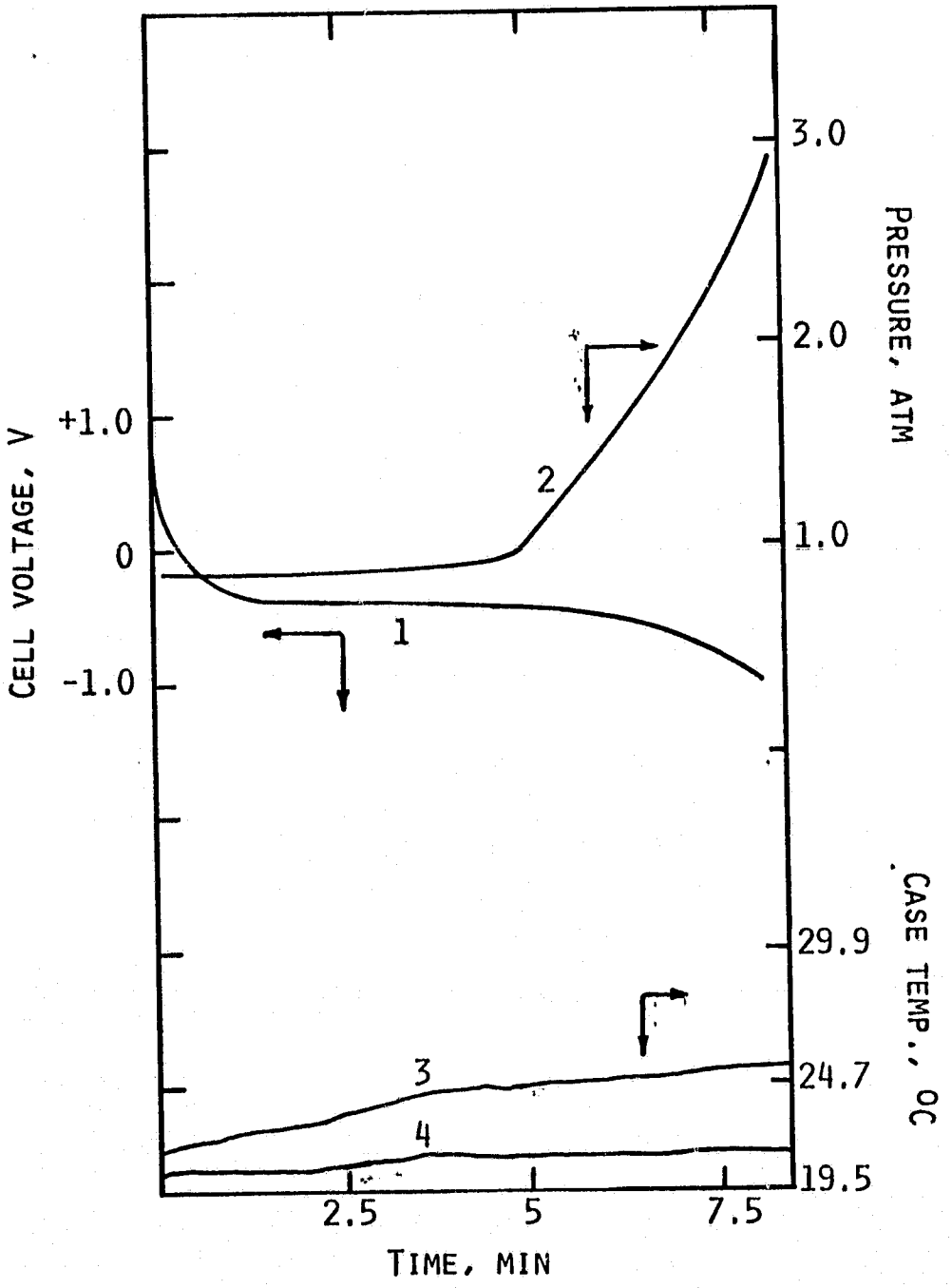

Fig. 66. Case temperature profiles of cell 35 during 90A overdischarge. Voltage (1), pressure (2), bottom (3) and top (4).

Table 5

ORIGINAL PAGE IS OF POOR QUALITY

Summary of Test Results

Set 1 (welded tabs 1/revolution)

		Cell Number				
		23	24	25	26	27
25A Charge	Mid Voltage, V	1.472	1.470	1.452	1.450	1.458
	Capacity, Ah	101	101	101	101	101
50A Dischg.	Mid Voltage, V	1.179	1.175	1.175	1.190	1.162
	Capacity, Ah	86.8	89.9	91.3	84.7	89.9
90A Charge	Mid Voltage, V	1.585	1.555	1.563	1.540	1.616
High Rate Dischg.	Mid Voltage, V	0.959	1.022	1.005	1.020	0.990
	Mid Current, A	158	153	146	160	-
	Capacity, Ah	74.2	73.6	76.3	74.1	-
High Rate Dischg.	Mid Voltage, V	0.950	1.01	1.03	1.01	1.02
	Mid Current, A	146	145	140	152	142
	Capacity, Ah	86.1	75.9	73.6	68.5	70.8
High Rate Dischg.	Mid Voltage, V	0.707	0.772	0.808	0.830	0.733
	Mid Current, A	214	225	236	239	243
	Capacity, Ah	78.5	73.1	82.6	85.1	81.0
Cell Impedance	Cycle 1, mΩ	1.5	1.2	1.2	1.2	1.4
	Cycle 5, mΩ	1.6	1.3	1.3	1.3	1.3
Overcharge	Voltage, V	1.535	1.535	1.529	1.545	1.545
	Pressure, atm	0.26	<1	0.66	0.36	0.46
	Voltage, V	1.55	1.537	1.533	1.515	1.527
	Pressure, atm	3.1	4.4	3.8	3.1	3.2
	Add'l Charge at 50A to 5 atm, Ah	15.3	9.3	11.9	22.6	19.6
Overdis-charge 90A	Cell Voltage, V	-0.55	-0.80	-0.79	-0.89	-1.0
	Pressure, atm	3.75	3.75	3.75	3.75	2.90
	Chargeout past 0V, Ah	20.5	21.8	17.0	16.5	13.5

Table 6

Summary of Test Results

Set 2 (welded tabs 2/revolution)

		Cell Number				
		32	33	34	35	36
25A Charge	Mid Voltage, V	1.475	1.481	1.471	1.467	1.475
	Capacity, Ah	125	125	125	125	125
50A Dischg.	Mid Voltage, V	1.192	1.188	1.198	1.196	1.188
	Capacity, Ah	94.1	93.6	90.4	95.2	95.4
90A Charge	Mid Voltage, V	1.545	1.571	1.532	1.536	1.535
High Rate Dischg.	Mid Voltage, V	1.000	0.992	1.079	1.071	1.085
	Mid Current, A	174	169	168	180	165
	Capacity, Ah	78.5	75.5	71.7	77.7	85.0
High Rate Dischg.	Mid Voltage, V	1.000	1.016	1.079	1.091	1.030
	Mid Current, A	176	172	167	186	191
	Capacity, Ah	51.4	78.2	69.8	85.2	86.5
High Rate Dischg.	Mid Voltage, V	0.838	0.798	0.897	0.873	0.861
	Mid Current, A	302	291	288	321	300
	Capacity, Ah	65.4	64.8	61.8	62.8	75.0
Cell Impedance	Cycle 1, mΩ	1.2	1.?	0.9	0.8	1.0
	Cycle 5, mΩ	1.2	1	0.8	0.7	1.0
Overcharge	Voltage, V	-	-	1.52	1.50	1.50
	Pressure, atm	0.80	1	0.36	0.40	0.43
	Voltage, V	-	-	1.50	1.52	1.52
	Pressure, atm	0.80	3.72	3.0	4.7	4.1
	Add'l Charge at 50A to 5 atm, Ah	-	8	20	5	8
Overdis-charge 90A	Cell Voltage, V	-0.70	-1.0	-0.67	-1.0	-1.0
	Pressure, atm	3.75	2.93	3.75	2.9	3.0
	Chargeout past 0V, Ah	14.6	14.2	13.9	12.6	20.5

Table 7

Summary of Test Results

Set 3 (edge contact, copper mesh)

		Cell Number				
		37	38	39	40	41
25A Charge	Mid Voltage, V	1.517	1.497	1.509	1.511	1.517
	Capacity, Ah	125	125	125	125	125
50A Dischg.	Mid Voltage, V	1.131	1.155	1.155	1.099	1.101
	Capacity, Ah	84.1	90.5	89.6	87.8	86.7
90A Charge	Mid Voltage, V	1.684	1.591	1.607	1.678	-
High Rate Dischg.	Mid Voltage, V	0.623	0.589	0.629	0.599	0.511
	Mid Current, A	112	177	174	174	162
	Capacity, Ah	32.2	63.5	82.5	70.7	3.37
High Rate Dischg.	Mid Voltage, V	0.520	0.629	0.554	0.589	-
	Mid Current, A	121	164	159	171	-
	Capacity, Ah	65.9	88.8	76.1	85.4	-
High Rate Dischg.	Mid Voltage, V	-	0.223	-	-	-
	Mid Current, A	-	40.9	-	-	-
	Capacity, Ah	-	10.6	-	-	-
Cell Impedance	Cycle 1, mΩ	2.1	2.0	1.9	2.6	2.9
	Cycle 5, mΩ	8.9	11.4	6.1	6.9	10.8
Overcharge	Voltage, V	1.693	1.576	1.599	1.575	2.51 (1)
	Pressure, atm	-	-	-	-	- (1)
	Voltage, V	1.663	1.612	1.610	1.599	-
	Pressure, atm	-	-	-	-	-
	Add'l Charge at 50A to 5 atm, Ah	15.0	15.0	16.7	18.3	0
Overdis-charge 90A	Cell Voltage, V	-1.0	-1.0	-1.0	-1.0	-1.0
	Pressure, atm	2.97	-	2.50	2.97	3.07
	Chargeout past 0V, Ah	19.8	21.8	17.5	19.0	13.0

(1) Cell reached 75°C limit after 39.2 Ah charge.

Table 8

Summary of Results

Set 4 (edge contact, springs)

		Cell Number				
		42	43	44	45	46
25A Charge	Mid Voltage, V	1.529	1.493	1.527	1.499	1.509
	Capacity, Ah	124	124	124	124	124
50A Dischg.	Mid Voltage, V	1.077	1.151	1.083	1.089	1.111
	Capacity, Ah	80.7	92.7	93.7	91.4	87.5
90A Charge	Mid Voltage, V	1.717	1.615	1.737	1.680	1.638
High Rate Dischg.	Mid Voltage, V	0.630	0.794	0.677	0.675	0.741
	Mid Current, A	164	185	-	165	164
	Capacity, Ah	34.9	69.4	-	52.3	65.6
High Rate Dischg.	Mid Voltage, V	0.642	0.747	0.638	0.685	0.743
	Mid Current, A	162	188	150	164	158
	Capacity, Ah	28.7	77.1	57.8	64.9	64.5
High Rate Dischg.	Mid Voltage, V	0.396	0.505	0.388	0.442	0.501
	Mid Current, A	177	246	177	204	224
	Capacity, Ah	28.0	112.3	87.02	90.9	75.1
Cell Impedance	Cycle 1, mΩ	2.8	1.8	3.2	2.6	2.4
	Cycle 5, mΩ	6.0	2.2	4.6	3.6	2.8
Overcharge	Voltage, V	1.723	1.527	1.612	1.529	-
	Pressure, atm	2.1	<1	1.2	2.5	4.1
	Voltage, V	1.616	1.543	1.580	1.555(1)	1.555(2)
	Pressure, atm	3.3	4.2	4.0	5.0(1)	5.0(2)
	Add'l Charge at 50A to 5 atm, Ah	15	5	6.7	0	0
Overdis-charge 90A	Cell Voltage, V	-0.80	-	-1.0	-0.99	-
	Pressure, atm	3.75	3.75	2.9	3.75	
	Chargeout past 0V, Ah	16.4	11.8	12.1	4.7	

(1) Cell reached 5 atm at 85.4 Ah charge.

(2) Cell reached 5 atm at 114 Ah charge.

General cell behavior followed that of conventional Ni/Cd cells. During C-rate charge oxygen pressure starts to build up at approximately 80% state of charge and reaches ~50 psig after about 10% overcharge. No optimization with regard to oxygen recombination, which strongly depends on the electrolyte fill level, was carried out. Case temperature increases from 10 to 30°C were observed. Generally the top of the case was noticeably warmer. The cells were tested without active cooling in ambient temperature air. In general, the results within each set are quite consistent. The main difference from set to set lies in the cell impedance and in its change with cycling. Set 2 featuring two tabs per revolution shows the lowest cell resistance. No significant change in cell resistance occurred during testing. The resistance of Set 1 (one welded tab) is only slightly higher and shows also no change. The two sets employing edge contacts behaved differently. They started with nearly identical initial resistance which was, however, about twice that of the welded tab cells. The resistance of Set 3 increased markedly during cycling and extended overcharge indicating a deterioration of the electrode contacts. Since the copper mesh had been gold plated we assume the primary problem to reside in the nickel electrode copper mesh contact probably due to oxidation of the nickel substrate contact surface. Set 4 shows much less change. However, here too, some increase in resistance was observed indicating that the contact appears not invariant with time.

A typical cell voltage recording during continuous cycling testing is shown in Figure 67. The results are summarized in Tables 9 to 12. They confirm the observation made above. Sets 1 and 2 showed very little change in the end of charge and end of discharge voltages over the 300 test cycles. Set 3 performed poorly and was not cycled extensively. Set 4 showed a moderate increase in cell impedance.

5. Summary Discussion and Conclusions

The objective of this program was to investigate the feasibility of a toroidal Ni/Cd cell configuration for potential use in large space power systems. The original concept was developed by NASA and involved cell closure by expanding the inside cell diameter and redrawing the outside cell diameter thus providing a compressive seal around a nylon insulator component. Better thermal management, higher energy density and lower cost were among the potential benefits.

Based on a thorough design review we suggested to overcome fundamental difficulties in the cell closure by localized swaging of grooves. Substantial strengthening of the cell case and positive interlocking are additional benefits. Practical parameters for the formation of swaged seals were developed and the principal feasibility was demonstrated by construction of prototype cells. Although possible hermetic seals with nylon are probably not practical due to the high elastic modulus and very

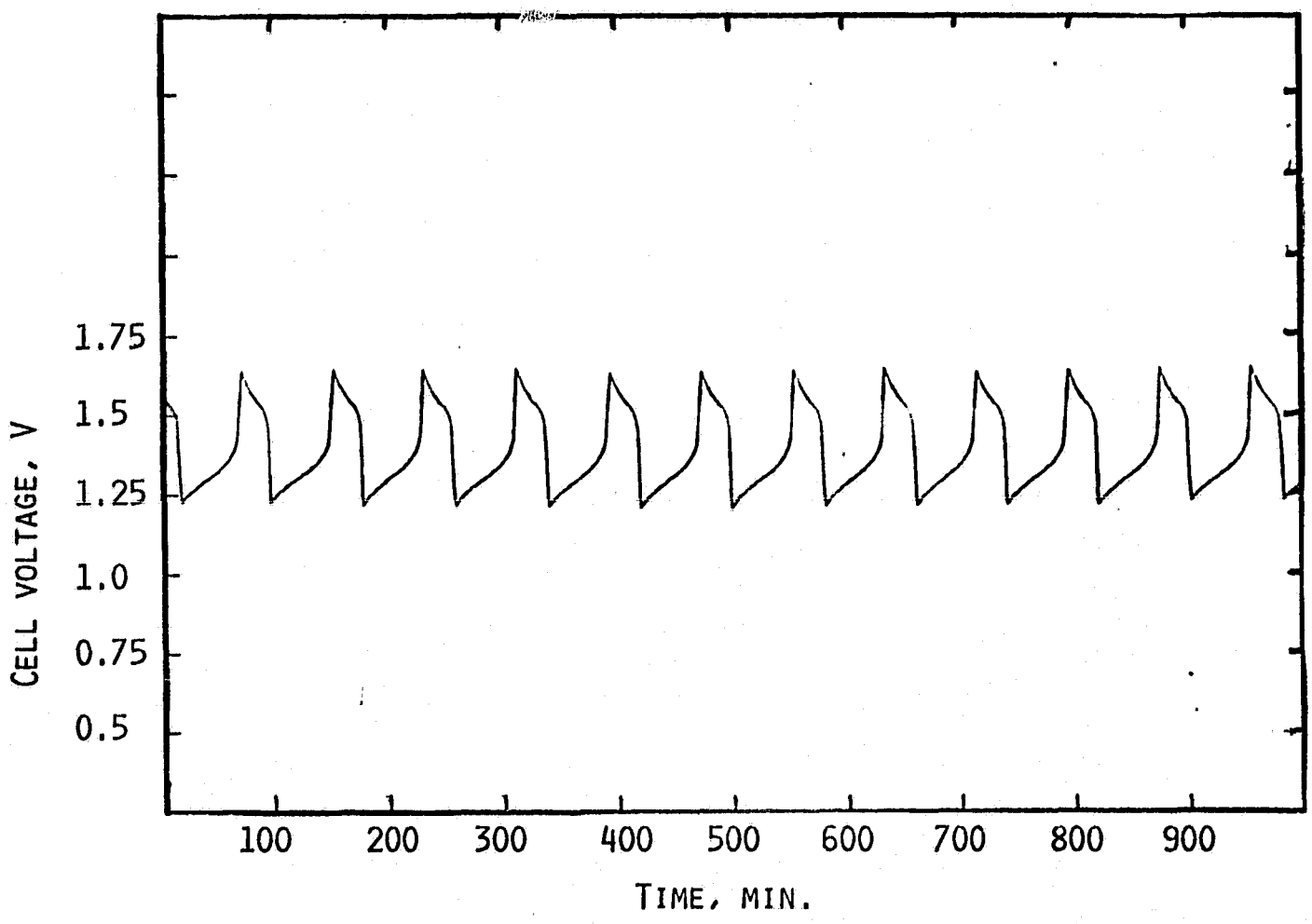

Fig. 67 . Voltage profile of cell 36 during continuous cycling (cycles 100-112). Cycle consisted of 50A charge for one hour followed by 90A discharge for one half hour.

Table 9

Cycle Test of Set 1 Cells

Cycle No.	Cell 26			
	Charge Current (A)	End of Charge Voltage (V)	Discharge Current (A)	End of Discharge Voltage (V)
1	50	1.525	90	1.100
5	50	1.537	30	1.125
10	30	1.532	30	.213
30	50	1.570	90	1.100
80	50	1.597	90	1.095
100	50	1.585	90	1.078
150	50	1.597	90	1.075
200	50	1.575	90	1.058
250	50	1.585	90	1.040
300	50	1.573	90	1.023

Table 10

Cycle Tests of Set 2 Cells

Cycle No.	Cell 34				Cell 35			
	Charge Current (A)	End of Charge Voltage (V)	Discharge Current (A)	End of Discharge Voltage (V)	Charge Current (A)	End of Charge Voltage (V)	Discharge Current (A)	End of Discharge Voltage (V)
1	50	1.505	90	1.168	50	1.520	90	1.150
5	50	1.508	90	1.155	50	1.520	30	1.225
10	50	1.525	90	1.150	30	1.510	30	1.225
30	50	1.543	90	1.130	50	1.533	90	1.138
80	50	1.525	90	1.093	50	1.550	90	1.125
100	50	1.528	90	1.088	50	1.550	90	1.113
150	50	1.533	90	1.075	50	1.550	90	1.108
200	50	1.520	90	1.055	50	1.530	90	1.125
250					50	1.543	90	1.110
300					50	1.536	90	1.051

Table 11

Cycle Tests of Set 3 Cells

Cycle No.	Cell 37				Cell 39			
	Charge Current (A)	End of Charge Voltage (V)	Discharge Current (A)	End of Discharge Voltage (V)	Charge Current (A)	End of Charge Voltage (V)	Discharge Current (A)	End of Discharge Voltage (V)
1	50	1.625	30	1.150	50	1.750	90	0.750
2	30	1.550	30	1.150	50	1.650	90	0.650
3	30	1.560	30	1.147	50	1.723	90	0.425
5	30	1.595	30	1.135				
8	30	1.608	30	1.100				
10[1]	30	1.550	30	1.095				
12	50	1.750	90	0.425				
13	50	1.745	90	0.375				
14	50	1.795	90	0.375				
15	50	1.775	90	0.350				

[1]Did not charge completely.

Table 12

Cycle Tests of Set 4 Cells

Cycle No.	Cell 43				Cell 46			
	Charge Current (A)	End of Charge Voltage (V)	Discharge Current (A)	End of Discharge Voltage (V)	Charge Current (A)	End of Charge Voltage (V)	Discharge Current (A)	End of Discharge Voltage (V)
1	50	1.575	90	1.058	50	1.600	90	1.023
5	50	1.600	30	1.175	50	1.600	90	0.998
10	30	1.550	30	1.175	50	1.603	90	0.960
30	50	1.610	90	0.980	50	1.625	90	0.938
80	50	1.613	90	1.000	50	1.610	90	0.875
100	50	1.630	90	0.937	50	1.623	90	0.855
150	50	1.650	90	0.913	50	1.635	90	0.800
200	50	1.633	90	0.875	50	1.632	90	0.695
250	50	1.648	90	0.853				
300	50	1.646	90	0.823				

limited elastic deformation range of this material. Other elastomeric insulators such as, e.g., Neoprene were found suitable for the formation of hermetic swaged seals.

Examination of the swaged toroidal Ni/Cd cell in particular with view on scale up to larger modules shows the following: Swaging of the outer seal becomes increasingly more difficult as the diameter is increased. The reason lies in the decreased resistance to buckling and out of round deformation in response to compressive swaging faces as the can curvature is decreased. To counter this, can thickness and thus weight, would have to be increased beyond that needed for stand alone structural strength. To eliminate this shortcoming we developed a swaged-welded toroidal Ni/Cd cell design. Here the toroidal can has only a single outer wall with an easy to perform and strong edge weld and an inner swaged compression seal. Manufacture of the cell can parts for this design is also greatly facilitated. We have built and demonstrated the performance of such cells. The major difficulties encountered were not related to cell can construction but rather to the electrical connections. The original toroidal cell design relied on large area mechanical contacts. Contacts solely at the ends of a larger electrode roll are only feasible for very low rate applications. Higher rates require periodic contacts or preferably continuous edge contacts. A variety of such configurations were explored in practice. To avoid gradual contact deterioration in the oxidative cell environment welded contacts or deterioration resistant surface finishes such as e.g., gold plating are necessary.

In summary we conclude that functioning toroidal Ni/Cd cells of large capacity can be manufactured. They can operate in a stand alone fashion without special restraining. The advantages of thermal management depends on the specific design and mode of cooling. We estimate the energy density as comparable to equally sized conventional design. There appears to be no significant cost advantage for high rate cells since contacts have to be either welded or of a fairly sophisticated mechanical nature with stable contact surfaces.

IV. REFERENCES

1. Roark, Raymond J., formulas for Stress and Strain, 4th Edition (New York: McGraw Hill, 1965).